

## 2. EXPLANATORY NOTES<sup>1</sup>

Shipboard Scientific Party<sup>2</sup>

### INTRODUCTION

We have assembled material in this chapter to help the reader understand the basis for our preliminary scientific conclusions and also to provide the interested investigator with the information needed to select samples for further analysis. This information concerns only shipboard operations and analyses described in the site reports in the Leg 181 *Initial Reports* volume of the *Proceedings of the Ocean Drilling Program*. Methods used by various investigators for shore-based analyses of Leg 181 data will be described in the individual scientific contributions published in the *Scientific Results* volume and in publications in various professional journals.

### Authorship of Site Chapters

The separate sections of the site chapters were written by the following shipboard scientists (authors are listed in alphabetical order, no seniority is implied):

Principal results: R. Carter, McCave

Background and objectives: R. Carter, McCave

Operations: Grout, Richter

Lithostratigraphy: Buret, L. Carter, Hall, Joseph, Smith, Winkler

Biostratigraphy: Aita, Di Stefano, Fenner, Gradstein, Hayward, Wei

Paleomagnetism: Hu, Wilson

Composite depths: Harris, Weedon

Age models and sedimentation rates: Gradstein, McCave, Wilson

Inorganic geochemistry: Khim, Suzuki

Organic geochemistry: Rinna

Physical properties: Lee, Millwood

Downhole measurements: Fothergill, Handwerker

---

<sup>1</sup>Examples of how to reference the whole or part of this volume.

<sup>2</sup>Shipboard Scientific Party addresses.

## Use of “Ma” vs. “m.y.”

1. *Ma* is equivalent to and replaces m.y.B.P. (million years Before Present), for example, 35–40 Ma.
2. *m.y.* is used in sentences such as “... for 5 m.y. in the early Miocene.”

## Drilling Characteristics

Information concerning sedimentary stratification in uncored or unrecovered intervals may be inferred from seismic data, wireline-logging results, and from an examination of the behavior of the drill string, as observed and recorded on the drilling platform. Typically, the harder a layer, the slower and more difficult it is to penetrate. A number of other factors may determine the rate of penetration, so it is not always possible to relate the drilling time directly to the hardness of the layers. Bit weight and revolutions per minute, recorded on the drilling recorder, also influence the penetration rate.

## Drilling Deformation

When cores are split, many show signs of significant sediment disturbance, including the concave-downward appearance of originally horizontal bands, haphazard mixing of lumps of different lithologies (mainly at the tops of cores), and the near-fluid state of some sediments recovered from tens to hundreds of meters below the seafloor. Core deformation probably occurs during cutting, retrieval (with accompanying changes in pressure and temperature), and core handling on deck.

## Shipboard Scientific Procedures

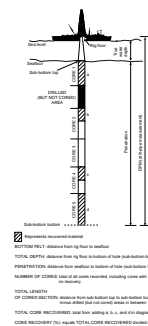
### Numbering of Sites, Holes, Cores, and Samples

Ocean Drilling Program (ODP) drill sites are numbered consecutively and refer to one or more holes drilled while the ship was positioned over one acoustic beacon. Multiple holes may be drilled at a single site by pulling the drill pipe above the seafloor (out of the hole), moving the ship some distance from the previous hole, and then drilling another hole.

For all ODP drill sites, a letter suffix distinguishes each hole drilled at the same site. The first hole drilled is assigned the site number modified by the suffix “A,” the second hole takes the site number and suffix “B,” and so forth. Note that this procedure differs slightly from that used by the Deep Sea Drilling Program (DSDP) (Sites 1 through 624), but prevents ambiguity between site- and hole-number designations. It is important to distinguish among holes drilled at a site, because recovered sediments or rocks from different holes usually do not come from exactly equivalent positions in each hole.

The cored interval is measured in meters below seafloor (mbsf). The depth interval assigned to an individual core begins with the depth below the seafloor that the coring operation began, and extends to the depth that the coring operation ended (Fig. F1). Each cored interval is generally 9.5 m long, which is the length of a core barrel. Coring intervals may be shorter and may not necessarily be adjacent if separated by drilled intervals. In soft sediments, the drill string can be “washed

F1. Coring and depth intervals, p. 40.



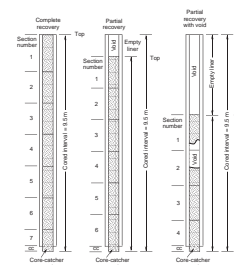
ahead” with the core barrel in place, without recovering sediments. This is achieved by pumping water down the pipe at high pressure to wash the sediment out of the way of the bit and up the space between the drill pipe and the wall of the hole. If thin, hard, rock layers are present, then it is possible to get “spotty” sampling of these resistant layers within the washed interval and thus to have a cored interval greater than 9.5 m.

Cores taken from a hole are numbered serially from the top of the hole downward. Core numbers, and their associated cored intervals in meters below seafloor, ideally are unique in a given hole. However, this may not be true if an interval is cored twice, if the borehole wall caves in, or other hole problems occur. Full recovery for a single core is 9.5 m of rock or sediment contained in a plastic liner (6.6-cm internal diameter) plus about 0.2 m (without a plastic liner) in the core catcher (Fig. F2). The core catcher is a device at the bottom of the core barrel that prevents the core from sliding out when the barrel is being retrieved from the hole. In many advanced hydraulic piston core (APC) or extended core barrel (XCB) cores, recovery exceeds the 9.5-m theoretical maximum by as much as 0.60 m. The cause of this expansion is not fully understood. The recovered core in its liner is divided into 1.5-m sections that are numbered serially from the top (Fig. F2). When full recovery is obtained, the sections are numbered from 1 through 7, with the last section generally being shorter than 1.5 m. Rarely, a core may require more than seven sections; this is usually the result of gas expansion having caused voids within some sections. When less than full recovery is obtained, as many sections as are needed to accommodate the length of the core will be recovered; for example, 4 m of core would be divided into two 1.5-m sections and a 1-m section. If cores are fragmented (recovery less than 100%), sections are numbered serially and intervening sections are noted as void, whether shipboard scientists believe that the fragments were contiguous in situ or not. In rare cases, a section less than 1.5 m may be cut to preserve features of interest. Sections less than 1.5 m in length are also sometimes cut when the core liner is severely damaged.

By convention, material recovered from the core catcher is placed immediately below the last section when the core is described and is labeled core catcher (CC); in sedimentary cores, it is treated as a separate section. In cases where material is only recovered in the core catcher it is assigned the depth of the top of the cored interval (this convention differs from that used in the early days of deep-sea drilling), although information from the driller or other sources may indicate from what depth it was actually recovered.

When the recovered core is shorter than the cored interval, the top of the core is equated with the top of the cored interval by convention to achieve consistency when handling analytical data derived from the cores. Samples removed from the cores are designated by distance, measured in centimeters from the top of the section to the top and bottom of each sample removed from that section. A complete identification number for a sample consists of the following information: leg, site, hole, core number, core type, section number, piece number (for hard rock), and interval in centimeters, measured from the top of section. For example, a sample identification of “Sample 181-1119A-11H-6, 10–12 cm” would be interpreted as representing a sample removed from the interval between 10 and 12 cm below the top of Section 6, Core 11 (H designates that this core was taken by the advanced hydraulic piston corer) of Hole 1119A during Leg 181. A computer routine was available

F2. Examples of numbered core sections, p. 41.



to calculate depth in mbsf from any correctly formulated ODP sample designation; this avoided inconsistencies that could have arisen on those occasions where some sections were cut to nonstandard lengths. Although depth mbsf is an invaluable convention, it is not ideal especially for high-resolution work; for further explanation, see “[Composite Depths](#),” p. 19.

All ODP core and sample identifiers indicate core type. The following abbreviations are used: H = hydraulic piston core (HPC; also referred to as APC, or advanced hydraulic piston core); X = extended core barrel (XCB); W = wash-core recovery; and M = miscellaneous material. APC and XCB cores were cut during Leg 181.

### **Core Handling**

As soon as each core was retrieved on deck, a sample taken from the core catcher was given to the paleontological laboratory for an initial age assessment. Special care was taken in transferring the core from the drill floor to a long horizontal rack on a catwalk near the core laboratory so that the core did not bend or twist excessively. The core was capped immediately, and gas samples were taken by piercing the core liner and withdrawing any gas into a vacuum tube. Voids within the core were sought as sites for gas sampling. Some of the gas samples were stored for shore-based study, but others were analyzed immediately as part of the shipboard safety and pollution-prevention program. Next, the core was marked into section lengths of 1.5 m, each section was labeled, and the core was cut into sections. Interstitial water (IW) and whole-round samples were also taken at this time. In addition, head-space gas samples were taken from the end of cut sections on the catwalk and sealed in glass vials for light hydrocarbon analysis. Afterward, each section was sealed at the top and bottom by gluing on color-coded plastic caps: blue to identify the top of a section and clear to identify its bottom. A yellow cap was placed on the section ends from which a whole-round sample was removed. The caps were usually attached to the liner by coating the end liner and the inside rim of the cap with acetone and then attaching the caps to the liners.

The cores were then carried into the laboratory where the sections were labeled with an engraver to permanently mark the complete designation of the section. The length of the core in each section and the core-catcher sample were measured to the nearest centimeter. This information was logged into the shipboard ORACLE database (JANUS).

Whole-round sections from APC and XCB cores were routinely run through the multisensor track (MST). The MST includes the gamma-ray attenuation porosity evaluator (GRAPE), a *P*-wave logger, natural gamma-ray emission measurement, and a volume magnetic susceptibility meter. The core-catcher sample is not run through the MST track, for which reason we avoided using it for final biostratigraphic work. Before MST analysis, the temperature of each core was measured. After the core had equilibrated to room temperature (~3 hr), soft sediments were measured for thermal conductivity. After MST analysis, cores were split lengthwise into working and archive halves. Soft cores were split with a wire. Hard cores were split using a diamond saw. The wire-cut cores were split from the bottom to top so that sediment below the voids or soupy intervals that were sometimes present at the top of Section 1 would not be drawn into the voids.

Archive core halves were described visually and then run through the ODP Minolta color scanner and the cryogenic magnetometer. Finally,

the cores were photographed with both black-and-white and color film, a whole core at a time. Close-up photographs (black-and-white and/or color) were taken of particular features, as requested by individual scientists, for illustrations in the summary of each site.

The working half of the core was measured first for sonic velocity. After physical properties and paleomagnetic sampling, the working half was sampled for reconnaissance-level and low-resolution shipboard and shore-based laboratory studies. Most sampling for detailed high-resolution paleoceanographic and paleoclimatic studies was deferred until after the cruise to optimize the sampling with the stratigraphic information from biostratigraphy, paleomagnetic stratigraphy, and lithologic correlations.

Each sample taken either for shipboard or shore-based analysis was logged into the ORACLE database (JANUS) by the location and the name of the investigator receiving the sample. Records of all of the samples removed are kept by the curator at ODP headquarters. The extracted samples were sealed in plastic vials or bags and labeled. Samples were routinely taken for shipboard physical properties and paleomagnetic analysis.

Both halves of the core were placed into labeled plastic tubes, which were then sealed and transferred to cold-storage space on board the drilling vessel. At the end of the leg, the cores were transferred from the ship in refrigerated air freight containers to cold storage at the ODP core repository in College Station.

## LITHOSTRATIGRAPHY

Core material recovered on Leg 181 was described according to ODP procedures and conventions. Shipboard procedures included visual core descriptions, smear-slide analysis, X-ray diffraction, and color spectrophotometry, all of which are outlined in general terms in the following section.

### Sediment Classification

Sediments collected on Leg 181 are classified using the scheme presented by Mazzullo et al. (1988). This classification method is descriptive as opposed to genetic and is based predominantly on texture and composition. However, as with other ODP legs (e.g., Leg 113; Shipboard Scientific Party, 1988), minor modifications have been made to the scheme (Table T1, also in [ASCII format](#)). According to Mazzullo et al.'s (1988) plan, cores from Leg 181 are primarily granular and pelagic sediments that incorporate varying proportions of siliciclastic and volcanoclastic components (Fig. F3):

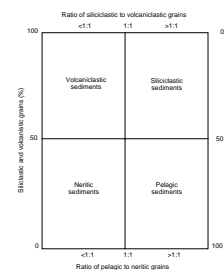
1. Pelagic biogenic components are most commonly the remains of foraminifers, nannofossils, diatoms and radiolarians, often accompanied by subordinate sponge spicules and silicoflagellates.
2. Siliciclastic components are rock fragments and minerals from metamorphic, sedimentary, and igneous sources.
3. Volcanoclastic components are minerals, glass, and rock fragments from volcanic sources. The classification reserves "volcanoclastic" for sediments deposited by volcanic processes. In the case of Leg 181, the dominant process is aerial dispersal and fallout from explosive rhyolitic eruptions.

---

T1. Outline of granular sediment classification scheme, [p. 58](#).

---

F3. Granular sediment class diagram, [p. 42](#).



The main lithologic classes are defined on the basis of the relative proportions of the aforementioned components. Therefore, pelagic sediments are those containing >50% biogenic planktonic grains, and siliciclastic sediments have >50% terrigenous grains. This contrasts with Mazzullo et al. (1988) who use a 60% cut-off value for the main classes, with components in the 40%–60% range being ascribed to a “mixed” class. A 50% cut-off eliminates the somewhat nonspecific “mixed” category.

### Nomenclature

Granular sediment has (1) a principal name that defines its class and (2) major and minor modifiers that capture the texture, composition, fabric, and other features of the granular components (Table T1). Pelagic sediments have principal names relating to the composition and degree of compaction. Thus, (1) ooze = unconsolidated calcareous and/or siliceous deposits; (2) chalk = firm pelagic sediment mainly composed of calcareous biogenic components; (3) limestone = hard pelagic sediment composed of calcareous biogenic components; (4) radiolarite, diatomite = firm pelagic sediment with a dominance of radiolarians or diatoms.

Siliciclastic sediments have principal names based on texture and are derived as follows:

1. The Udden-Wentworth scale (Wentworth, 1922) provides the range of grain sizes and the names of the textural groups (gravel, sand, silt, and clay) and subgroups (e.g., fine sand, coarse silt).
2. Where two or more textural groups are present, names are assigned in order of increasing abundance and in accordance with the scheme presented in Figure F4 (e.g., fine sandy silt is mainly silt with a subordinate fine sand component). In the case of sediments containing unspecified amounts of silt and clay but not strongly dominated by either, the term “mud” is used (its graphic symbol is that for “silty clay”), though where possible use of this term has been avoided.

Lithified sediments have the suffix “-stone” added to the textural group/subgroup term. Again, where silt and clay concentrations are unspecified, “mudstone” is used and if fissile, “shale.”

Volcaniclastic sediments are described as “tephra” where deposits are unconsolidated and grains are <2 mm diameter. Consolidated deposits are termed “tuff.”

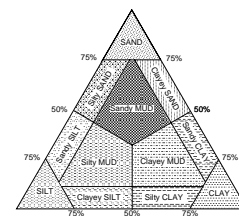
### Modifiers

Major (>25%) and minor (~10%–25%) modifiers describe the composition and textures of the sediment in greater detail. Components with concentrations of <10% are not named unless they are of special significance to the interpretation. Major modifiers can also be used to describe color, grain fabric, and shape. The principal name is preceded by the major modifier and then the minor modifier, which is accompanied by the term “-bearing” (e.g., tephra-bearing).

Examples:

A soft, fine-grained sediment with 60% foraminifers and 20% radiolarians (a radiolarian-bearing foraminifer ooze);

F4. Siliciclastic sediment ternary diagram, p. 43.





- A firm, fine-grained sediment with 50% nannofossils, 30% foraminifers, and 15% tephra (a tephra-bearing, foraminifer nannofossil chalk); and
- A soft sediment with 60% fine quartz sand with 15% foraminifers and 10% mica (a mica- and foraminifer-bearing fine quartz sand).

### Core Description Techniques

Cores are designated using leg, site, hole, core number, and core type (See “Introduction,” p. 1) and the cored interval (mbsf and meters composite depth [mcd]; see “Composite Depths,” p. 19).

### Sediment Barrel Sheets

The visual description of each core was summarized using core description sheets (“barrel sheets”; Fig. F5). Barrel sheets were generated using AppleCORE (v. 0.7.5g) and are presented with whole-core photographs (see the “Core Descriptions” contents list). The lithology of the recovered material is represented on barrel sheets by a column titled “Graphic Lithology.” In addition, a wide variety of features that characterize the sediment is indicated in the columns to the right of the graphic log. These features are briefly described below. The legend of symbols used in the barrel sheets is shown in Figure F6. Symbols are placed as close as possible to their proper stratigraphic position although they remain schematic.

### Descriptive Lithology Text

The lithologic text description consists of three parts: (1) a heading that lists all the major sediment lithologies observed in the core, (2) a general description of major and minor lithologies, and (3) a general description of the core including the location and type of any significant features in the core. The terminology for the thickness of sedimentary beds and laminae follows McKee and Weir (1953), who use the following categories: very thick bedded (>100 cm), thick bedded (30–100 cm), medium bedded (10–30 cm), thin bedded (3–10 cm), thickly laminated (0.3–3 cm), and thinly laminated (<0.3 cm). Included in this text is any information regarding sediment disturbance produced by natural processes or coring/drilling procedures.

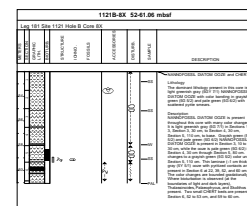
### Sedimentary Disturbance (Drilling and Natural)

Any deformation and disturbance of the recovered sediment interpreted as resulting from the coring process is listed in the “Drilling Disturbance” column. The absence of drilling disturbance is indicated by a blank column. The degree of drilling “disturbance” is described for soft and firm sediments using the following categories:

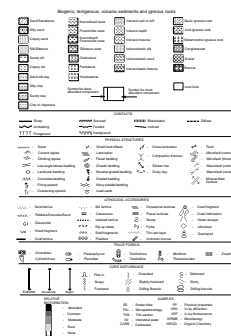
- Slightly = bedding contacts were slightly bent;
- Moderately = bedding contacts were extremely bent;
- Highly = bedding completely disturbed, possibly showing symmetrical diapir-like or flow structures parallel to the liner walls; and
- Soupy = water saturated with no clear bedding.

For indurated sediments the degree of “fracturing” was described using the following categories:

F5. Leg 181 “barrel sheet” example, p. 44.



F6. Core description graphic textures and symbols, p. 45.



Slightly = core pieces were in place and contained little or no drilling slurry or breccia;

Moderately = core pieces were either in place or partly displaced, but original orientation was preserved or recognizable;

Highly = pieces were from the cored interval and most probably in the correct stratigraphic sequence but their original orientation was not determinable; and

Drilling breccia = core pieces have lost their original orientation and stratigraphic position and may have been mixed with drilling slurry.

### **Induration**

Standard ODP nomenclature was used (Mazzullo et al., 1988).

### **Ichnofossils (Trace Fossils)**

Ichnologic analysis included both an evaluation of the extent of bioturbation and, where possible, the identification of ichnofossil types.

The degree of bioturbation was semiquantitatively assessed using a slightly modified version of the Droser and Bottjer (1991) ichnofabric index (e.g., barren or no bioturbation, rare, moderate, common, and abundant; see Fig. F6). These indices are illustrated using grayscale shading in the “Relative Bioturbation” column of the barrel sheets.

Identification of ichnofossil types was restricted to intervals where biogenic structures were discrete (e.g., where burrows exhibited sharp walls or had fills that contrasted well with the surrounding sediments in terms of texture, composition, or color). Discrete biogenic structures (burrows, burrow systems, borings, and so on) were identified on the basis of their morphology as observed on the core surface. Identifiable biogenic structures are illustrated in the “Ichnofossils” column of the barrel sheets, using symbols depicted in Figure F6.

### **Smear Slides**

Visual description of the sediment was complemented by data from smear slides. Tables summarizing these data may be found in the “**Core Descriptions**” contents list. These tables include information about the sample location together with the estimated abundances of the sand, silt, and clay fractions and the major biogenic components. An indication is also provided as to whether the sample represents a dominant or a minor lithology in the core.

Identification of finer grained mineral particles is difficult using only a binocular microscope, and the quantity of sand-sized particles tends to be underestimated in smear slides because they cannot be incorporated evenly into the smear. Therefore, it is stressed that smear-slide data provide only estimates of the relative abundances of detrital constituents. The mineralogy of some smear-slide components was validated by X-ray diffraction.

### **Samples**

The positions of samples taken from each core for analysis are indicated by letters in the “Sample” column of the barrel sheets as follows: SS (smear slide), PAL (micropaleontology), IW (interstitial water), and XRD (X-ray diffraction).



## Summary Lithologic Columns

Graphic summaries of the lithology from each Leg 181 site are presented for each site chapter and are derived from information given on the barrel sheets. Components with concentrations of <10% are omitted from the Summary Columns as are beds and layers of <20 cm thick. Thus, the lithology columns only show the major lithologic units and subunits. Additional columns outlining 550-nm light reflectance, natural gamma ray, magnetic susceptibility, and calcium carbonate are also included where available. Reflectance and susceptibility, in particular, provide a high-resolution record of downcore change. Stratigraphic control is provided by biostratigraphic zones derived from foraminifers, nannofossils, radiolarians, and diatoms with additional control from magnetic polarity data.

## Color and Spectrophotometry

Included in the core description is a qualitative impression of sediment color estimated by the sedimentologists using the standard Munsell color chart. In addition, the reflectance of visible light from each core was determined using a Minolta Spectrophotometer CM-2002, mounted on the split-core analysis track (SCAT). This instrument determines the reflectance at 31 separate 10-nm-wide spectral bands from 400 to 700 nm, covering the visible spectrum. Measurements were taken as soon as possible after the cores were split. Strips of very thin, transparent plastic film were used to cover the cores to prevent fouling the spectrophotometer lens, which was lowered to almost touch the core for measurement (except at Site 1119). Routine measurements were made at 2-cm intervals down each core section, but spacings were sometimes modified according to void space and sedimentary layering.

Before obtaining measurements from each core, the spectrophotometer was calibrated by attaching a white calibration cap covered with film (Balsam et al., 1997). Spectrophotometric measurements were then recorded using the program Spectrolog (v. 3.0). Additional detailed information about measurement and interpretation of spectral data with the Minolta spectrophotometer can be found in Schneider et al. (1995) and Balsam et al. (1997).

## X-Ray Diffraction

In selected core samples, the relative abundances of the main silicate and carbonate minerals were determined using a Philips model PW-1729 X-ray diffractometer with Cu-K<sub>α</sub> radiation (Ni filter) and automatic divergence slit. Bulk-sediment samples were freeze-dried, ground, and mounted with a random orientation in an aluminum sample holder. The instrument conditions were 40 kV, 35 mA, goniometer scan from 2° to 70° (2θ) for bulk samples, step size 0.01% (2θ), scan speed at 1.2°/min, count time 0.5 s. Peak intensities were converted to values appropriate for a fixed slit width.

Graphic evaluation of the diffractograms was performed using the interactive MacDiff (v. 3.3 PPC) software. The main minerals were identified according to peak position and the relative abundances established on the basis of both peak intensities and integrated peak areas. The ratios and relative abundances reported in this volume should be considered only as providing a general characterization of the sediments and not as a detailed quantitative measure.

## BIOSTRATIGRAPHY

### Introduction

One aim of ODP Leg 181 was to develop a detailed southern mid- to high-latitude biochronology and magnetostratigraphy for the Oligocene through Pleistocene, for the ocean between the Subantarctic Front (SAF) and just north of the Subtropical Convergence (STC), immediately east of New Zealand. A key objective was to monitor global climate fluctuations as reflected in the waxing and waning of the northeast-flowing Deep Western Boundary Current (DWBC), which is a key driving force in global circulation. During Leg 181, nannofossils, radiolarians, diatoms, and foraminifers were studied at seven sites, which were triple, double, or single cored with the APC and XCB systems. The presence of silicoflagellates, chrysophycean cysts, opal phytoliths, sponge spicules, bolboformids, ebridians, and calcareous dinoflagellate cysts were routinely monitored. With most of the sites cored above the carbonate compensation depth, excellent suites of both calcareous and siliceous microfossil assemblages were recovered.

The only existing Neogene site in this region, DSDP Leg 90, Site 594, just south of the STC on the Chatham Rise, provided a low-resolution late Neogene biozonation (Martini and Jenkins, 1986), with provisional ties to the detailed regional chronostratigraphy developed for New Zealand (e.g., Hornibrook and Jenkins, 1994). The ODP Leg 181 sites, strategically chosen on the Hikurangi Plateau, Chatham Rise, and Campbell Plateau to detail both the Neogene global climate change and the growth of the giant drifts redistributed by the DWBC, will greatly expand such calibration. Because Leg 181 analyses simultaneously develop magnetostratigraphy, isotope stratigraphy, and biostratigraphy, they will provide definitive links to the standard time scale for the subantarctic and subtropical New Zealand zonal schemes of nannofossil and planktonic foraminiferal datums, that is, ties to the Cenozoic New Zealand stages (e.g., Edwards et al., 1988; Hornibrook et al., 1989; Hornibrook, 1990; Scott et al., 1990; Morgans et al., 1996; Naish et al., 1998). Northern sites contain numerous volcanic tephra erupted from New Zealand and distributed eastward in the prevailing westerly winds, which will allow further calibration to standard time scales (e.g., Shane et al., 1995), as will the cyclostratigraphic record from the spliced triple- and double-cored APC holes.

ODP Legs 113, 114, 117, 119, 120, and 177 laid the foundation for a circumpolar southern high-latitude biostratigraphy and chronostratigraphy. Cenozoic sequences recovered during these legs provided biostratigraphic zonations based on calcareous and siliceous microfossils and on key species ranges that could be tied directly to the geomagnetic time scale (e.g., Gersonde et al., 1990; Thomas et al., 1990; Barron et al., 1991; Harwood et al., 1992; Wei, 1992; Wei et al., 1993). Leg 181 drilling of a latitudinal transect across the STC will allow further improvement and refinement of these biostratigraphic schemes, and the intercalibration of high- and mid-latitude zonations and species ranges in key microfossil groups for biochronology. Improved dating of Neogene biostratigraphic ranges can be accomplished by correlation with Leg 181 magnetostratigraphy, by using orbitally tuned signals from stable isotope analysis, or using other data sets with high temporal resolution, such as color reflectance, magnetic susceptibility, and biota abundance records. In addition, data from the transect of sites will lead to a understanding of the evolutionary processes (patterns, modes, and

timing of speciation and diversification) of taxa, of the migration of taxa across the STC, and of the origin and development of the Southern Hemisphere bioprovinces.

### Time Scale

Ages were assigned primarily based upon core-catcher samples. Samples from within the cores were examined when a more refined age determination was necessary. Correlations to standard chronostratigraphic frameworks will be improved by integration of data from post-cruise magnetobiostratigraphic studies and oxygen isotope stratigraphy.

Ages for calcareous nannofossil, foraminiferal, diatom, and radiolarian events in the Paleogene and Miocene are according to the Geomagnetic Polarity Time Scale (GPTS) of Cande and Kent (1995) in Berggren et al. (1995a, 1995b), with minor modifications for the Pliocene and Pleistocene using the astrochronology of Lourens et al. (1996). Although refined astrochronologies do exist for Miocene and even older sections, none is yet firmly calibrated to either standard biochronology or standard magnetostratigraphy (F. Hilgen, pers. comm., 1998), which led us to prefer the Oligocene–Miocene GPTS for calibration of the microfossil datums. For the Pliocene and Pleistocene, the GPTS and the astrochronologies of Mediterranean sapropels and the oceanic stable isotope records are concordant. A compilation of microfossil events ages updated from the literature for four major microfossil groups was made (Tables T2, T3, T4, T5, all also in ASCII format; Figs. F7, F8). These tables were prepared as an aid to quickly look up the definition of biostratigraphic events and chronostratigraphic boundaries and their links to the time scale.

The Oligocene/Miocene boundary is defined at the 35-m level of the Rigorosa Formation in the Carrosio-Lemme section, northwest Italy, corresponding to the base of polarity chron C6Cn.2n and the first appearance of *Globorotalia kugleri*. The age estimate in GPTS is 23.8 Ma. This level correlates to middle Waitakian in New Zealand (Morgans et al., 1996; Fig. F7).

The Miocene/Pliocene boundary is defined at the onset of marine conditions in the Mediterranean at the base of the Zanclean, correlated to polarity Chron C3r in the GPTS and 5.32 Ma in the astrochronology of Hilgen (1991a, 1991b). Biostratigraphically, the boundary is bracketed by the highest occurrence of *Discoaster quinqueramus* and *Triquetrorhabdulus rugosus* and the lowest occurrence of *Ceratolithus acutus* (see review in Berggren, 1995b). In New Zealand, the boundary interval occurs within the upper Kapitean stage (Morgans et al., 1996; Fig. F7), immediately below the Opoitian stage.

The Pliocene/Pleistocene boundary, defined in the Vrica Section (Calabria, Italy), is located near the top of magnetic polarity Chron C2n, with an estimated age of 1.81 Ma (Lourens et al., 1996). Biostratigraphically, the boundary may be approximated with the lowest occurrence of medium-sized *Gephyrocapsa* spp. (bmG event) (Raffi et al., 1993) and the highest occurrence of *Discoaster brouweri* and *D. triradiatus* (Berggren et al., 1995a). In New Zealand the boundary occurs within the Nukumaruan stage (Fig. F7).

### New Zealand Stages

In the previous section, mention was made of the need to correlate the Leg 181 biostratigraphy and chronostratigraphy both to standard

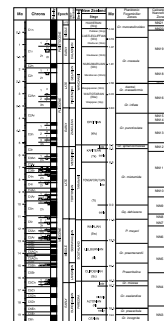
T2. Calcareous nannofossil datums used during Leg 181, p. 59.

T3. Foraminiferal and bolboformid datums used during Leg 181, p. 60.

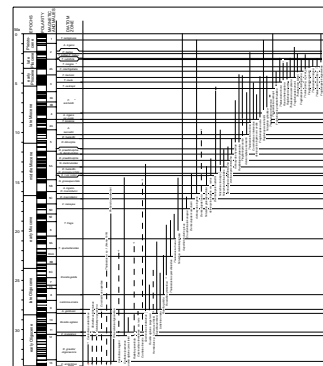
T4. Age assignments of biostratigraphic diatom zones used during Leg 181, p. 63.

T5. Ages of biostratigraphically useful radiolarian datums in the New Zealand region, p. 64.

F7. Combined biostratigraphic zonal schemes, p. 46.



F8. Diatom zonation and stratigraphic ranges of diatom species, p. 49.





diachroneity (Wei et al., 1993). It is conceivable that the distribution, evolution, and extinction of calcareous nannofossils in the studied areas have been modulated by the development of oceanic front systems, and, therefore, many of these datum levels could be time transgressive. Detailed magnetostratigraphies across the studied area will assist with estimates of their numerical ages of bioevents in various holes. The depth of each datum level was recorded at the midpoint between observed samples.

## **Methods**

Standard smear slides were made for all samples using Norland Optical Adhesive as a mounting medium. Calcareous nannofossils were examined by means of a light-polarized microscope at 1000× magnification. Unless otherwise noted, we followed taxonomic concepts summarized in Perch-Nielsen (1985).

Regarding state of preservation, we consider that etching and overgrowth are the most important features. In order to establish a ranking of preservation we have followed the code systems prescribed in the JANUS database system:

- VG = very good (no evidence of dissolution and/or secondary overgrowth of calcite; diagnostic characters perfectly preserved);
- G = good (little or no evidence of dissolution and/or secondary overgrowth of calcite; diagnostic characters fully preserved);
- M = moderate (dissolution and/or secondary overgrowth: partially altered primary morphological characteristics: however, nearly all specimens can be identified at the species level); and
- P = poor (severe dissolution, fragmentation, and/or secondary overgrowth with primary features largely destroyed; many specimens cannot be identified at the species level and/or generic level).

Five categories of relative abundance of individual taxa were applied:

- D = dominant (>50% of the total assemblage = 100 per field of view [fov]);
- A = abundant (10%–50% of the total assemblage = 10–100/fov);
- C = common (1%–10% of the total assemblage = 1–10/fov);
- F = few (0.1%–1% of the total assemblage = 1/1–10 fov); and
- R = rare (<0.1% of the total assemblage = <1/10 fov).

For Site 1121, an additional category was added:

- T = trace (present when more than 10 fields of view were examined).

Total abundance of calcareous nannofossils for each sample was estimated as follows:

- VA (very abundant) = >100 nannofossils/fov;
- A (abundant) = 10–100 nannofossils/fov;
- C (common) = 1–10 nannofossils/fov;
- R (rare) = <1 nannofossil/10 fov; and
- B (barren).

## Foraminifers and Bolboformids

Several planktonic foraminiferal zonal schemes have been developed for the mid- and high-latitudes of the Southern Hemisphere (e.g., Jenkins and Srinivasan, 1986; Berggren, 1992a; Berggren et al., 1995a). Based on previous work (Brunner, 1991; Pujol and Bourrouilh, 1991), the late Neogene subantarctic zonation scheme by Jenkins and Srinivasan (1986), as modified by Scott et al. (1990) and Hornibrook and Jenkins (1994) (Fig. F7), was deemed best to divide the sequences recovered during Leg 181. However, because of the absence or low abundance of several marker species, this zonation scheme was not fully applicable to the foraminiferal assemblages recovered during Leg 181, and both planktonic and local New Zealand benthic datums (Table T3) were used extensively to assist with age assignments.

The generic and species classification used for Neogene planktonic foraminifers mainly follows Kennett and Srinivasan (1983) and Scott et al. (1990, 1995). The latter deals exclusively with genus *Globorotalia*. Species identification of Paleogene and early Neogene planktonic foraminifers are based on Hornibrook et al. (1989), Stott and Kennett (1990), and Berggren (1992b).

Benthic foraminifers provide limited biostratigraphic age control as currently applied to Leg 181 samples. Individual benthic foraminiferal datums recognized are mostly regional datums established for on-land and nearshore New Zealand (e.g., Hornibrook et al., 1989) and are discussed for each site. Benthic foraminiferal taxonomy follows van Morkhoven et al. (1986), Hornibrook et al. (1989), Thomas (1990), and Mackensen and Spiegler (1992).

Bolboformid taxonomy is based on Qvale and Spiegler (1989), Spiegler (1991, in press), Mackensen and Spiegler (1992), Grützmacher (1993), and Spezzaferri and Spiegler (1998). It is questionable if the local stratigraphies derived from the bolboformid zonations in the North Atlantic and Indian Oceans are applicable to the Leg 181 region, hence the biostratigraphy derived from this group has been used with caution.

## Methods

To obtain planktonic and benthic foraminifers and bolboformids from core-catcher samples, a 20–50 cm<sup>3</sup> sample was soaked in tap water, disaggregated, and washed over a 63- $\mu$ m sieve. At deeper levels in Site 1123, the low abundance of foraminifers and high degree of chalk cementation required larger samples to be broken down using a combination of water, hydrogen peroxide, and ultrasonic bath. The sieves were immersed in a methylene blue solution between successive samples in order to stain specimens left in the sieves from previous samples. All samples were dried under heat lamps.

Species abundances (as percentages of the total planktonic foraminiferal, benthic foraminiferal, or bolboformid assemblages) were defined as follows:

- D = dominant >30%;
- A = abundant 10%–30%;
- F = few/frequent 5%–10%;
- R = rare 1%–5%; and
- P = present <1%.



Preservation was categorized as

Good (G) = dissolution effects are rare,

Moderate (M) = dissolution damages, such as etched, partially broken tests are common, and fragments are frequent; and

Poor (P) = the degree of fragmentation is often high and the specimens present are often small, compact and encrusted.

The abundance of planktonic foraminifers, benthic foraminifers, and/or bolboformids as groups relative to the total residue were categorized as

Abundant (A) = >50%;

Common (C) = 25%–50%;

Few (F) = 10%–25%;

Rare (R) = <5% of the residue;

Trace (T) = used where only a few broken tests were recorded in a sample; and

Barren (B) = no specimens in samples.

## Diatoms

During Leg 181 the diatom zonation for the Neogene by Harwood and Maruyama (1992) was used with slight changes as proposed by Gersonde and Zielinski (Shipboard Scientific Party, 1999) in their study of ODP Leg 177 samples (Fig. F8). Gersonde and Zielinski replace the *Thalassiosira insigna*-*T. vulnifica* Zone of Harwood and Maruyama (1992) with the *Thalassiosira insigna* Zone, because the first occurrence of *Thalassiosira vulnifica* is probably diachronous. Instead, these authors use the total range of *T. insigna*. Also, these authors place the base of the *Fragilariopsis reinholdii* Zone, marked by the first occurrence (FO) of the nominate taxon, in polarity Chron C4 at around 8.1 Ma, an age that is close to the age of its FO in the Equatorial Pacific, as reported by Barron (1992). For the Oligocene, the diatom zonation for the high southern latitudes by Fenner (1984, 1985) and modified by Harwood and Maruyama (1992) is followed.

The ages of diatom datums (Table T4) follow Gersonde and Bárcena (1998) and Gersonde et al. (1998). The ages are based on the correlation of the stratigraphic ranges of the marker species to the GPTS of Berggren et al. (1995a, 1995b). This correlation to magnetostratigraphy, which started with work on piston cores (e.g., McCollum, 1975; Ciesielski, 1983) was refined as a result of Legs 113, 114, 119, and 120 (e.g., Gersonde and Burckle, 1990; Fenner, 1991; Baldauf and Barron, 1991; Harwood and Maruyama, 1992; Gersonde and Bárcena, 1998). Because of the occurrence of warm and temperate species in the northernmost sites of Leg 181, additional stratigraphic ranges have been added following the compilation of Barron (1992). The ages for the diatom datums given for the Oligocene in Table T4 follow Harwood and Maruyama (1992) and the Shipboard Scientific Party (1999) for Leg 177.

The diatom assemblages observed in sediments recovered from Leg 181 also provide environmental information, which helps in reconstructing (1) the thermal isolation of the Southern Ocean, (2) the initiation of Antarctic Bottom Water Currents, (3) changes in the late Quaternary surface-water temperatures, and (4) definition of water masses and positions of oceanic fronts.

The presence of freshwater and benthic marine diatoms at Leg 181 sites indicates input from New Zealand and its coastal regions, but may also be in part aeolian input from Australia through the prevailing strong westerly winds. The common presence of reworked diatoms in the sites from the Campbell Plateau allowed the recognition of phases of intensified currents. Displaced subantarctic diatoms from the Bounty Trough area characterize the Chatham Drift sediments.

## **Methods**

Depending on overall diatom abundance, two types of slides were prepared for diatom analysis. For intervals rich in biogenic silica, smear slides were prepared from a small amount of raw material from a core catcher or from additional core material when required. At most sites the sediments were too rich in calcium carbonate and/or terrigenous detritus to allow this method to be used. Hence, for most samples it was necessary to boil the sediment in 10% HCl to remove calcium carbonate. The carbonate-free residue was repeatedly washed with distilled water to remove the acid. In each case, aliquots of raw and cleaned sample were mounted on microslides, covered with 18-mm-diameter cover glasses using Mountex mounting medium. All slides were scanned with a Zeiss microscope at a magnification of 400× for stratigraphic markers and paleoenvironmentally sensitive taxa. Species identification was confirmed when necessary at 1000×. For documentation of poorly known or undescribed taxa, photomicrographs were taken using a video-print system at 1500× final magnification.

Overall diatom abundance in the HCl-insoluble residue, as well as species abundance within the diatom assemblages, were estimated based on smear-slide evaluation at 400×, using the following categories:

- D (dominant) = >50% of assemblage;
- A (abundant) = 10%–50%;
- C (common) = 5%–10%;
- F (few) = 1%–5%;
- R (rare) = 0.1%–1%;
- T (trace) = <0.1%; and
- B (barren) = no diatoms in sample.

Preservation of diatoms was differentiated as follows:

- G (good) = thinly silicified forms present, few fragments of valves, assemblages are diverse;
- M (moderate) = thinly silicified forms missing, valve fragments present, but no strongly etched valve relicts observed; and
- P (poor) = only few species with thickly silicified valves present, fragmentation and etching of valves is evident.

At several sites, preservation and abundance estimates were plotted vs. depth to visualize the distribution of diatom abundance and preservation.

## **Radiolarians**

Neogene radiolarian biostratigraphy during Leg 181 in the Southwest Pacific was based largely on the southern mid- to high-latitude zona-

tions established by Caulet (1986, 1991), Abelmann (1992), and Lazarus (1992). Because the Leg 181 transect sites cover the SAF and STC, the Neogene radiolarian assemblages include low- to mid-latitude zonal markers, which prevented application of the Antarctic/subantarctic zonal scheme. Tentative age assignments, therefore, were based on the mid-latitude zonation of Foreman (1975) and Morley (1985) established in the North Pacific region. The Paleogene radiolarian zonation used in this study follows those by Takemura (1992) and Hollis (1997). Low-latitude radiolarian zonation and code numbers, which were tied to the GPTS of Berggren et al. (1995a, 1995b) by Sanfilippo and Nigrini (1998), were compiled for the purpose of correlation between mid- and high-latitude zonations. The ages of radiolarian datums follow Sugiyama (Shipboard Scientific Party, 1999) with some additions. Figure F10 and Table T5 show radiolarian zonations and datums used during Leg 181, respectively.

### Methods

To obtain radiolarians from core-catcher samples, about 10 cm<sup>3</sup> of sediment was disaggregated and boiled with 10% H<sub>2</sub>O<sub>2</sub>, 10% HCl, and about 1% Calgon solutions. Brief treatment of samples in an ultrasonic bath was followed by washing on a 63- $\mu$ m mesh sieve. The residue was moved into a beaker, and a strewn slide was made using a pipette. Canada Balsam was used as a mounting medium. Additional random-strewn slides will be prepared onshore to locate biostratigraphic events more accurately within cores.

Overall radiolarian abundance was determined based on strewn-slide evaluation at 100 $\times$ , using the following convention:

- A (abundant) = >100 specimens per slide traverse;
- C (common) = 50–100 specimens per slide traverse;
- F (few) = 10–50 specimens per slide traverse;
- R (rare) = <10 specimens per slide traverse;
- T (trace) = <1 specimen per slide traverse; and
- B (barren) = no radiolarians in sample.

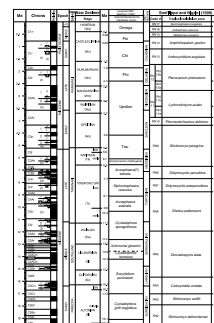
The abundance of individual species was recorded relative to the fraction of the total assemblage as follows:

- A (abundant) = >10% of the total assemblage;
- C (common) = 5%–10% of the total assemblage;
- F (few) = <5% of the total assemblage;
- R (rare) = a few or more specimens per slide;
- T (trace) = present in slide; and
- B (barren) = absent.

Preservation was recorded as follows:

- E (excellent) = nearly pristine, complete skeleton, lacking any indication of dissolution, recrystallization, or breakage;
- G (good) = majority of specimens complete, with minor dissolution, recrystallization, and/or breakage;
- M (moderate) = minor but common dissolution, with a small amount of recrystallization or breakage of specimens; and

F10. Cenozoic radiolarian biostratigraphic zonation schemes, p. 51.



P (poor) = strong dissolution, recrystallization, or breakage, many specimens unidentifiable.

## PALEOMAGNETISM

Paleomagnetic studies conducted on the *JOIDES Resolution* during Leg 181 consisted of remanent magnetization measurements of archive-half sections before and after alternating field (AF) demagnetization, magnetic remanence measurements on discrete samples collected from the working half of core sections, magnetic susceptibility measurements on whole-core sections, and a limited set of rock-magnetic measurements on discrete samples. Discrete samples were collected from working halves in standard 8-cm<sup>3</sup> plastic cubes with the arrow on the bottom of the sampling cube pointing up-core. The sampling frequency was generally two samples per core at one hole per site. Intervals with drilling-related core deformation were avoided.

### Instruments and Measurement Procedure

Measurements of remanent magnetization were carried out using an automated pass-through cryogenic DC-SQUID (direct current superconducting quantum interference device) magnetometer (2-G Enterprises Model 760-R) with an in-line alternating field (AF) demagnetizer (2-G Enterprises Model 2G600), capable of producing peak fields of 80 mT with a 200-Hz frequency. The background noise level of the magnetometer on-board environment is  $\sim 3 \times 10^{-10}$  Am<sup>2</sup>. The large volume of core material within the sensing region of the magnetometer, which is on the order of 100 cm<sup>3</sup>, permits the accurate measurements of cores with remanent intensities as weak as  $\sim 10^{-5}$  A/m.

The standard ODP magnetic coordinate system was used (+X: vertical upward from the split surface of archive halves, +Y: left along split surface when looking upcore, +Z: downcore).

Natural remanent magnetization (NRM) was routinely measured for all archive-half sections at 5- to 10-cm intervals. Measurements at core and section ends and within intervals of drilling-related core deformation were edited during data processing. AF demagnetizations were applied at 10 and 20 mT when time permitted; otherwise, cores were only demagnetized at a single AF step at 20 mT. All discrete sample measurements were also made on the pass-through magnetometer using a sample boat that held seven discrete cube samples at 20-cm intervals.

Discrete samples were demagnetized by AF using the in-line demagnetizer installed on the pass-through cryogenic magnetometer at 5-mT steps to 30 mT and then at 10-mT steps to 60 or 80 mT, depending on remaining sample intensity. An Analytical Services Company model IM-10 impulse magnetizer, which can apply pulsed fields from 20 to 1200 mT, was used for studies of the acquisition of stepwise isothermal remanent magnetization (IRM), saturation IRM (SIRM), and backfield SIRM of selected discrete samples. When time permitted, the SIRM of discrete samples was thermally demagnetized using a Schonstedt Model TSD-1 Thermal Specimen Demagnetizer at 40°C or 50°C steps to 640°C. However, heating was stopped if sample intensity became too weak or if routine magnetic susceptibility indicated alteration of the magnetic mineralogy from heating. Spurious fields inside the oven do not exceed 100 nT and are generally <5 nT inside the cooling chamber. Tempera-

ture gradients over the central 30.5-cm length of the oven are  $\sim 10^{\circ}\text{C}$ , with an absolute temperature accuracy within  $20^{\circ}\text{C}$  of the set value.

Magnetic susceptibility was measured for each whole-core section as part of the MST analysis (see “Physical Properties,” p. 24). The MST susceptibility meter (a Bartington MS2 meter containing an MS2C sensor with a coil diameter of 88 mm and an inducing-field frequency of 0.565 kHz) was set on SI units and the values were stored in the JANUS database in raw meter units. To convert to true SI volume susceptibilities, these values should be multiplied by  $10^{-5}$  and then multiplied by a correction factor to take into account the volume of material that passed through the susceptibility coils. The correction factor for a standard ODP core is about 0.66 ( $=1/1.5$ ). This correction was applied for all figures illustrating magnetic susceptibilities in the “Paleomagnetism” sections in this report. The end effect of each section was not corrected.

### Core Orientation

Core orientation of the advanced hydraulic piston cores was achieved with a Tensor tool mounted on the core barrel. The Tensor tool consists of a three-component fluxgate magnetometer and a three-component accelerometer rigidly attached to the core barrel. The information from both sets of sensors allows the azimuth and dip of the hole to be measured as well as the azimuth of the double-line orientation mark on the core liner. Orientation is not usually attempted for the top three cores (about 30 mbsf) until the bottom-hole assembly is sufficiently stabilized in the sediment. Core orientation by the Tensor tool was relative to magnetic north.

### Magnetostratigraphy

Where AF demagnetization successfully isolated the primary component of remanent magnetization, paleomagnetic inclinations were used to assign a magnetic polarity to the stratigraphic column. Interpretations of the magnetic polarity stratigraphy, with constraints from the biostratigraphic data, are presented in the site chapters. The magnetic polarity time scale of Cande and Kent (1995) and the time scale of Berggren et al. (1995b) were used.

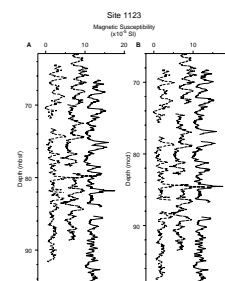
We encountered several types of secondary magnetization acquired during coring, which sometimes hampered magnetostratigraphic interpretation. Details of the magnetic overprints are presented in the site chapters.

## COMPOSITE DEPTHS

### Composite Section Construction

The purpose of composite section construction is to reconstruct a complete sedimentary sequence at each site, an objective crucial to the paleoceanographic objectives of this leg and to orbital time scale development. To recover complete sequences, two or three holes were drilled at each site, with deliberate hole-to-hole offsets in depth. This drilling strategy increases the likelihood that intervals missing from one APC hole as a result of gaps between successive cores are recovered in an adjacent hole. The need for drilling multiple holes and for composite section development is illustrated in Figure F11. Previous ODP legs with

F11. Magnetic susceptibility records (mbsf) and composite section example, p. 54.



paleoceanographic objectives have successfully used this strategy to recover complete sedimentary sequences. On Leg 181, we used methods similar to those employed on Legs 138 (Hagelberg et al., 1992), 154 (Curry, Shackleton, Richter, et al., 1995), 162 (Jansen, Raymo, Blum, et al., 1996), 167 (Lyle, Koizumi, Richter, et al., 1997), and 177 (Gersonde, Hodell, Blum, et al., 1999).

High-resolution (2- to 16-cm intervals), nondestructive measurements of gamma-ray attenuation porosity evaluator (GRAPE), bulk density, magnetic susceptibility, natural gamma-ray emissions, and *P*-wave velocity were made by the MST on each whole-round core section after the cores had equilibrated to room temperature (~2–3 hr after retrieval). After splitting, reflectance spectra in the visible range (400–700 nm) were measured on each archive-core half using the MST. For composite section development, we used magnetic susceptibility, natural gamma-ray emissions, and spectral reflectance at 550 nm as the primary data sets for hole-to-hole correlations. Voids, identified by anomalously low GRAPE density values, and disturbed intervals were omitted from the composite sections. Use of more than one data type provided a cross-check on correlations between holes and was helpful in intervals where one data set produced ambiguous correlations. Biostratigraphic data from multiple holes provided an additional check on correlations among holes.

To construct composite sections, we used an interactive software package (“Splicer” v. 2.0) developed specifically for this purpose by the Borehole Research Group at Lamont-Doherty Earth Observatory. This program is based on correlation software developed for Leg 138 (Hagelberg et al., 1992). The software allows the operator to align corresponding features in data from adjacent holes, based on visual graphics and the correlation coefficient for a user-defined depth interval (typically 2 m long). Features were aligned by linearly adjusting the ODP coring depths (mbsf), measured from the length of drill string advanced, on a core-by-core basis. For each core in each hole, we used a single tie to one other core from a different hole; no depth adjustments (stretching or squeezing) were made within a core. The resulting adjusted depth scale is the meters composite depth scale (mcd) and the section produced by the aligned cores is termed a composite depth section (Fig. **F11B**).

Offsets between the mbsf and mcd scales arise both from random uncertainty in mbsf depths resulting from ship motion and heave, and from differential distortion of cores during the coring and retrieval process, for example, core expansion caused by rebound. The composite section is thus longer than the in situ section, typically by about 10%. Because the depth of each core is adjusted by a single constant, and distortion of any specific interval is different in different holes, this procedure does not align all features between holes. Depth adjustments/tie points were chosen to both optimize the correlation among multiple holes and to facilitate construction of a single representative “spliced record” from aligned cores. Where an appropriate depth adjustment for a single core was uncertain, or overlapping data from other holes were unavailable, the depth adjustment applied was the cumulative offset from the overlying aligned cores.

A table in each site chapter summarizes core offsets for conversion from the mbsf to the mcd scales. For each section of each core, the depth adjustment required to convert from the mbsf depth scale to the mcd scale is given. The last two columns in each table give the cumulative depth offset added to the ODP curatorial sub-bottom depth (mbsf)



and the composite depth (in mcd), respectively. The mcd depth for any sample equals the mbsf depth plus the offset.

### Splice Construction

After composite section construction, we assembled a single spliced record representative of the complete recovered sedimentary sequence at each site. Conceptually, building the “splice” consists of patching the intervals missing in a single hole with data from adjacent holes. The advantage of the spliced record is that it provides a single representative record of any lithologic parameter (e.g., magnetic susceptibility, spectral reflectance, or GRAPE), and it is ideally suited to guide sampling plans for high-resolution paleoceanographic studies. The output of this procedure is called the “spliced record.”

Splice tie points ideally were made between adjacent holes at the level of visually obvious features that are strongly correlated between holes and where the parameter measured differs by less than 10% between holes. Because there is some stretching and/or compression within cores, the precise length of the splice depends on which intervals of core were selected to build it. Each splice was constructed by beginning at the mud line at the top of the composite section and working downwards. Intervals were chosen for the splice so that section continuity was maintained while disturbed intervals were avoided. An example is given in Figure F12. Splice tie points always connect features with exactly the same composite depths. As a result, the final alignment of the adjacent holes may be slightly different (Fig. F12) from the one giving the best overall visual or quantitative hole-to-hole correlation. Further adjustments to the composite depth section by expanding and compressing the depth scale within individual core intervals is required to align all features exactly (e.g., Hagelberg et al., 1995). Tables that give the tie points for construction of the spliced records are presented in each site chapter.

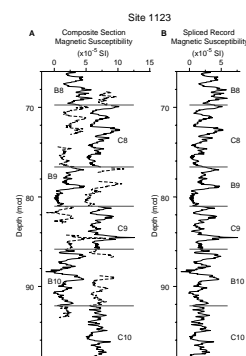
## INORGANIC GEOCHEMISTRY

### Interstitial Water Sampling and Chemistry

Shipboard interstitial water analyses for Leg 181 were performed on 5–10-cm whole-round sediment sections, which were cut and capped immediately after the core arrived on deck. Specific details of the sampling resolution are described in the individual site chapters. Before squeezing, samples were removed from the core liner and the outside surface of each whole-round section was carefully scraped off with a spatula to minimize potential contamination. Whole rounds were placed into a titanium and stainless steel squeezing device and squeezed at ambient temperature by applying pressure up to 40,000 lb ( $\sim 4150$  psi =  $2.918 \times 10^6$  kg/m<sup>2</sup>) with a hydraulic press (Manheim and Sayles, 1974).

Interstitial water was extruded through a prewashed Whatman no. 1 filter, fitted above a titanium screen. All interstitial water samples were filtered through 0.45- $\mu$ m Gelman polysulfone disposable filters and collected into acid-washed (10% HCl) 50-mL plastic syringes. The interstitial water samples were subsequently refiltered through 0.45- $\mu$ m Gelman polysulfone disposable filters. The samples were stored in plas-

F12. Magnetic susceptibility records and resulting spliced record, p. 55.



tic vials for shipboard analyses or archived in glass ampoules and/or heat-sealed in acid-washed plastic tubes for shore-based analyses.

Interstitial water analyses followed the procedures outlined by Gieskes et al. (1991). Interstitial water samples were routinely analyzed for salinity as total dissolved solids (g/kg) with a Goldberg optical hand-held refractometer made by Reichart. Alkalinity was measured by Gran titration with a Brinkmann pH electrode and a Metrohm autotitrator, and pH was measured on the NBS scale as part of the alkalinity titration. It should be noted that pH measurements obtained in this fashion are not always reliable given that the algorithm employed for pH measurement before the start of the alkalinity titration is adversely influenced by degassing. Dissolved chloride ( $\text{Cl}^-$ ) was determined by titration with  $\text{AgNO}_3$ . Dissolved  $\text{SiO}_2$  ( $\text{H}_4\text{SiO}_4$ ), ammonium ( $\text{NH}_4^+$ ), and phosphorous ( $\text{PO}_4^{3-}$ ) concentrations were determined by spectrophotometric methods with a Milton Roy Spectronic 301 spectrophotometer (Gieskes et al., 1991). As a result of the shortage of fresh phenol, the reproducibility of  $\text{NH}_4^+$  measurements decreased during the cruise. International Association of Physical Sciences Organizations (IAPSO) standard seawater was used for calibrating most techniques. The reproducibility of these analyses, determined by repeated measurements of standards, are alkalinity = <1.5%;  $\text{Cl}^-$  = <0.3%;  $\text{H}_4\text{SiO}_4$  = <3%; and  $\text{PO}_4^{3-}$ , and  $\text{NH}_4^+$  = ~3%.

Sodium ( $\text{Na}^+$ ), potassium ( $\text{K}^+$ ), magnesium ( $\text{Mg}^{2+}$ ), calcium ( $\text{Ca}^{2+}$ ), chloride ( $\text{Cl}^-$ ), and sulfate ( $\text{SO}_4^{2-}$ ) concentrations were measured by ion chromatography on 1/200 diluted aliquots in nanopure water using a Dionex DX-100. In general, the results obtained from this technique for some elements are less accurate than alternative methods, such as titration for  $\text{Cl}^-$  and charge balance calculations for  $\text{Na}^+$ . However, the relative trends are usually similar and can serve as a second check of results generated by the other methods. The precision of results measured by ion chromatography was generally within 3%–5%. The  $\text{Cl}^-$  and  $\text{Na}^+$  measurements by ion chromatography are not reported here.

Lithium ( $\text{Li}^+$ ) and strontium ( $\text{Sr}^{2+}$ ) concentrations were quantified using flame atomic emission (AES) and absorption (AAS) spectrometry, respectively, on a Varian SpectrAA-20. Tenfold dilutions of the interstitial water samples were used for lithium and five- to twentyfold dilutions were employed for strontium analyses. Air-acetylene ( $\text{Li}^+$ ) and nitrous oxide-acetylene ( $\text{Sr}^{2+}$ ) flames were used for these analyses. Standards for all flame AAS/AES techniques were matrix matched as closely as possible to the samples ( $\text{Li}^+$  and  $\text{Sr}^{2+}$ ). A more detailed description of analytical methods and standards used can be found in *ODP Technical Note 15* (Gieskes et al., 1991). Standard deviations ( $1\sigma$ ) were better than 2% for  $\text{Li}^+$ , and better than 3%–4% for  $\text{Sr}^{2+}$ . Sodium ( $\text{Na}^+$ ) was estimated by charge balance on the assumption that total cation charge equals total anion charge ( $\Sigma$  [cation charge] =  $\Sigma$  [anion charge]). The chemical data for interstitial water are reported in molar concentration units in each site report.

## ORGANIC GEOCHEMISTRY

The shipboard organic geochemistry program for Leg 181 included (1) real-time monitoring of volatile hydrocarbons as required by ODP safety regulations, (2) measurement of inorganic (carbonate) content of the sediments, (3) elemental analyses of total nitrogen, sulfur, and car-

bon, and (4) characterization of organic matter by Rock-Eval pyrolysis (Espitalié et al., 1986). All methods followed and instruments used during Leg 181 are described in detail by Emeis and Kvenvolden (1986), Kvenvolden and McDonald (1986), and in the “Explanatory Notes” chapter of Leg 156 (Shipboard Scientific Party, 1995).

### Volatile Hydrocarbons

For safety and pollution prevention, concentrations and distribution of light hydrocarbon gases, mainly methane ( $C_1$ ), ethane ( $C_2^+$ ), and propane ( $C_3$ ), were monitored for each core following the standard headspace sampling method described by Kvenvolden and McDonald (1986). A 5-cm<sup>3</sup> sediment sample was collected with a calibrated borer tool while the core was still on deck and placed in a 21.5-cm<sup>3</sup> glass serum vial. The sample was sealed with a septum and metal crimp cap. When consolidated or lithified samples were encountered, chips of material were placed in the vial and sealed. Before gas analyses, the vial was heated to 60°C for 30 min. A 5-cm<sup>3</sup> subsample of the headspace gas was then extracted from each vial using a standard glass syringe for gas chromatography (GC) analysis. When gas was encountered, vacutainer samples were collected by penetrating the core liner using a syringe connected to a penetration tool.

The constituents of the gas were analyzed with a HP5890 II gas chromatograph equipped with a flame ionization detector (FID). When heavier hydrocarbons ( $C_3^+$ ) were suspected or detected, the sample was analyzed by a natural gas analyzer (NGA). The NGA is used to quantify  $C_1$  to  $C_6$  and also nitrogen, oxygen, and carbon dioxide. Helium was used as a carrier gas. Data acquisition and processing were performed by a HP Chemstation. Chromatographic response was calibrated against authentic standards and the results reported as parts per million (ppm).

### Inorganic Carbon

Inorganic carbon was determined using a Coulometrics 5011 Carbon Dioxide Coulometer equipped with a System 140 carbonate carbon analyzer. A sample of 10–12 mg of freeze-dried ground sediment was weighed and then reacted with 2M HCl to liberate  $CO_2$ . The  $CO_2$ , which formed a titratable acid with a blue monoethanolamine indicator, was electrochemically titrated. The percentage of calcium carbonate was calculated from the inorganic carbon content, assuming that all the  $CO_2$  evolved was derived from dissolution of calcium carbonate by the following equation:

$$CaCO_3 \text{ [wt\%]} = IC \text{ [wt\%]} (\text{inorganic carbon}) \times 8.33 \quad (1)$$

The amount of carbonate is expressed as weight percent (wt%), assuming all the carbonate was present as calcite. No corrections were made for other carbonate minerals.

### Elemental Analysis

Total carbon, nitrogen, and sulfur were analyzed using a Carlo Erba 1500 CNS Analyzer. An aliquot of 12 to 15 mg of freeze-dried ground sediment with a  $V_2O_5$  catalyst was combusted at 1000°C in a stream of oxygen. Nitrogen oxides were reduced to  $N_2$ , and the mixture of  $N_2$ ,

CO<sub>2</sub>, and SO<sub>2</sub> gases was separated by gas chromatography. Detection of elements was performed by a thermal conductivity detector (TCD). All measurements were calibrated by comparison to natural standards. The amount of total organic carbon (TOC) was calculated as the difference between total carbon (TC) and inorganic carbon (IC), i.e:

$$\text{TOC [wt\%]} = \text{TC [wt\%]} - \text{IC [wt\%]} \quad (2)$$

### **Organic Matter Characterization and Maturity Determination**

The type of organic matter in a selected group of samples was characterized by pyrolysis using a Delsi Nermag Rock-Eval II system. This method is based on a whole-rock pyrolysis technique designed to identify the type and the degree of maturity of organic matter and to detect the petroleum potential of sediments (Espitalié et al., 1986). The Rock-Eval system includes a temperature program that first releases volatile hydrocarbons (S<sub>1</sub>) at 300°C for 3 min. Hydrocarbons are then released via thermal cracking of kerogen (S<sub>2</sub>) as the temperature is increased to 550°C at 25°C min<sup>-1</sup>. S<sub>1</sub> and S<sub>2</sub> hydrocarbons are measured by a flame ionization detector (FID) and reported in milligrams per gram of dry sediment. The temperature at which the kerogen yields the maximum amount of hydrocarbons during the S<sub>2</sub> program provides the parameter T<sub>max</sub>, which is used to assess the maturity of the organic matter. Between 300°C and 390°C of the stepped pyrolysis, CO<sub>2</sub> released from the thermal degradation of organic matter (S<sub>3</sub>) is trapped, measured by a TCD and reported in milligrams per gram dry sediment. Rock-Eval II parameters help in characterizing organic matter by allowing the following indices to be calculated: Hydrogen Index (HI; S<sub>2</sub>/TOC × 100), Oxygen Index (OI; S<sub>3</sub>/TOC × 100), and S<sub>2</sub>/S<sub>3</sub> value. Interpretation of Rock-Eval data is considered to be compromised for samples containing less than 0.5% TOC.

## **PHYSICAL PROPERTIES**

The objectives of physical properties measurements are (1) to obtain the basic data for the correlation between adjacent holes at a given site and construct complete stratigraphic sequences, (2) to detect changes in lithology and diagenetic zones within the sediment, (3) to identify potential stratigraphic hiatuses that are presented as inflections, discontinuities, or reversals in physical properties, and (4) to determine the sediment's consolidation characteristics, such as shear strength and porosity.

### **Multisensor Track (MST)**

Compressional wave velocity (*P*-wave), wet-bulk density, magnetic susceptibility, and natural gamma-ray emission were measured continuously and nondestructively on whole-round core sections on the MST.

#### ***P*-wave Velocity**

*P*-wave velocity varies with the lithology, the degree of consolidation, and the occurrence of gassy sediment and hydrates. Together with

GRAPE (gamma-ray attenuation porosity evaluator) density,  $P$ -wave velocity is used to calculate acoustic impedance and the reflection coefficient, which are then used to estimate the depth of reflectors observed in seismic profiles.

$P$ -wave velocity was measured, orthogonal to the core axis, using the  $P$ -wave logger (PWL) mounted on the MST. The PWL transmits a 500-kHz compressional wave pulse through the core at a repetition rate of 1 kHz.  $P$ -wave velocity was determined by picking the first arrival of wavelets. The travel time of the acoustic signal was measured to an accuracy of 50 ns. This corresponds to an instrument resolution of 1.5 m/s. The accuracy of velocity, however, was about 5 m/s because of the liner wall thickness (Schultheiss and McPhail, 1989).

The PWL system requires two types of calibration, which are performed at the beginning of each core section measurement. The first calibration is carried out for the displacement of the transducers, using the nominal diameter of an aluminum core and a standard core liner. The displacement of the transducer measures the core thickness and uses this measurement to calculate compressional wave velocity in the sediment. The distance traveled is measured with an accuracy of 0.1 mm. The second calibration,  $P$ -wave offset (time delay), adjusts to give the expected theoretical velocity in water at laboratory temperature. The  $P$ -wave offset is made by running the water standard core to compensate for sound propagation through the core liner and the electronic delay.  $P$ -wave velocity was only measured in hydraulic piston cores in a period of 4 s at 4-cm intervals.

All  $P$ -wave velocities were corrected to 20°C temperature values according to the following equation:

$$V_{20} = V_T + 3 (20 - T_s),$$

where  $V_{20}$  = velocity at 20°C, and  $T_s$  = the sediment temperature at which the measurement is made (°C). The measured velocity ( $V_T$ m/s) at temperature  $T_s$  is defined as

$$V_T = (d + CDD - 2W) / (t_s - X),$$

where  $d$  is the diameter of the inner core liner,  $CDD$  is core diameter deviation from the standard nominal core,  $W$  is the wall thickness of the core liner,  $t_s$  is the travel time through the sediment core and core liner, and  $X$  is the  $P$ -wave offset.

Note: Because of poor quality of the PWL results, all  $P$ -wave velocity measured by the PWL are not presented in the Leg 181 *Initial Reports* but are available from the ODP database.

### GRAPE Density

GRAPE density provides a precise and high-resolution record of lithology and porosity changes. Together with  $P$ -wave velocity, GRAPE density can provide acoustic impedance and reflection coefficients to construct synthetic seismograms.

Estimates of wet-bulk density have been obtained from continuous logging of whole-round core sections with the GRAPE mounted on the MST. A 10-mCi Cesium-137 capsule was used as the gamma-ray source. A narrow gamma-ray beam with energy principally at 0.662 MeV was attenuated on passing through the diameter of the core. For most sediments, the incident photons are scattered by the electrons with a partial

energy loss at this energy level (Boyce, 1976). The primary mechanism for the attenuation of gamma rays is by Compton scattering. The Compton attenuation is therefore directly related to the number of electrons encountered by the gamma-ray beam. This device measures the count rate per second of gamma-ray attenuation, which is related logarithmically to density times the thickness of sediment. Using a calibration based on aluminum standards of different thicknesses with distilled water inside the core liner, and ascertaining the slope of regression, the GRAPE density was obtained. Sediment was sampled at 2-s and 4-cm intervals. Longer counting times would allow greater precision. To maintain satisfactory precision of density measurement, aluminum standards have to be run with each core section to have calibration parameters ready for density calculation.

### **Magnetic Susceptibility**

Magnetic susceptibility is used mostly as a proxy indicator of changes in composition that can be linked to paleoclimate-controlled depositional processes. This measurement also is extremely useful for correlation among adjacent holes at a given site.

Magnetic susceptibility was measured with the Bartington Instruments MS2C system using an 8-cm diameter loop, an inducing field frequency of 0.565 kHz, and a low sensitivity setting of 1.0. Sediment was measured at 4-s and 4-cm intervals. The susceptibility instrument was set on SI units and the raw values are stored in the JANUS database. To convert to true SI volume susceptibilities, these values should be multiplied by  $10^{-5}$  and then multiplied by a correction factor (0.66) to take into account the volume of material that passed through the susceptibility coils.

### **Natural Gamma-Ray Emission**

Natural gamma-ray measurements are used for three purposes: (1) correlation of core and downhole data in multiple holes, (2) evaluation of the clay/shale content of a formation, and (3) abundance estimates for K, U, and Th.

The natural gamma-ray system consists of four shielded scintillation counters arranged at  $90^\circ$  from each other in a plane orthogonal to the core track. The scintillation counters contain doped sodium iodide crystals and photomultipliers to produce countable pulses (Blum, 1997). Natural gamma-ray measurements were taken for a period of 20 s at 15-cm intervals.

## **Physical Properties Measurements**

### **Thermal Conductivity**

Thermal conductivity was measured immediately after the MST measurements using whole-round core from intervals where downhole temperature measurements were taken. The needle probe method was used in full space configuration. The probes were calibrated based on three standards: red rubber, macor ceramic, and black rubber. Thermal conductivities of these three standards are 0.96 W/(m·K), 1.61 W/(m·K), and 0.54 W/(m·K), respectively.

For each measurement, a needle probe was inserted into whole-round core. While the needle was heated, the temperature ( $T$ ) was mea-



sured as a function of time ( $t$ ). The temperature is related to the thermal conductivity of the sediment by

$$T(t) = (q / 4\pi k) \cdot \ln(t) + L(t),$$

where  $q$  is heat input per unit length of wire per unit time (W/m·s),  $k$  is the apparent thermal conductivity in W/(m·K), and  $L(t)$  is a linear change in temperature with time, including temperature drift during measurement as well as instrumental errors.

All measurements were corrected for a linear offset between measured and true thermal conductivities. That is, the least-squares fit of the linear regression was used to obtain the true thermal conductivity based on a measured probe reading.

### **Index Properties**

Water content, grain density (to calculate bulk density, porosity, and related properties), and vane shear strength measurements were obtained from split cores.

An additional estimate of wet-bulk density was determined by measuring water content and grain density to check the accuracy of the density measured on the MST. Water content is determined by weighing a sample of sediment and then drying the sample in an oven at a temperature of 105°–110° C for a period of 24 hr and re-weighing. Water content as a percentage of water mass over dry mass is determined by

$$W_{\text{dry}} = [M_w / (M_d - M_{\text{salt}})] \cdot 100,$$

where  $W_{\text{dry}}$  = dry water content (%),  $M_w$  is water mass,  $M_d$  is dry mass, and  $M_{\text{salt}}$  is the salt in the fluid:

$$M_{\text{salt}} = s \cdot M_w / (1 - s),$$

where  $s$  is salinity (0.035).

Wet-bulk density is then defined as the ratio of mass to volume of wet sediment:

$$\rho_b = (M_d + M_w) / [(M_d - M_{\text{salt}}) / \rho_g + (M_w + M_{\text{salt}}) / \rho_f],$$

where  $\rho_g$  = grain density (see below) and  $\rho_f$  is fluid density (1.025 g/cm<sup>3</sup>).

Porosity ( $\emptyset$ ) is defined as the ratio of the water volume to the total volume and was determined using the following relationship:

$$\emptyset = (\rho_g - \rho_b) / (\rho_g - \rho_f).$$

Grain density is defined as the mass of the grains divided by the volume of the grains:

$$\rho_g = (M_d - M_{\text{salt}}) / (V_d - M_{\text{salt}} / \rho_{\text{salt}}),$$

where  $V_d$  = dry volume and  $\rho_{\text{salt}}$  is the density of salt (2.257 g/cm<sup>3</sup>).

Dry volumes were determined using a helium-displacement Quantachrome Penta-Pycnometer by employing Archimedes' principle of

fluid displacement. The displaced fluid is a helium gas that can penetrate pores as fine as one Angstrom ( $10^{-10}$  m). The pycnometer measures the volume of each sample to an approximate precision of  $\pm 0.02$  cm<sup>3</sup>. Determinations were made five times, or until 0.01 of the standard deviation was achieved, and then averaged.

### Automated Vane Shear Strength Measurements

Undrained shear strength was determined using the Wykeham-Farrence motorized miniature vane shear apparatus, following ASTM D4648-94 procedure (ASTM, 1995). A four-bladed vane was inserted into the split-core and rotated to determine the torque required to cause a cylindrical surface to be sheared by the vane. Torque at failure was converted through a calibrated spring into a measure of the sediment's undrained shear strength given in units of kPa. The results of a series of undrained shear tests were represented by measuring the value of cohesion.

The vane used for all measurements has a 1:1 blade ratio with a dimension of 12.7 mm. A rotation rate of 90°/min was used. The vane shear strength of sediment can be calculated from the equation:

$$S_u = T / K,$$

where  $S_u$  = undrained shear strength in kN/m<sup>2</sup> or kPa,  $T$  is torque at failure to shear the sediment in Nm,  $K$  is a constant (in m<sup>3</sup>) depending on overall vane width,  $d$ , and vane length,  $h$ :

$$K = \pi (d^2h/2 + d^3/6),$$

where  $d$  and  $h$  are equal to 12.7 mm; therefore,  $K = 4.29 \times 10^{-6}$  m<sup>3</sup>.

The springs used to measure torque must be calibrated to the angles of rotation. ODP personnel are responsible for this occasional calibration. The spring constant,  $B$ , is defined as

$$B = \theta / T,$$

where  $T$  is the torque (provided in kg·cm by the manufacturer) and  $\theta$  is the corresponding deflection angle. ODP personnel enter the data into a calibration utility that converts the data to N·m and determines the regression slope that corresponds to  $B$ . The conversion is

$$T (\text{N} \cdot \text{m}) = 0.0981 \times T (\text{kg} \cdot \text{cm}).$$

The calibration constant for spring no. 4 that was used during Leg 181 is 0.045146.

### Digital Sound Velocimeter (DSV)

In addition to the measurement by the  $P$ -wave logger mounted on the MST,  $P$ -wave velocity was also measured on each split core section on the DSV.

Two types of sound propagation measurements were obtained. First, two piezoelectric transducer pairs, PW1 and PW2, were inserted into soft sediment, parallel and orthogonal to the core axis, respectively. Sound was propagated through the sediment without the effect of the

core liner. Transducers are separated by about 7 cm and firmly fixed at one end to a steel plate. Secondly, a modified Hamilton frame velocimeter, PW3, was used to measure sound speed orthogonal to the split core section, with transducers at the top and the bottom of the core section. In well-compacted or indurated sediment, discrete samples are required for good transducer contact. The DSV measurements were made at the same intervals where index properties and vane shear strength were taken. Calibration and calculation of the DSV are similar to those of the *P*-wave logger on the MST. A correction for the core liner, when present, is made.

## DOWNHOLE MEASUREMENTS

### Introduction

Well logs show a continuous, in situ record of geophysical parameters within a borehole. They can be used to assess the physical, chemical, and structural characteristics of formations penetrated by drilling, thus providing a means of reconstructing and interpreting geological environments.

Well-logging is typically undertaken in the deepest hole drilled at any one site. Where core recovery is poor, downhole logs are often the most reliable source of information; where core recovery is good, log data can be correlated with core data to produce more detailed and emphatic results.

Downhole logging operations begin after the hole has been cored and flushed with a viscous drilling fluid. The drilling assembly is then pulled up to ~80 mbsf and the logging tools are passed through the drill pipe into the open hole. The logging tools are joined together into tool strings so that compatible tools are run together (Fig. F13). Each tool string is lowered separately to the base of the hole and then measurement takes place as the tool string is raised at a constant velocity between 275–500 m/h (see individual site chapters). A wireline heave compensator is used to minimize the effect of the ship's heave on the tool position in the borehole (Goldberg, 1990).

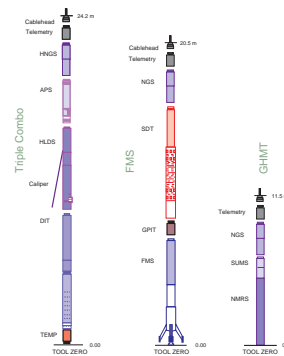
Three tool strings were used during Leg 181: the triple combination, the Formation MicroScanner (FMS-sonic), and the Geologic High-Resolution Magnetic Tool (GHMT) (Fig. F13; Table T6, also in ASCII format). The principles underlying the use of these tools are explained in Serra (1984, 1986, 1989), Timur and Toksöz (1985), and Tittman (1986), and some examples of their applications are given by Ellis (1987) and Rider (1996). Following is a brief description and explanation of the tools used.

### Tool String Configurations

#### Triple Combination Tool String

The Natural Gamma Ray Sonde (NGS) and the Hostile-Environment Natural Gamma-Ray Sonde (HNGS) measure the gamma radiation of uranium (U), potassium (K), and thorium (Th), which occur naturally in sediments. Because of the relative abundance of U, Th, and K within many clay minerals, a high gamma-ray reading is often indicative of a relatively high clay content in the sediment, while a low gamma-ray reading often indicates quartz sands and carbonates (e.g., Serra and

F13. Tool strings used, p. 56.



T6. Tool strings used and properties measured, p. 65.

Sulpice, 1975). It should be mentioned, however, this is not always the case (see Rider, 1990).

A gamma-ray sonde was fitted to all of the tool strings to enable depth correlation between each individual logging run. The natural gamma reading was also used for measuring the depth to the seafloor, as natural gamma radiation shows a sharp increase at the mudline.

The Accelerator Porosity Sonde (APS) emits fast neutrons, which lose energy as they collide with hydrogen nuclei in the formation. Once the neutrons have slowed down to reach thermal energies (0.025 eV), they are captured by the nuclei of chlorine and various heavy elements. This results in a gamma-ray emission. The APS measures the number of neutrons arriving at five different detectors at varying distances from the source. This measurement is inversely proportional to the concentration of hydrogen in the formation. Because the majority of hydrogen is contained in the pore water, the APS measurement can be used to derive a porosity. However, hydrogen bound in minerals such as clays also contributes to the APS measurement, so that the raw porosity value is often an overestimate.

The Hostile Environment Lithodensity Sonde (HLDS) consists of a  $^{137}\text{Cs}$  radioactive source and two gamma-ray detectors mounted on a shielded sidewall skid that is pressed against the formation by a hydraulically activated arm. The arm also provides a caliper measurement of borehole diameter. The gamma rays emitted by the source interact with the electrons in the formation and lose energy as a result of Compton scattering. When the gamma rays reach a low energy (<150 keV), photoelectric absorption takes place. This tool is sensitive to hole conditions, as the detectors need to be in contact with the borehole wall to produce reliable data.

The number of gamma rays that reach the detectors in the HLDS is directly related to the number of electrons in the formation, which is in turn related to the bulk density. The photoelectric effect (PEF) can be assessed by comparing the counts from the far detector, which is in the high energy region where only Compton scattering occurs, with those of the near detector, which is in the low energy region where the photoelectric effect is dominant.

The bulk density value measured by the HLDS can be used to calculate a porosity, using the following equation:

$$F = (\rho_{gr} - \rho_b) / (\rho_{gr} - \rho_w),$$

where  $\rho_{gr}$  = mean grain density, given by physical properties measurements (typically 2.7 g/cm<sup>3</sup>),  $\rho_w$  = pore water density, taken to be 1.03 g/cm<sup>3</sup> for seawater, and  $\rho_b$  = bulk density, given by the HLDS.

Photoelectric absorption is strongly dependent on the atomic number of the constituents of the formation. The PEF values, therefore, can give an indication of the chemical composition of the rock.

The Dual Induction Tool (DIT) provides three different measurements of electrical resistivity based on multiple depths of investigation: deep induction (IDPH), medium induction (IMPH), and shallow, spherically focused resistivity (SFL). The two induction devices produce an alternating magnetic field, which induces Foucault currents around the borehole. These currents produce a new inductive signal, proportional to the conductivity of the formation. The measured conductivities are then converted to resistivity ( $\Omega\text{m}$ ). The SFL measures the current necessary to maintain a constant voltage drop across a fixed interval and is a

direct measurement of resistivity. Because the solid constituents of rocks are essentially infinitely resistive relative to the pore fluids, resistivity is controlled mainly by the nature of the pore fluids, porosity, and the tortuosity of the pore spaces.

The Lamont-Doherty Temperature Logging Tool (TLT) is a high-precision, self-recording logging tool that measures the temperature of the water in the hole. Data are recorded as a function of time, with conversion to depth based on a synchronized time-cable depth record. Data from the TLT provide an insight into the thermal regime of the formation penetrated by drilling.

### FMS-Sonic Tool String

The Sonic Digital Tool (SDT) measures the traveltime of sound waves along the borehole wall, between two transmitters and two receivers, over distances of 2.4, 3.0, and 3.6 m. Full waveforms are recorded by this tool, allowing shore-based processing to estimate shear and Stoneley wave velocities, as well as amplitude attenuation. Logs are edited for cycle-skipping and obvious bad values. The sonic velocity is related to porosity, as sediments have a higher sonic wave velocity than pore fluids. Sonic velocity, therefore, typically increases with compaction and lithification. Furthermore, an impedance log (density  $\times$  velocity) can be created to generate synthetic seismograms for comparison with the seismic survey sections.

The General Purpose Inclinometry Tool (GPIT) uses acceleration measurements to calculate the amount of tool displacement that occurs during logging. These data enable logging depths to be determined more accurately.

The Formation MicroScanner (FMS) produces high-resolution microresistivity images. This tool consists of four orthogonal imaging pads, each containing 16 microelectrodes (Fig. F14). The pads, which are in direct contact with the borehole wall, emit a focused current into the formation. The current intensity fluctuations are measured, then converted to color images that reflect microresistivity variations: the lighter the color, the greater the resistivity (Ekstrom et al., 1987). These images have a vertical resolution of  $\sim 0.5$  cm and a measurement interval of 0.25 cm (Serra, 1989). Roughly 30% of a 25-cm diameter borehole is imaged.

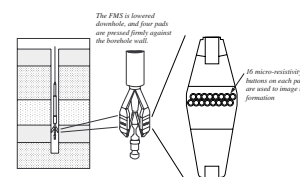
The development of the FMS tool has added a new dimension to wireline-logging (Luthi, 1990; Lovell et al., 1998; Salimullah and Stow, 1992). The formation can now be viewed in its complete state, and often it can be grouped into facies assemblages. Features such as bedding, fracturing, slump folding, and bioturbation can be resolved, and the fact that the images are oriented means that fabric can be analyzed and bed orientations can be measured.

### GHMT Tool String

The Susceptibility Magnetic Sonde (SUMS) measures magnetic susceptibility by means of low-frequency induction in the surrounding sediment. It responds primarily to magnetic minerals (mainly magnetite, hematite, and iron sulfide), which are often contained in the detrital sediment fraction, and, therefore, it can be used as a proxy indicator of paleoenvironmental change.

The Nuclear Resonance Magnetic Sonde (NMRS) measures the total magnetic field, using a proton precession magnetometer. The data from

F14. The Formation MicroScanner (FMS), p. 57.



the SUMS and the NMRS tools can be used to construct a polarity stratigraphy, using the method outlined below.

The total magnetic field ( $B$ ) measured in the borehole is composed of five variables:

$$B = B_o + B_p + B_t + B_i \pm B_r,$$

where

- $B_o$  is the Earth's magnetic field, generated in the Earth's core with an intensity of ~57,000 nT for the region of Leg 181;
- $B_p$  is the magnetic field caused by the bottom-hole assembly (BHA) and pipe, and can be as large as ~2000 nT, decaying away from the BHA;
- $B_t$  is the time-varying field. Two passes of the GHMT are run to check that this is negligible. If only one pass of the GHMT is run, then  $B_t$  is assumed to be negligible;
- $B_i$  is the field induced in the borehole by the effect of the earth's field acting on the sediments. It is given by the formula  $B_i = (J_i/2) \cdot (1 - 3\sin^2 I)$ , where  $J_i = B_o \cdot \chi$ ;  $\chi$  is the sediment susceptibility, measured by the SUMS, and  $I$  is the magnetic inclination of the modern earth's field ( $B_o$ ) at the borehole location; and
- $B_r$  is the remanent field in the borehole. In the Southern Hemisphere, negative  $B_r$  signifies a normal polarity and positive  $B_r$  signifies reversed polarity.
- $B_i$  and  $B_r$  are the fields of interest. Subtracting  $B_o$ ,  $B_p$ , and  $B_t$  from the GHMT yields  $B_i \pm B_r$ . A stratigraphy based solely on positive or negative remanence is a reasonable estimate of the true magnetic stratigraphy. Further processing, involving regression analysis of the Koenigsberger coefficient ( $B_r/B_i$ ) using a sliding depth scale, with anticorrelation showing normal polarity and positive correlation showing reversed polarity, will give a more reliable stratigraphy. This analysis is typically done on shore.



## REFERENCES

- Abelmann, A., 1992. Early to middle Miocene radiolarian stratigraphy of the Kerguelen Plateau, Leg 120. In Wise, S.W., Jr., Schlich, R., et al., *Proc. ODP, Sci. Results*, 120: College Station, TX (Ocean Drilling Program), 757–783.
- ASTM, 1995. Standard test method for laboratory miniature vane shear test for saturated fine-grained clayey soils, Designation D 4648-94. In *Annual Book of ASTM Standards*, Section 4—Construction (Vol. 04.08): Philadelphia (Am. Soc. Testing and Mater.).
- Baldauf, J.G., and Barron, J.A., 1991. Diatom biostratigraphy: Kerguelen Plateau and Prydz Bay regions of the Southern Ocean. In Barron, J., Larsen, B., et al., *Proc. ODP, Sci. Results*, 119: College Station, TX (Ocean Drilling Program), 547–598.
- Balsam, W.L., Damuth, J.E., and Schneider, R.R., 1997. Comparison of shipboard vs. shore-based spectral data from Amazon Fan cores: implications for interpreting sediment composition. In Flood, R.D., Piper, D.J.W., Klaus, A., and Peterson, L.C. (Eds.), *Proc. ODP, Sci. Results*, 155: College Station, TX (Ocean Drilling Program), 193–215.
- Barron, J.A., 1992. Neogene diatom datum levels in the equatorial and North Pacific. In Ishizaki, K., and Saito, T. (Eds.), *The Centenary of Japanese Micropaleontology*: Tokyo (Terra Sci. Publ.), 413–425.
- Barron, J.A., Baldauf, J.G., Barrera, E., Caulet, J.-P., Huber, B.T., Keating, B.H., Lazarus, D., Sakai, H., Thierstein, H.R., and Wei, W., 1991. Biochronologic and magneto-chronologic synthesis of Leg 119 sediments from the Kerguelen Plateau and Prydz Bay, Antarctica. In Barron, J., Larsen, B., et al., *Proc. ODP, Sci. Results*, 119: College Station, TX (Ocean Drilling Program), 813–847.
- Berggren, W.A., 1992a. Neogene planktonic foraminifer magnetobiostratigraphy of the southern Kerguelen Plateau (Sites 747, 748, and 751). In Wise, S.W., Jr., Schlich, R., et al., *Proc. ODP, Sci. Results*, 120 (Pt. 2): College Station, TX (Ocean Drilling Program), 631–647.
- , 1992b. Paleogene planktonic foraminifer magnetobiostratigraphy of the Southern Kerguelen Plateau (Sites 747–749). In Wise, S.W., Jr., Schlich, R., et al., *Proc. ODP, Sci. Results*, 120 (Pt. 2): College Station, TX (Ocean Drilling Program), 551–568.
- Berggren, W.A., Hilgen, F.J., Langereis, C.G., Kent, D.V., Obradovich, J.D., Raffi, I., Raymo, M.E., and Shackleton, N.J., 1995a. Late Neogene chronology: new perspectives in high-resolution stratigraphy. *Geol. Soc. Am. Bull.*, 107:1272–1287.
- Berggren, W.A., Kent, D.V., Swisher, C.C., III, and Aubry, M.-P., 1995b. A revised Cenozoic geochronology and chronostratigraphy. In Berggren, W.A., Kent, D.V., Aubry, M.-P., and Hardenbol, J. (Eds.), *Geochronology, Time Scales and Global Stratigraphic Correlation*. Spec. Publ.—Soc. Econ. Paleontol. Mineral. (Soc. Sediment. Geol.), 54:129–212.
- Blum, P., 1997. Physical Properties Handbook: a Guide to the Shipboard Measurements of Physical Properties of Deep-sea Cores. *ODP Tech. Note*, 26.
- Boyce, R.E., 1976. Definitions and laboratory techniques of compressional sound velocity parameters and wet-water content, wet-bulk density, and porosity parameters by gravimetric and gamma-ray attenuation techniques. In Schlanger, S.O., Jackson, E.D., et al., *Init. Repts. DSDP*, 33: Washington (U.S. Govt. Printing Office), 931–958.
- Brassell, S.C., Eglinton, G., Marlowe, I.T., Pflaumann, U., and Sarnthein, M., 1986. Molecular stratigraphy: a new tool for climatic assessment. *Nature*, 320:129–133.
- Brunner, C.A., 1991. Latest Miocene to Quaternary biostratigraphy and paleoceanography, Site 704, subantarctic South Atlantic Ocean. In Ciesielski, P.F., Kristoffersen, Y., et al., *Proc. ODP, Sci. Results*, 114: College Station, TX (Ocean Drilling Program), 201–215.

- Bukry, D., 1973. Low-latitude coccolith biostratigraphic zonation. *In* Edgar, N.T., Saunders, J.B., et al., *Init. Repts. DSDP*, 15: Washington (U.S. Govt. Printing Office), 685–703.
- , 1975. Coccolith and silicoflagellate stratigraphy, northwestern Pacific Ocean, Deep Sea Drilling Project Leg 32. *In* Larson, R.L., Moberly, R., et al., *Init. Repts. DSDP*, 32: Washington (U.S. Govt. Printing Office), 677–701.
- , 1978. Biostratigraphy of Cenozoic marine sediment by calcareous nanofossils. *Micropaleontology*, 24:44–60.
- Cande, S.C., and Kent, D.V., 1995. Revised calibration of the geomagnetic polarity timescale for the Late Cretaceous and Cenozoic. *J. Geophys. Res.*, 100:6093–6095.
- Carter, R.M., and Naish, T.R., 1998. Have local stages outlived their usefulness for the New Zealand Pliocene–Pleistocene? *N. Z. J. Geol. Geophys.*, 41:271–279.
- Caulet, J.P., 1986. Radiolarians from the southwest Pacific. *In* Kennett, J.P., von der Borch, C.C., et al., *Init. Repts. DSDP*, 90: Washington (U.S. Govt. Printing Office), 835–861.
- , 1991. Radiolarians from the Kerguelen Plateau, Leg 119. *In* Barron, J., Larsen, B., et al., *Proc. ODP, Sci. Results*, 119: College Station, TX (Ocean Drilling Program), 513–546.
- Ciesielski, P.F., 1983. The Neogene and Quaternary diatom biostratigraphy of subantarctic sediments, Deep Sea Drilling Project Leg 71. *In* Ludwig, W.J., Krasheninnikov, V.A., et al., *Init. Repts. DSDP*, 71 (Pt. 2): Washington (U.S. Govt. Printing Office), 635–666.
- Curry, W.B., Shackleton, N.J., Richter, C., et al., 1995. *Proc. ODP, Init. Repts.*, 154: College Station, TX (Ocean Drilling Program).
- Dowsett, H.J., 1988. Diachroneity of Late Neogene microfossils in the Southwest Pacific Ocean: application of the graphic correlation method. *Paleoceanography*, 3:209–222.
- Droser, M.L., and Bottjer, D.J., 1991. Trace fossils and ichnofabric in Leg 119 cores. *In* Barron, J., Larsen, B., et al., *Proc. ODP, Sci. Results*, 119: College Station, TX (Ocean Drilling Program), 635–641.
- Edwards, A.R., Hornibrook, N. de B., Raine, J.I., Scott, G.R., Stevens, G.R., Strong, C.P., and Wilson, G.J., 1988. A New Zealand Cretaceous–Cenozoic geological time scale. *N. Z. Geol. Surv. Rec.*, 35:135–149.
- Edwards, A.R., and Perch-Nielsen, K., 1975. Calcareous nanofossils from the southern Southwest Pacific, DSDP Leg 29. *In* Kennett, J.P., Houtz, R.E., et al., *Init. Repts. DSDP*, 29: Washington (U.S. Govt. Printing Office), 469–539.
- Ekstrom, M.P., Dahan, C., Chen, M.-Y., Lloyd, P., and Rossi, D.J., 1987. Formation imaging with microelectrical scanning arrays. *Log Analyst*, 28:294–306.
- Ellis, D.V., 1987. *Well Logging for Earth Scientists*: New York (Elsevier).
- Emeis, K.-C., and Kvenvolden, K.A., 1986. Shipboard organic geochemistry on JOIDES Resolution. *ODP Tech. Note*, 7.
- Espitalié, J., Deroo, G., and Marquis, F., 1986. La pyrolyse Rock-Eval et ses applications, Partie III. *Rev. Inst. Fr. Pet.*, 41:73–89.
- Fenner, J., 1985. Late Cretaceous to Oligocene planktic diatoms. *In* Bolli, H.M., Saunders, J.B., and Perch-Nielsen, K. (Eds.), *Plankton Stratigraphy*: Cambridge (Cambridge Univ. Press), 713–762.
- Fenner, J.M., 1984. Eocene–Oligocene planktic diatom stratigraphy in the low latitudes and the high southern latitudes. *Micropaleontology*, 30:319–342.
- , 1991. Late Pliocene–Quaternary quantitative diatom stratigraphy in the Atlantic sector of the Southern Ocean. *In* Ciesielski, P.F., Kristoffersen, Y., et al., *Proc. ODP, Sci. Results*, 114: College Station, TX (Ocean Drilling Program), 97–121.
- Foreman, H.P., 1975. Radiolaria from the North Pacific, Deep Sea Drilling Project, Leg 32. *In* Larson, R.L., Moberly, R., et al., *Init. Repts. DSDP*, 32: Washington (U.S. Govt. Printing Office), 579–676.
- Gersonde, R., Abelmann, A., Burckle, L.H., Hamilton, N., Lazarus, D., McCartney, K., O'Brien, P., Spieß, V., and Wise, S.W., Jr., 1990. Biostratigraphic synthesis of Neo-

- gene siliceous microfossils from the Antarctic Ocean, ODP Leg 113 (Weddell Sea). *In* Barker, P.F., Kennett, J.P., et al., *Proc. ODP, Sci. Results*, 113: College Station, TX (Ocean Drilling Program), 915–936.
- Gersonde, R., and Bárcena, M.A., 1998. Revision of the late Pliocene–Pleistocene diatom biostratigraphy for the northern belt of the Southern Ocean. *Micropaleontology*, 44:1–15.
- Gersonde, R., and Burckle, L.H., 1990. Neogene diatom biostratigraphy of ODP Leg 113, Weddell Sea (Antarctic Ocean). *In* Barker, P.F., Kennett, J.P., et al., *Proc. ODP, Sci. Results*, 113: College Station, TX (Ocean Drilling Program), 761–789.
- Gersonde, R., Hodell, D.A., Blum, P., et al., 1999. *Proc. ODP, Init. Repts.*, 177: College Station, TX (Ocean Drilling Program).
- Gersonde, R., Spieß, V., Flores, J. A., Hagen, R., and Kuhn, G., 1998. The sediments of Gunnerus Ridge and Kainan Maru Seamount (Indian sector of Southern Ocean). *Deep-Sea Res.*, 45:1515–1540.
- Gieskes, J.M., Gamo, T., and Brumsack, H., 1991. Chemical methods for interstitial water analysis aboard *JOIDES Resolution*. *ODP Tech. Note*, 15.
- Goldberg, D., 1990. Test performance of the Ocean Drilling Program wireline heave motion compensator. *Sci. Drill.*, 1:206–209.
- Gradstein, F.M., and Berggren, W.A., 1981. Flysch-type agglutinated foraminifera and the Maestrichtian to Paleogene history of the Labrador and North seas. *Mar. Micropaleontology*, 6:211–269.
- Grützmacher, U., 1993. Die Veränderungen der paläogeographischen Verbreitung von *Bolboforma*: Ein Beitrag zur Rekonstruktion und Definition von Wassermassen im Tertiär. *Geomar Rep.*, 22:1–104.
- Hagelberg, T., Shackleton, N., Pisias, N., and Shipboard Scientific Party, 1992. Development of composite depth sections for Sites 844 through 854. *In* Mayer, L., Pisias, N., Janecek, T., et al., *Proc. ODP, Init. Repts.*, 138 (Pt. 1): College Station, TX (Ocean Drilling Program), 79–85.
- Hagelberg, T.K., Pisias, N.G., Shackleton, N.J., Mix, A.C., and Harris, S., 1995. Refinement of a high-resolution, continuous sedimentary section for studying equatorial Pacific Ocean paleoceanography, Leg 138. *In* Pisias, N.G., Mayer, L.A., Janecek, T.R., Palmer-Julson, A., and van Andel, T.H. (Eds.), *Proc. ODP, Sci Results*, 138: College Station, TX (Ocean Drilling Program), 31–46.
- Harwood, D.M., Lazarus, D.B., Abelmann, A., Aubry, M.-P., Berggren, W.A., Heider, F., Inokuchi, H., Maruyama, T., McCartney, K., Wei, W., and Wise, S.W., Jr., 1992. Neogene integrated magnetobiostratigraphy of the central Kerguelen Plateau, Leg 120. *In* Wise, S.W., Jr., Schlich, R., et al., *Proc. ODP, Sci. Results*, 120: College Station, TX (Ocean Drilling Program), 1031–1052.
- Harwood, D.M., and Maruyama, T., 1992. Middle Eocene to Pleistocene diatom biostratigraphy of Southern Ocean sediments from the Kerguelen Plateau, Leg 120. *In* Wise, S.W., Jr., Schlich, R., et al., *Proc. ODP, Sci. Results*, 120: College Station, TX (Ocean Drilling Program), 683–733.
- Hayward, B.W., 1983. Planktic foraminifera (Protozoa) in New Zealand: a taxonomic review. *N. Z. J. Zool.*, 10:63–74.
- , 1986. A guide to paleoenvironmental assessment using New Zealand Cenozoic foraminiferal faunas. *N. Z. Geol. Surv. Rep.*, 109:1–72.
- Hilgen, F.J., 1991a. Astronomical calibration of Gauss to Matuyama sapropels in the Mediterranean and implications for the geomagnetic polarity time scale. *Earth Planet. Sci. Lett.*, 107:226–244.
- , 1991b. Extension of the astronomically calibrated (polarity) time scale to the Miocene/Pliocene boundary. *Earth Planet. Sci. Lett.*, 107:349–368.
- Hollis, C.J., 1997. Cretaceous–Paleocene Radiolaria of eastern Marlborough, New Zealand. *Monogr.—Inst. Geol. Nucl. Sci.*, 17:1–152.
- Hornibrook, N.de B., 1990. The Neogene of New Zealand—a basis for regional events. *In* Tsuchi, R. (Ed.), *Pacific Neogene Events*: Tokyo: (Univ. Tokyo Press), 195–206.

- Hornibrook, N. de B., Brazier, R.C., and Strong, C.P., 1989. Manual of New Zealand Permian to Pleistocene foraminiferal biostratigraphy. *Paleontol. Bull. N. Z. Geol. Surv.*, 56:1–175.
- Hornibrook, N. de B., and Jenkins, D.G., 1994. DSDP 594, Chatham Rise, New Zealand—Late Neogene planktonic foraminiferal biostratigraphy revisited. *J. Micro-paleontol.*, 13:93–101.
- Jansen, E., Raymo, M.E., Blum, P., et al., 1996. *Proc. ODP, Init. Repts.*, 162: College Station, TX (Ocean Drilling Program).
- Jenkins, D.G., and Srinivasan, M.S., 1986. Cenozoic planktonic foraminifers from the equator to the sub-antarctic of the southwest Pacific. In Kennett, J.P., von der Borch, C.C., et al., *Init. Repts. DSDP*, 90: Washington (U.S. Govt. Printing Office), 795–834.
- Kennett, J.P., and Srinivasan, M.S., 1983. *Neogene Planktonic Foraminifera: A Phylogenetic Atlas*: Stroudsburg, PA (Hutchinson Ross).
- Kvenvolden, K.A., and McDonald, T.J., 1986. Organic geochemistry on the JOIDES Resolution—an assay. *ODP Tech. Note*, 6.
- Lazarus, D., 1992. Antarctic Neogene radiolarians from the Kerguelen Plateau, Legs 119 and 120. In Wise, S.W., Jr., Schlich, R., et al., *Proc. ODP, Sci. Results*, 120: College Station, TX (Ocean Drilling Program), 785–809.
- Lohman, W.H., 1986. Calcareous nannoplankton biostratigraphy of the southern Coral Sea, Tasman Sea, and southwestern Pacific Ocean, Deep Sea Drilling Project Leg 90: Neogene and Quaternary. In Kennett, J.P., von der Borch, C.C., et al., *Init. Repts. DSDP*, 90: Washington (U.S. Govt. Printing Office), 763–793.
- Lourens, L.J., Antonarakou, A., Hilgen, F.J., Van Hoof, A.A.M., Vergnaud-Grazzini, C., and Zachariasse, W.J., 1996. Evaluation of the Plio-Pleistocene astronomical time-scale. *Paleoceanography*, 11:391–413.
- Lovell, M.A., Harvey, P.K., Brewer, T.S., Williams, C., Jackson, P.D., and Williamson, G., 1998. Application of FMS images in the Ocean Drilling Program: an overview. In Cramp, A., MacLeod, C.J., Lee, S.V., and Jones, E.J.W. (Eds.), *Geological Evolution of Ocean Basins: Results from the Ocean Drilling Program*. Geol. Soc. Spec. Publ. London, 131:287–303.
- Luthi, S.M., 1990. Sedimentary structures of clastic rocks identified from electrical borehole images. In Hurst, A., Lovell, M.A., and Morton, A.C. (Eds.), *Geological Applications of Wireline Logs*. Geol. Soc. Spec. Publ. London, 48:3–10.
- Lyle, M., Koizumi, I., Richter, C., et al., 1997. *Proc. ODP, Init. Repts.*, 167: College Station, TX (Ocean Drilling Program).
- Mackensen, A., and Spiegler, D., 1992. Middle Eocene to early Pliocene *Bolboforma* (algae?) from the Kerguelen Plateau, southern Indian Ocean. In Wise, S.W., Jr., Schlich, R., et al., *Proc. ODP, Sci. Results*, 120: College Station, TX (Ocean Drilling Program), 675–682.
- Manheim, F.T., and Sayles, F.L., 1974. Composition and origin of interstitial waters of marine sediments, based on deep sea drill cores. In Goldberg, E.D. (Ed.), *The Sea* (Vol. 5): *Marine Chemistry: The Sedimentary Cycle*: New York (Wiley), 527–568.
- Martini, E., 1971. Standard Tertiary and Quaternary calcareous nannoplankton zonation. In Farinacci, A. (Ed.), *Proc. 2nd Int. Conf. Planktonic Microfossils Roma*: Rome (Ed. Tecnosci.), 2:739–785.
- Martini, E., and Jenkins, D.G., 1986. Biostratigraphic synthesis, Deep Sea Drilling Project Leg 90 in the southwest Pacific Ocean. In Kennett, J.P., von der Borch, C.C., et al., *Init. Repts. DSDP*, 90: Washington (U.S. Govt. Printing Office), 1459–1470.
- Mazzullo, J.M., Meyer, A., and Kidd, R.B., 1988. New sediment classification scheme for the Ocean Drilling Program. In Mazzullo, J., and Graham, A.G. (Eds.), *Handbook for Shipboard Sedimentologists*. ODP Tech. Note, 8:45–67.
- McCollum, D.W., 1975. Diatom stratigraphy of the southern Ocean. In Hayes, D.E., Frakes, L.A., et al., *Init. Repts. DSDP*, 28: Washington (U.S. Govt. Printing Office), 515–571.

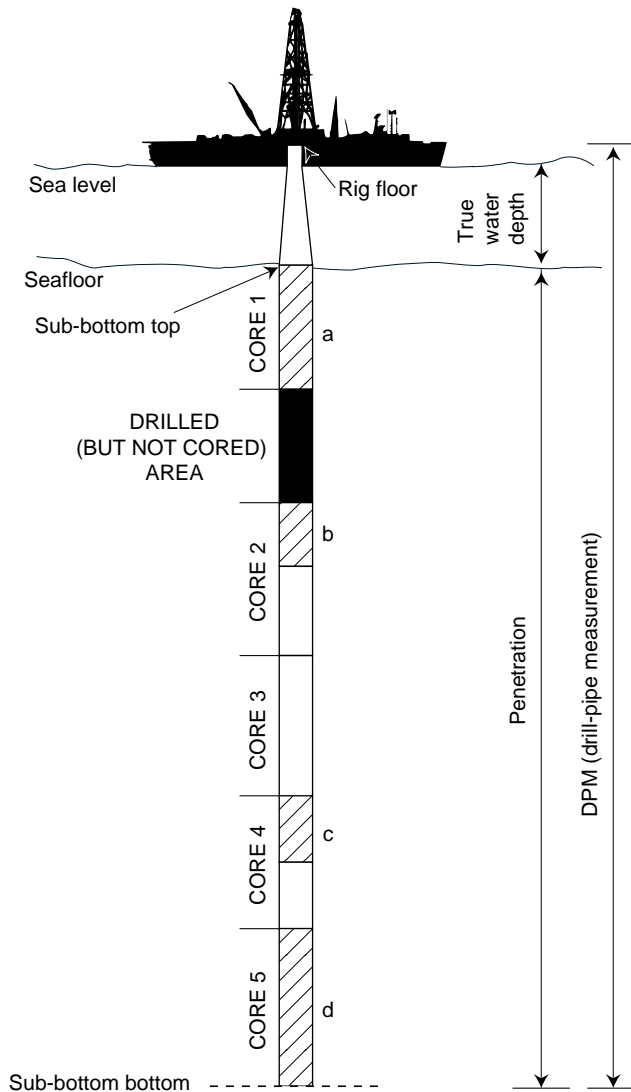
- McKee, E.D., and Weir, G.W., 1953. Terminology for stratification and cross-stratification in sedimentary rocks. *Geol. Soc. Am. Bull.*, 64:381–390.
- Morgans, H.E.G., Scott, G.H., Beu, A.G., Graham, I.J., Mumme, T.C., George, W.St., and Strong, C.P., 1996. New Zealand Cenozoic Time Scale (version 11/96). *Rep.—Inst. Geol. Nucl. Sci.*, 96/38:1–12.
- Morley, J.J., 1985. Radiolarians from the Northwest Pacific, Deep Sea Drilling Project Leg 86. *In* Heath, G.R., Burckle, L.H., et al., *Init. Repts. DSDP*, 86: Washington (U.S. Govt. Printing Office), 399–422.
- Naish, T., Abbott, S., Alloway, B., Beu, A., Carter, R., Edwards, A., Journeaux, T., Kamp, P., Pillans, B., Saul, G, and Woolfe, K., 1998. Astronomical calibration of a southern hemisphere Plio-Pleistocene reference section, Wanganui Basin. *N. Z. Quat. Sci. Rev.*, 17:695–710.
- Okada, H., and Bukry, D., 1980. Supplementary modification and introduction of code numbers to the low-latitude coccolith biostratigraphic zonation (Bukry, 1973; 1975). *Mar. Micropaleontol.*, 5:321–325.
- Perch-Nielsen, K., 1985. Cenozoic calcareous nannofossils. *In* Bolli, H.M., Saunders, J.B., and Perch-Nielsen, K. (Eds.), *Plankton Stratigraphy*: Cambridge (Cambridge Univ. Press), 427–554.
- Pujol, C., and Bourrouilh, R., 1991. Late Miocene to Holocene planktonic foraminifers from the subantarctic South Atlantic. *In* Ciesielski, P.F., Kristoffersen, Y., et al., *Proc. ODP, Sci. Results*, 114: College Station, TX (Ocean Drilling Program), 217–232.
- Qvale, G., and Spiegler, D., 1989. The stratigraphic significance of *Bolboforma* (algae, Chrysophyta) in Leg 104 samples from the Vøring Plateau. *In* Eldholm, O., Thiede, J., Taylor, E., et al., *Proc. ODP, Sci. Results*, 104: College Station, TX (Ocean Drilling Program), 487–495.
- Rade, J., 1977. Tertiary biostratigraphic zonation based on calcareous nannoplankton in eastern Australia nearshore basins. *Micropaleontology*, 23:270–296.
- Raffi, I., Backman, J., Rio, D., and Shackleton, N.J., 1993. Plio-Pleistocene nannofossil biostratigraphy and calibration to oxygen isotopes stratigraphies from Deep Sea Drilling Project Site 607 and Ocean Drilling Program Site 677. *Paleoceanography*, 8:387–408.
- Rider, M., 1990. Gamma-ray log shape used as a facies indicator: critical analysis of an oversimplified method. *In* Hurst, A., Lovell, M.A., and Morton, A.C. (Eds.), *Geological Application of Wireline Logs II*. Geol. Soc. Spec. Publ. London, 48:27–37.
- , 1996. *The Geological Interpretation of Well Logs*: Caithness (Whittles Publishing).
- Salimullah, A.R.M., and Stow, D.A.V., 1992. Application of FMS images in poorly recovered coring intervals: examples from ODP Leg 129. *In* Hurst, A., Griffiths, C.M., and Worthington, P.F. (Eds.), *Geological Application of Wireline Logs II*. Geol. Soc. Spec. Publ. London, 65:71–86.
- Sanfilippo, A., and Nigrini, C., 1998. Code numbers for Cenozoic low latitude radiolarian biostratigraphic zones and GPTS conversion tables. *Mar. Micropaleontol.*, 33:109–156.
- Sato, T., and Kameo, K., 1996. Pliocene to Quaternary calcareous nannofossil biostratigraphy of the Arctic Ocean, with reference to late Pliocene glaciation. *In* Thiede, J., Myhre, A.M., Firth, J.V., Johnson, G.L., and Ruddiman, W.F. (Eds.), *Proc. ODP, Sci. Results*, 151: College Station, TX (Ocean Drilling Program), 39–59.
- Schneider, R.R., Cramp, A., Damuth, J.E., Hiscott, R.N., Kowsmann, R.O., Lopez, M., Nanayama, F., Normark, W.R., and Shipboard Scientific Party, 1995. Color-reflectance measurements obtained from Leg 155 cores. *In* Flood, R.D., Piper, D.J.W., Klaus, A., et al., *Proc. ODP, Init. Repts.*, 155: College Station, TX (Ocean Drilling Program), 697–700.
- Schultheiss, P.J., and McPhail, S.D., 1989. An automated P-wave logger for recording fine-scale compressional wave velocity structures in sediments. *In* Ruddiman, W., Sarnthein, M., et al., *Proc. ODP, Sci. Results*, 108: College Station, TX (Ocean Drilling Program), 407–413.


- Scott, G.H., Bishop, S., and Burt, B.J., 1990. *Guide to Some Neogene Globorotalids (Foraminiferida) from New Zealand*. N. Z. Geol. Surv. Paleontol. Bull., 61:1–135.
- Scott, G.H., Nelson, C.S., and Stone, H.H., 1995. Planktic foraminiferal events in early Miocene zones N6 and N7 at southwest Pacific DSDP site 593: relation with climatic changes in oxygen isotope zone Mi1b. *Mar. Micropaleontol.*, 25:29–45.
- Serra, O., 1984. *Fundamentals of Well-Log Interpretation* (Vol. 1): *The Acquisition of Logging Data*: Dev. Pet. Sci., 15A: Amsterdam (Elsevier).
- , 1986. *Fundamentals of Well-Log Interpretation* (Vol. 2): *The Interpretation of Logging Data*. Dev. Pet. Sci., 15B.
- , 1989. *Formation MicroScanner Image Interpretation*: Houston (Schlumberger Educ. Services), SMP-7028.
- Serra, O., and Sulpice, L., 1975. Sedimentological analysis of shale-sand series from well logs. *Trans. SPWLA 16th Ann. Logging Symp.*, pap. W.
- Shane, P., Froggatt, P., Black, T., and Westgate, J., 1995. Chronology of Pliocene and Quaternary bioevents and climatic events from fission-track ages on tephra beds, Wairarapa, New Zealand. *Earth Planet. Sci. Lett.*, 130:141–154.
- Shipboard Scientific Party, 1988. Explanatory notes. In Barker, P.F., Kennett, J.P., et al., *Proc. ODP, Init. Repts.*, 113: College Station, TX (Ocean Drilling Program), 13–32.
- , 1995. Explanatory notes. In Shipley, T.H., Ogawa, Y., Blum, P., et al., *Proc. ODP, Init. Repts.*, 156: College Station, TX (Ocean Drilling Program), 39–68.
- , 1999. Explanatory notes. In Gersonde, R., Hodell, D.A., Blum, P., et al. *Proc. ODP, Init. Repts.*, 177, 1–57 [CD-ROM]: College Station, TX (Ocean Drilling Program).
- Spezzaferri, S., and Spiegler, D., 1998. *Bolboforma* biostratigraphy from the southeast Greenland Margin, Hole 918D. In Saunders, A.D., Larsen, H.C., and Wise, S.W., Jr. (Eds.), *Proc. ODP, Sci. Results*, 152: College Station, TX (Ocean Drilling Program), 201–208.
- Spiegler, D., 1991. Occurrence of *Bolboforma* (algae, Chrysophyta) in the subantarctic (Atlantic) Paleogene. In Ciesielski, P.F., Kristoffersen, Y., et al., *Proc. ODP, Sci. Results*, 114: College Station, TX (Ocean Drilling Program), 325–334.
- , in press. *Bolboforma* biostratigraphy from the Hatton-Rockall Basin (North Atlantic). In Raymo, M.E., Jansen, E., Blum, P., and Herbert, T.D. (Eds.), *Proc. ODP, Sci. Results*, 162: College Station, TX (Ocean Drilling Program).
- Stott, L.D., and Kennett, J.P., 1990. Antarctic Paleogene planktonic foraminifer biostratigraphy: ODP Leg 113, Sites 689 and 690. In Barker, P.F., Kennett, J.P., et al., *Proc. ODP, Sci. Results*, 113: College Station, TX (Ocean Drilling Program), 549–569.
- Takemura, A., 1992. Radiolarian Paleogene biostratigraphy in the southern Indian Ocean, Leg 120. In Wise, S.W., Jr., Shlich, R., et al., *Proc. ODP, Sci. Results*, 120: College Station, TX (Ocean Drilling Program), 735–756.
- Thomas, E., 1990. Late Cretaceous through Neogene deep-sea benthic foraminifers (Maud Rise, Weddell Sea, Antarctica). In Barker, P.F., Kennett, J.P., et al., *Proc. ODP, Sci. Results*, 113: College Station, TX (Ocean Drilling Program), 571–594.
- Thomas, E., Barrera, E., Hamilton, N., Huber, B.T., Kennett, J.P., O'Connell, S.B., Pospichal, J.J., Speiß, V., Stott, L.D., Wei, W., and Wise, S.W., Jr., 1990. Upper Cretaceous-Paleogene stratigraphy of Sites 689 and 690, Maud Rise (Antarctica). In Barker, P.F., Kennett, J.P., et al., *Proc. ODP, Sci. Results*, 113: College Station, TX (Ocean Drilling Program), 901–914.
- Timur, A., and Toksöz, M.N., 1985. Downhole geophysical logging. *Annu. Rev. Earth Planet. Sci.*, 13:315–344.
- Tittman, J., 1986. *Geophysical Well Logging*: London (Academic Press).
- van Morkhoven, F.P.C.M., Berggren, W.A., and Edwards, A.S., 1986. Cenozoic cosmopolitan deep-water benthic foraminifera. *Bull. Cent. Rech. Explor.—Prod. Elf-Aquitaine*, Mem. 11.
- Wei, W., 1992. Paleogene chronology of Southern Ocean drill holes: an update. In Kennett, J.P., and Warnke, D.A. (Eds.), *The Antarctic Paleoenvironment: a Perspective on Global Change*. *Antarct. Res. Ser.*, 56:75–96.



- Wei, W., Pospichal, J.J., and Wise, S.W., Jr., 1993. Cenozoic calcareous nannofossil magnetobiochronology of the Southern Ocean. *In* Hamršmid, B., and Young, J.R. (Eds.), *Nannoplankton Research*. Proc. 4th INA Conf., 2:93–104.
- Wentworth, C.K., 1922. A scale of grade and class terms of clastic sediments. *J. Geol.*, 30:377–392.

Figure F1. Coring and depth intervals.



 Represents recovered material

**BOTTOM FELT:** distance from rig floor to seafloor

**TOTAL DEPTH:** distance from rig floor to bottom of hole (sub-bottom bottom)

**PENETRATION:** distance from seafloor to bottom of hole (sub-bottom bottom)

**NUMBER OF CORES:** total of all cores recorded, including cores with no recovery

**TOTAL LENGTH**

**OF CORED SECTION:** distance from sub-bottom top to sub-bottom bottom minus drilled (but not cored) areas in between

**TOTAL CORE RECOVERED:** total from adding a, b, c, and d in diagram

**CORE RECOVERY (%):** equals TOTAL CORE RECOVERED divided by TOTAL LENGTH OF CORED SECTION times 100

Figure F2. Examples of numbered core sections.

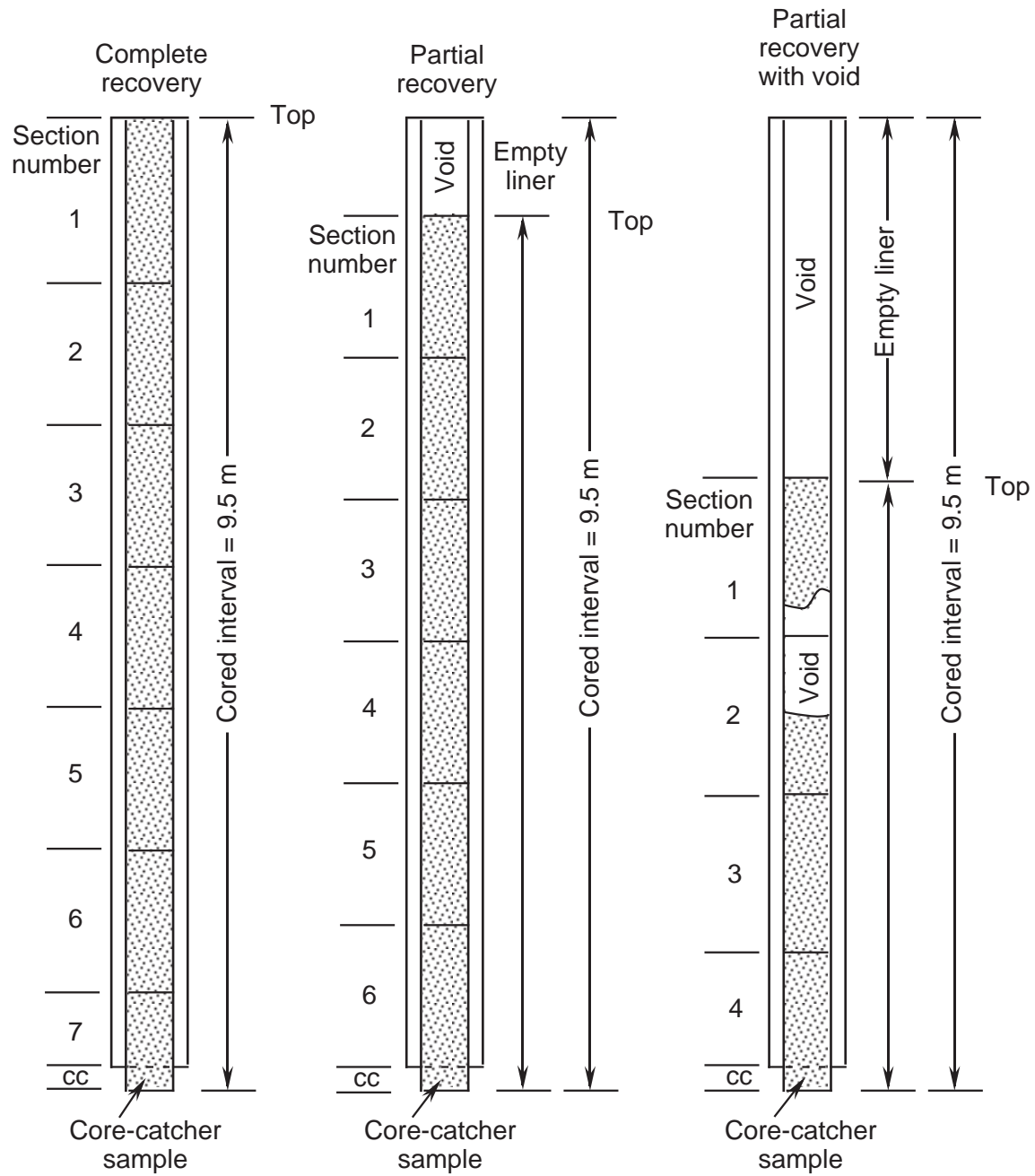


Figure F3. Diagram outlining the classes of granular sediments (modified from Mazzullo et al., 1987).

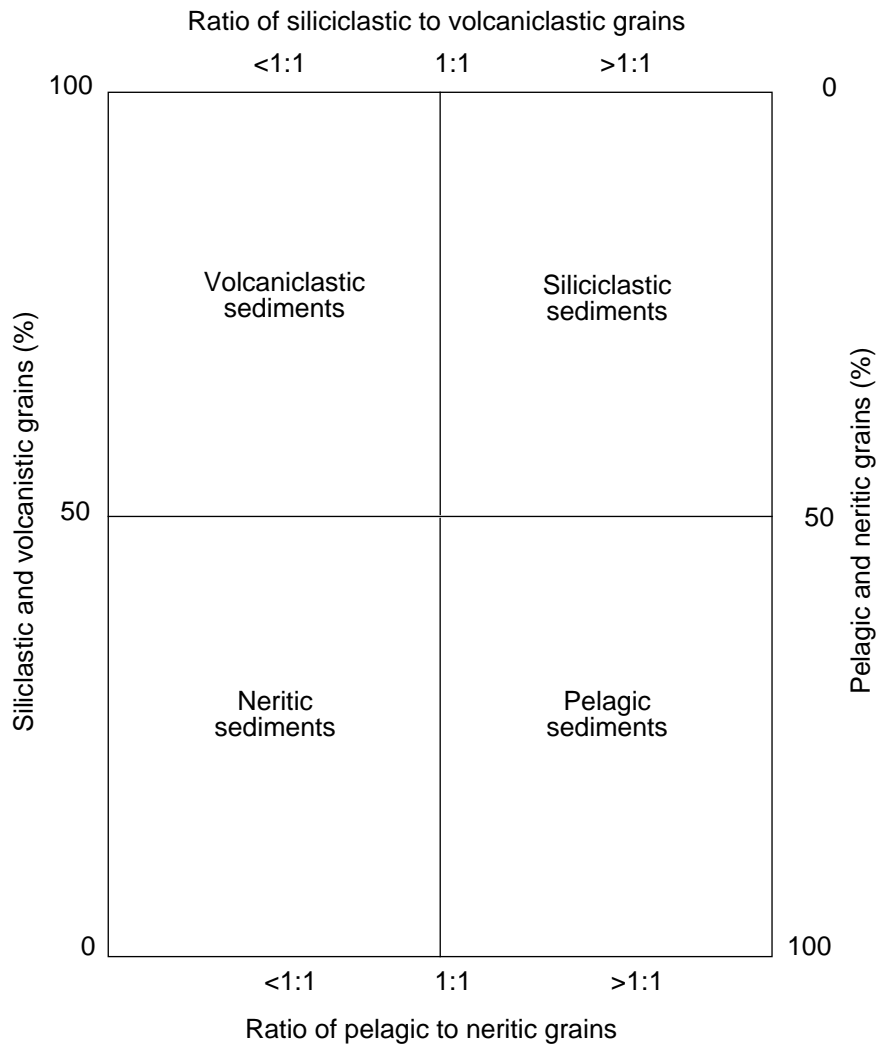


Figure F4. Ternary diagram showing the principal names of the siliciclastic sediments.

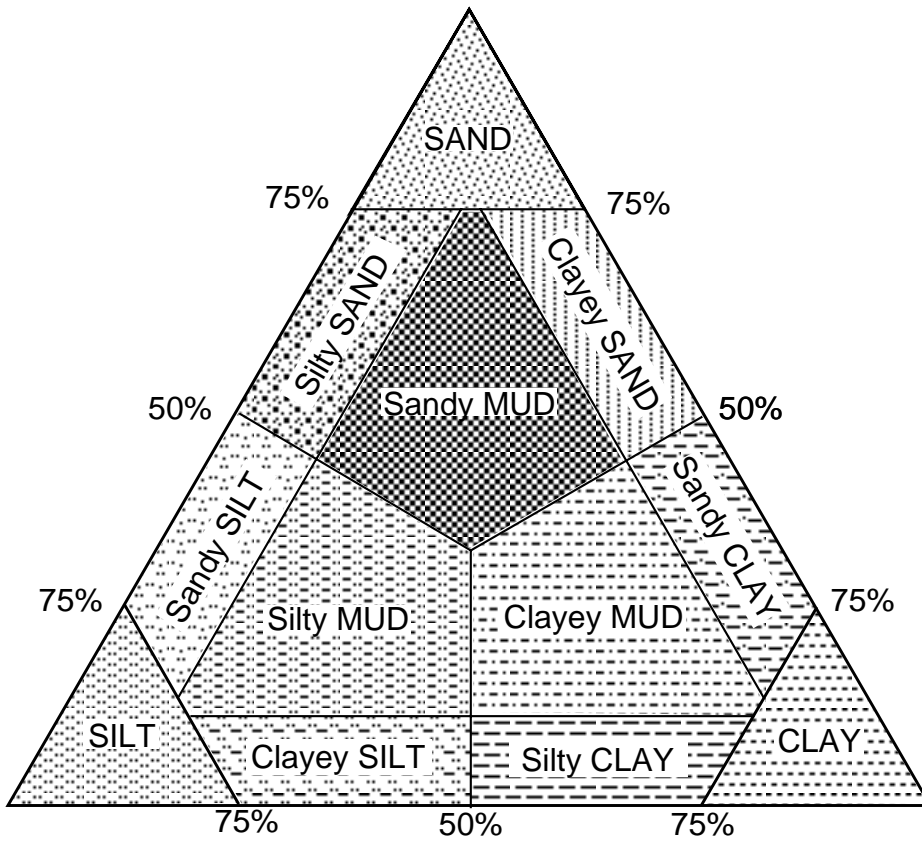
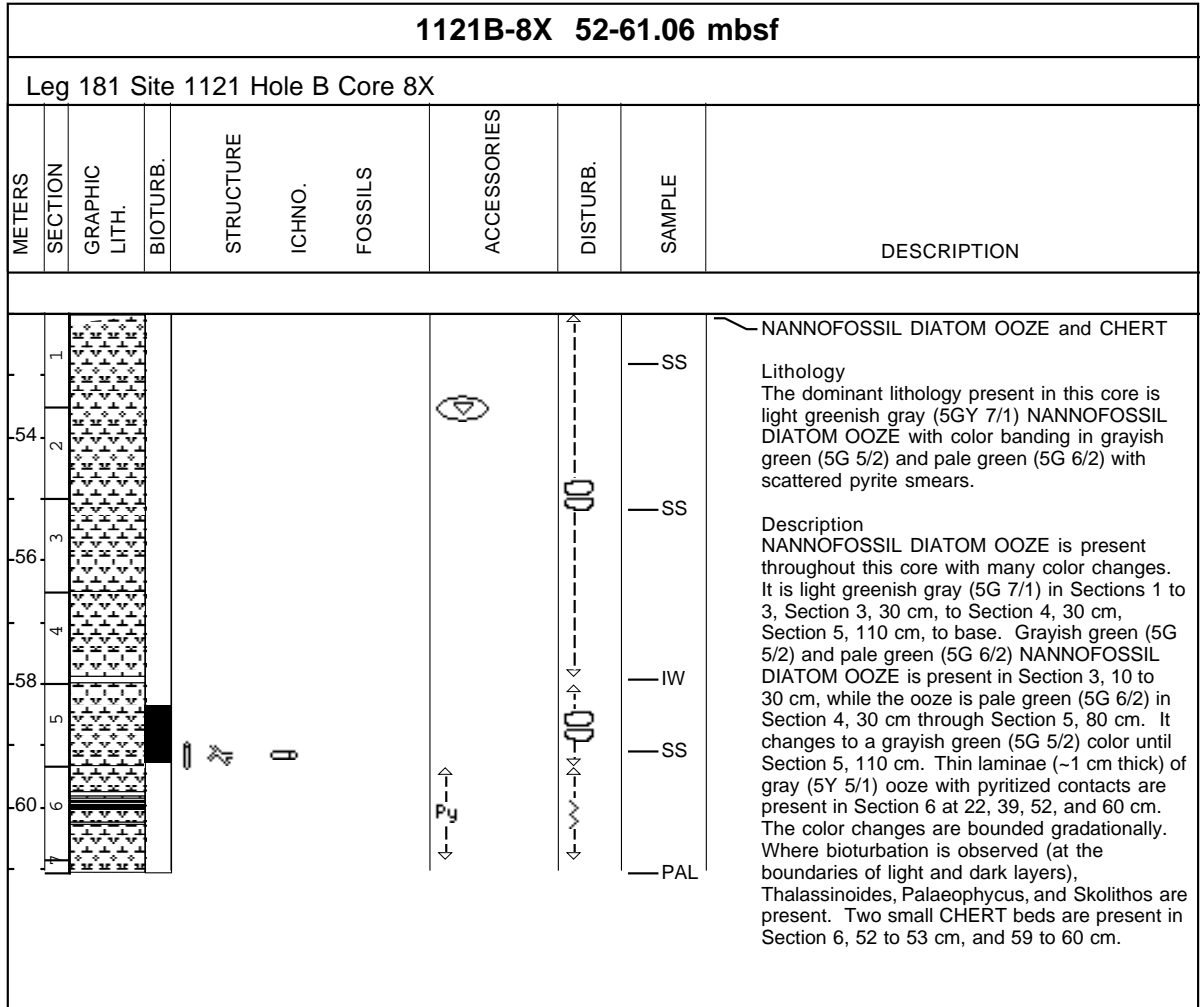


Figure F5. Example of a core description “barrel sheet” generated on Leg 181. The key to the graphic textures and symbols is presented in Figure F6, p. 45.





**Figure F6.** Graphic textures and symbols used for the core description “barrel sheets” and the Summary Graphic Lithology column of figures in the “Lithostratigraphy” sections in each site chapter.

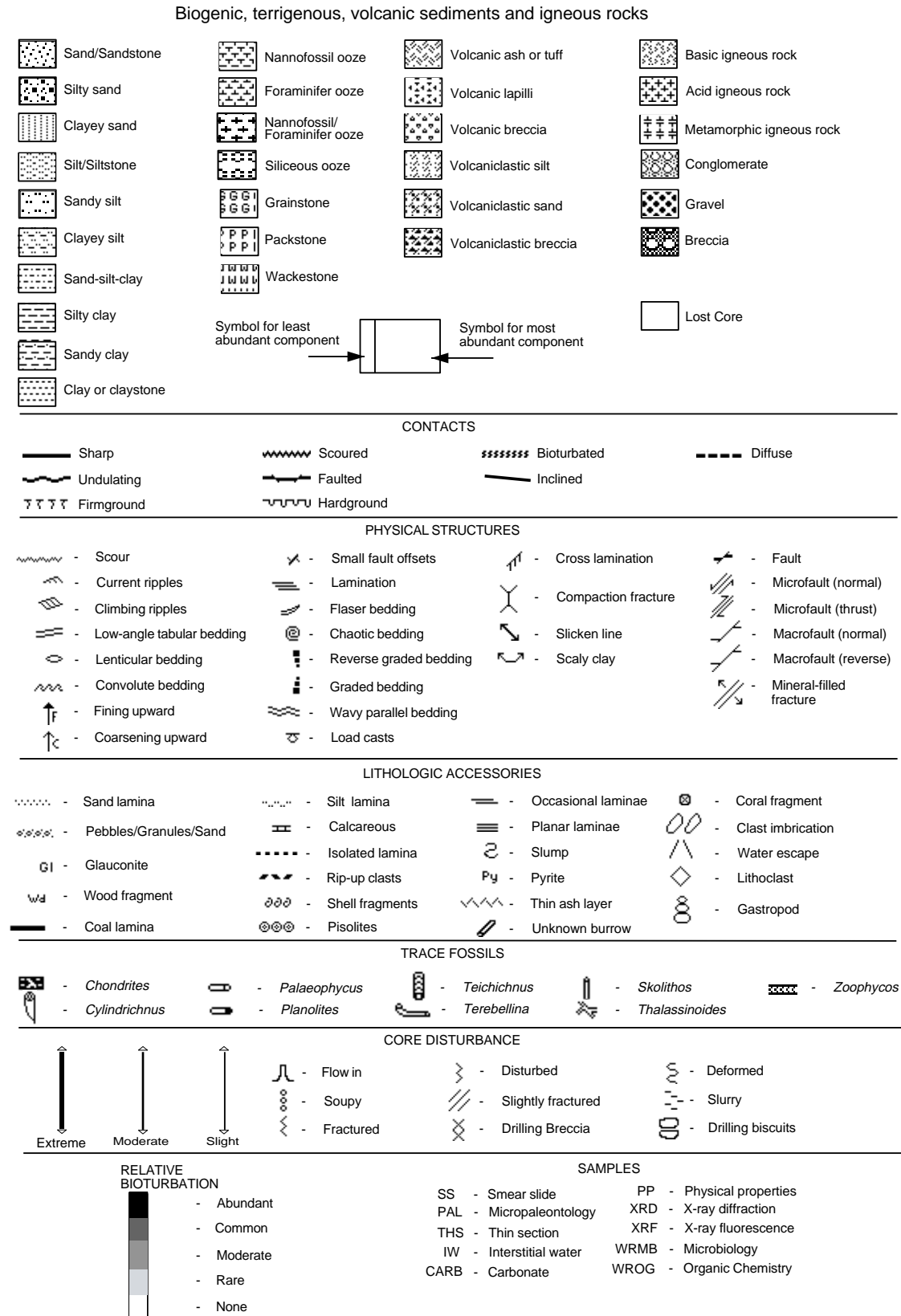


Figure F7. Combined calcareous nannofossil, planktonic foraminiferal, diatom and radiolarian biostratigraphic zonal schemes tied to the geomagnetic polarity time scale (Berggren et al., 1995b) and the New Zealand and European stages used during Leg 181 for the New Zealand region. The gray shaded area spanning the interval 55.5–54.6 Ma indicates the current range of differing usages of the Paleocene–Eocene boundary (after Berggren et al., 1995, p. 139). (Continued on next two pages.)

Ma	Chronos	Polarity	Epoch	Inter-national Series	New Zealand		Ma	Planktonic Foraminifer Zones	Calcareous Nannofossil Zones
					Stage	Series			
0.5 1 1.5 2 2.5 3 3.5 4 4.5 5	C1n		PLEISTOCENE	LATE	HAWERAN (Wq)	WANGANUI	0.34	<i>Gr. truncatulinoides</i>	NN21
		1 r	EARLY	CALABRIAN	Putikian (Wcp)	Hautawan (Wnh)	1.07	<i>Gr. crassula</i>	NN19
	C1r	1r			CASTLECLIFFIAN (Wc)				
		2r	LATE	GELASIAN	Marahanan (Wnm)	Mangapanian (Wm)	2.58	dextral <i>Gr. crassaformis</i>	NN18
	C2n	1 r			PIACENZIAN				
		2r	Waipipian (Wp)	3.60		<i>Gr. inflata</i>	NN17		
		3n	EARLY		ZANCLEAN			OPOITIAN (Wo)	5.2
		4n		TARANAKI		KAPITEAN (Tk) early	5.5		
			LATE		MESSINIAN			TONGAPORUTUAN late	6.6
		EARLY		ZANCLEAN		OPOITIAN (Wo)	5.2		
			LATE		TARANAKI			KAPITEAN (Tk) early	5.5
		EARLY		ZANCLEAN		OPOITIAN (Wo)	5.2		
			LATE		TARANAKI			KAPITEAN (Tk) early	5.5
		EARLY		ZANCLEAN		OPOITIAN (Wo)	5.2		
			LATE		TARANAKI			KAPITEAN (Tk) early	5.5
		EARLY		ZANCLEAN		OPOITIAN (Wo)	5.2		
			LATE		TARANAKI			KAPITEAN (Tk) early	5.5
		EARLY		ZANCLEAN		OPOITIAN (Wo)	5.2		
			LATE		TARANAKI			KAPITEAN (Tk) early	5.5
		EARLY		ZANCLEAN		OPOITIAN (Wo)	5.2		
			LATE		TARANAKI			KAPITEAN (Tk) early	5.5
		EARLY		ZANCLEAN		OPOITIAN (Wo)	5.2		
			LATE		TARANAKI			KAPITEAN (Tk) early	5.5
		EARLY		ZANCLEAN		OPOITIAN (Wo)	5.2		
			LATE		TARANAKI			KAPITEAN (Tk) early	5.5
		EARLY		ZANCLEAN		OPOITIAN (Wo)	5.2		
			LATE		TARANAKI			KAPITEAN (Tk) early	5.5
		EARLY		ZANCLEAN		OPOITIAN (Wo)	5.2		
			LATE		TARANAKI			KAPITEAN (Tk) early	5.5
		EARLY		ZANCLEAN		OPOITIAN (Wo)	5.2		
			LATE		TARANAKI			KAPITEAN (Tk) early	5.5
		EARLY		ZANCLEAN		OPOITIAN (Wo)	5.2		
			LATE		TARANAKI			KAPITEAN (Tk) early	5.5
		EARLY		ZANCLEAN		OPOITIAN (Wo)	5.2		
			LATE		TARANAKI			KAPITEAN (Tk) early	5.5
		EARLY		ZANCLEAN		OPOITIAN (Wo)	5.2		
			LATE		TARANAKI			KAPITEAN (Tk) early	5.5
		EARLY		ZANCLEAN		OPOITIAN (Wo)	5.2		
			LATE		TARANAKI			KAPITEAN (Tk) early	5.5
		EARLY		ZANCLEAN		OPOITIAN (Wo)	5.2		
			LATE		TARANAKI			KAPITEAN (Tk) early	5.5
		EARLY		ZANCLEAN		OPOITIAN (Wo)	5.2		
			LATE		TARANAKI			KAPITEAN (Tk) early	5.5
		EARLY		ZANCLEAN		OPOITIAN (Wo)	5.2		
			LATE		TARANAKI			KAPITEAN (Tk) early	5.5
		EARLY		ZANCLEAN		OPOITIAN (Wo)	5.2		
			LATE		TARANAKI			KAPITEAN (Tk) early	5.5
		EARLY		ZANCLEAN		OPOITIAN (Wo)	5.2		
			LATE		TARANAKI			KAPITEAN (Tk) early	5.5
		EARLY		ZANCLEAN		OPOITIAN (Wo)	5.2		
			LATE		TARANAKI			KAPITEAN (Tk) early	5.5
		EARLY		ZANCLEAN		OPOITIAN (Wo)	5.2		
			LATE		TARANAKI			KAPITEAN (Tk) early	5.5
		EARLY		ZANCLEAN		OPOITIAN (Wo)	5.2		
			LATE		TARANAKI			KAPITEAN (Tk) early	5.5
		EARLY		ZANCLEAN		OPOITIAN (Wo)	5.2		
			LATE		TARANAKI			KAPITEAN (Tk) early	5.5
		EARLY		ZANCLEAN		OPOITIAN (Wo)	5.2		
			LATE		TARANAKI			KAPITEAN (Tk) early	5.5
		EARLY		ZANCLEAN		OPOITIAN (Wo)	5.2		
			LATE		TARANAKI			KAPITEAN (Tk) early	5.5
		EARLY		ZANCLEAN		OPOITIAN (Wo)	5.2		
			LATE		TARANAKI			KAPITEAN (Tk) early	5.5
		EARLY		ZANCLEAN		OPOITIAN (Wo)	5.2		
			LATE		TARANAKI			KAPITEAN (Tk) early	5.5
		EARLY		ZANCLEAN		OPOITIAN (Wo)	5.2		
			LATE		TARANAKI			KAPITEAN (Tk) early	5.5
		EARLY		ZANCLEAN		OPOITIAN (Wo)	5.2		
			LATE		TARANAKI			KAPITEAN (Tk) early	5.5
		EARLY		ZANCLEAN		OPOITIAN (Wo)	5.2		
			LATE		TARANAKI			KAPITEAN (Tk) early	5.5
		EARLY		ZANCLEAN		OPOITIAN (Wo)	5.2		
			LATE		TARANAKI			KAPITEAN (Tk) early	5.5
		EARLY		ZANCLEAN		OPOITIAN (Wo)	5.2		
			LATE		TARANAKI			KAPITEAN (Tk) early	5.5
		EARLY		ZANCLEAN		OPOITIAN (Wo)	5.2		
			LATE		TARANAKI			KAPITEAN (Tk) early	5.5
		EARLY		ZANCLEAN		OPOITIAN (Wo)	5.2		
			LATE		TARANAKI			KAPITEAN (Tk) early	5.5
		EARLY		ZANCLEAN		OPOITIAN (Wo)	5.2		
			LATE		TARANAKI			KAPITEAN (Tk) early	5.5
		EARLY		ZANCLEAN		OPOITIAN (Wo)	5.2		
			LATE		TARANAKI			KAPITEAN (Tk) early	5.5
		EARLY		ZANCLEAN		OPOITIAN (Wo)	5.2		
			LATE		TARANAKI			KAPITEAN (Tk) early	5.5
		EARLY		ZANCLEAN		OPOITIAN (Wo)	5.2		
			LATE		TARANAKI			KAPITEAN (Tk) early	5.5
		EARLY		ZANCLEAN		OPOITIAN (Wo)	5.2		
			LATE		TARANAKI			KAPITEAN (Tk) early	5.5
		EARLY		ZANCLEAN		OPOITIAN (Wo)	5.2		
			LATE		TARANAKI			KAPITEAN (Tk) early	5.5
		EARLY		ZANCLEAN		OPOITIAN (Wo)	5.2		
			LATE		TARANAKI			KAPITEAN (Tk) early	5.5
		EARLY		ZANCLEAN		OPOITIAN (Wo)	5.2		
			LATE		TARANAKI			KAPITEAN (Tk) early	5.5
		EARLY		ZANCLEAN		OPOITIAN (Wo)	5.2		
			LATE		TARANAKI			KAPITEAN (Tk) early	5.5
		EARLY		ZANCLEAN		OPOITIAN (Wo)	5.2		
			LATE		TARANAKI			KAPITEAN (Tk) early	5.5
		EARLY		ZANCLEAN		OPOITIAN (Wo)	5.2		
			LATE		TARANAKI			KAPITEAN (Tk) early	5.5
		EARLY		ZANCLEAN		OPOITIAN (Wo)	5.2		
			LATE		TARANAKI			KAPITEAN (Tk) early	5.5
		EARLY		ZANCLEAN		OPOITIAN (Wo)	5.2		
			LATE		TARANAKI			KAPITEAN (Tk) early	5.5
		EARLY		ZANCLEAN		OPOITIAN (Wo)	5.2		
			LATE		TARANAKI			KAPITEAN (Tk) early	5.5
		EARLY		ZANCLEAN		OPOITIAN (Wo)	5.2		
			LATE		TARANAKI			KAPITEAN (Tk) early	5.5
		EARLY		ZANCLEAN		OPOITIAN (Wo)	5.2		
			LATE		TARANAKI			KAPITEAN (Tk) early	5.5
		EARLY		ZANCLEAN		OPOITIAN (Wo)	5.2		
			LATE		TARANAKI			KAPITEAN (Tk) early	5.5
		EARLY		ZANCLEAN		OPOITIAN (Wo)	5.2		
			LATE		TARANAKI			KAPITEAN (Tk) early	5.5
		EARLY		ZANCLEAN		OPOITIAN (Wo)	5.2		
			LATE		TARANAKI			KAPITEAN (Tk) early	5.5
		EARLY		ZANCLEAN		OPOITIAN (Wo)	5.2		
			LATE		TARANAKI			KAPITEAN (Tk) early	5.5
		EARLY		ZANCLEAN		OPOITIAN (Wo)	5.2		

Figure F7 (continued).

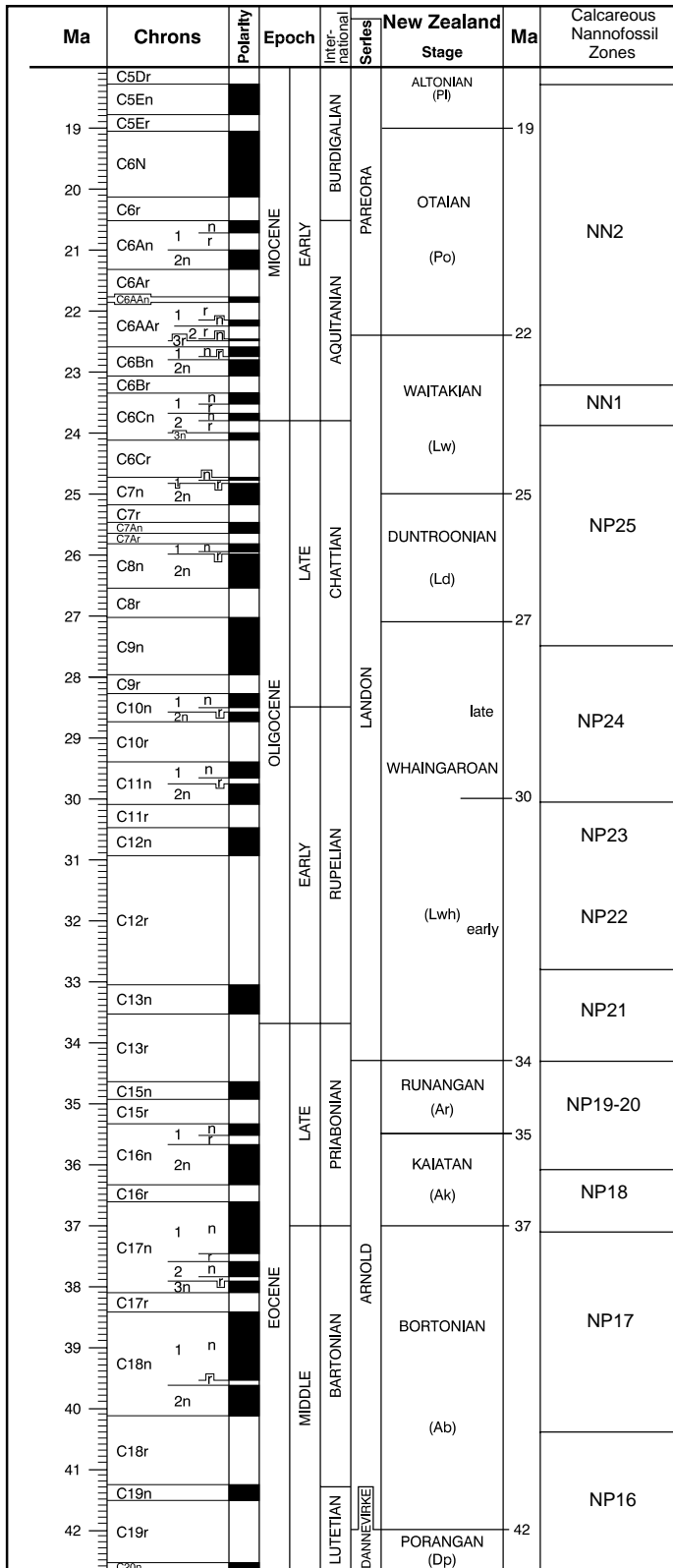


Figure F7 (continued).

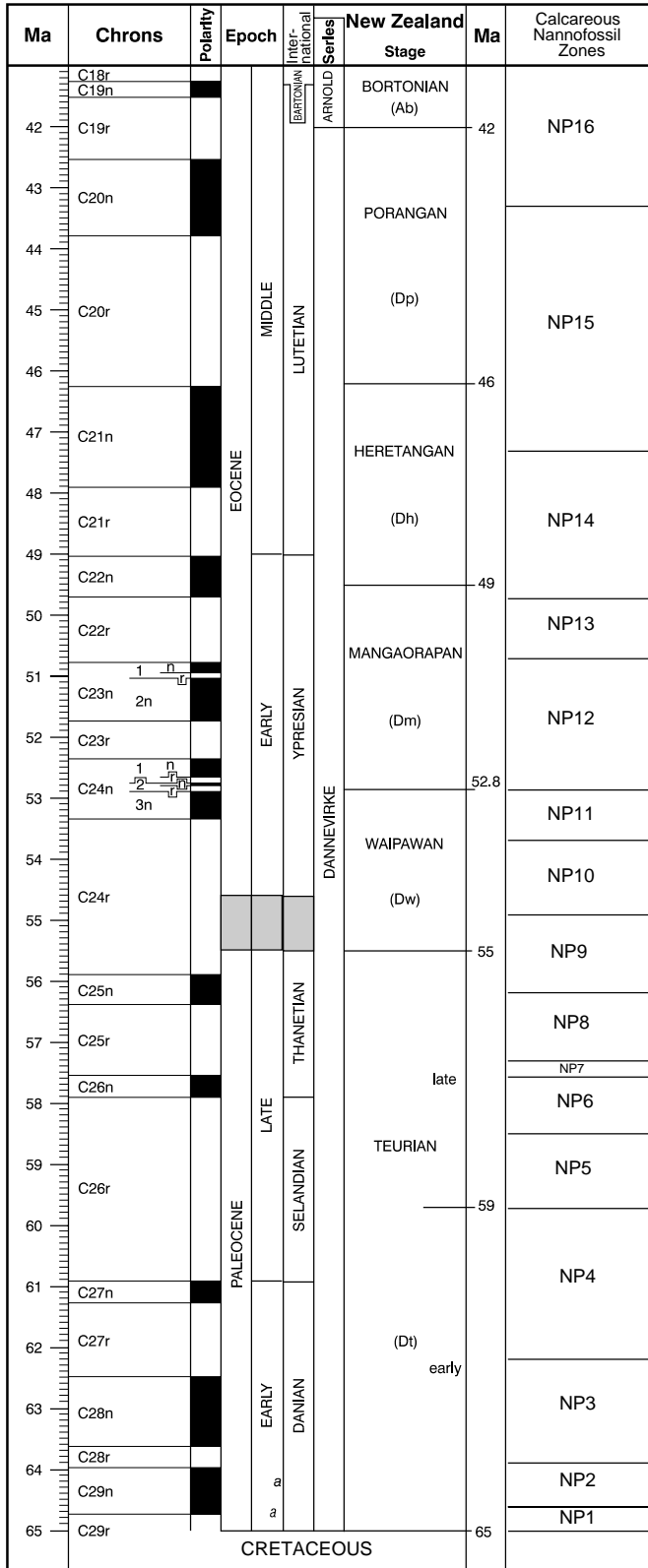




Figure F9. Latitudinal ranges of Holocene planktonic foraminifers around New Zealand used in the interpretation of paleo-sea-surface water masses (from Hayward, 1983).

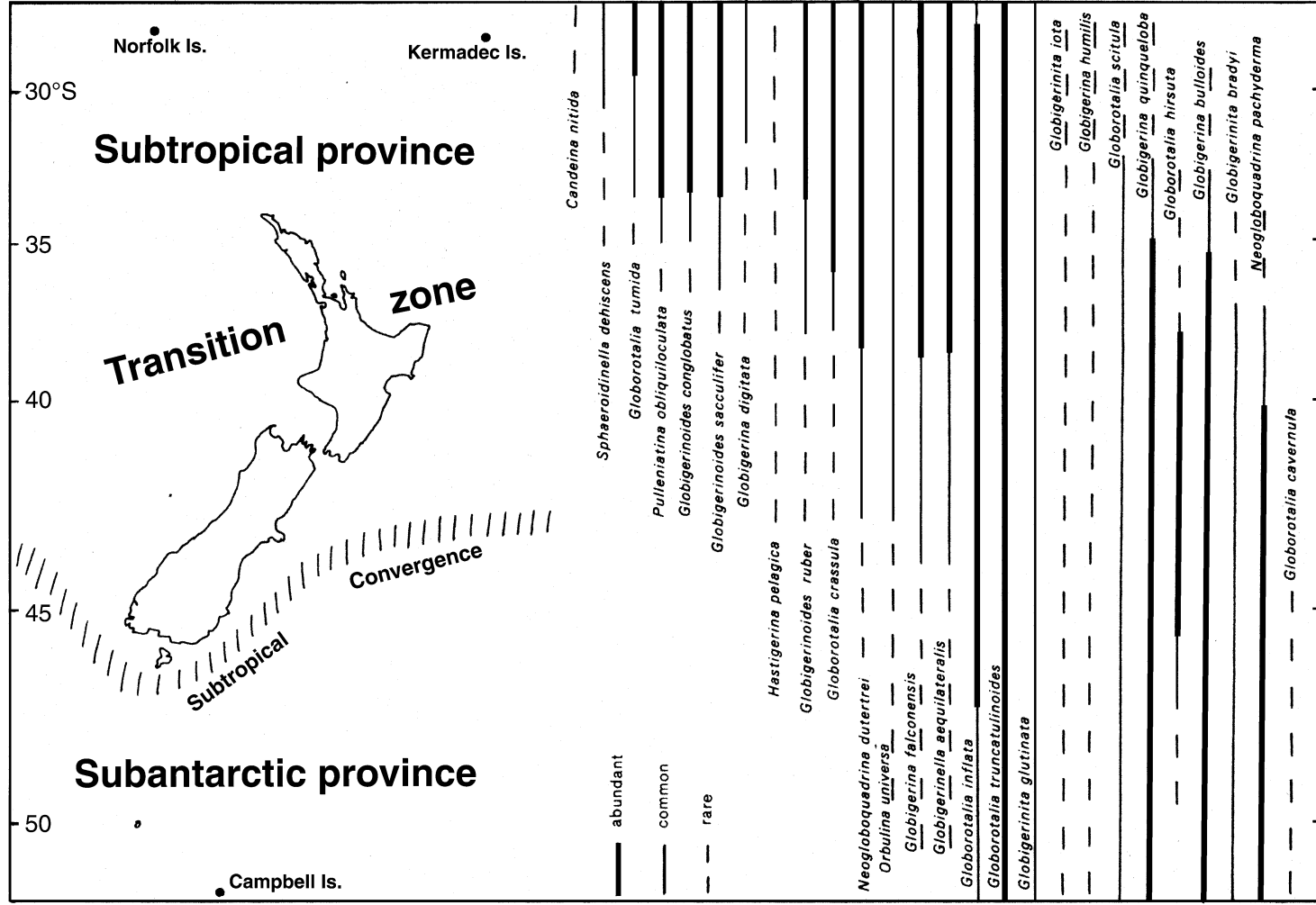




Figure F10. Cenozoic radiolarian biostratigraphic zonation schemes tied to the geomagnetic polarity time scale (Berggren et al., 1995b) and the New Zealand stages, which were used during Leg 181. The gray shaded area spanning the interval 55.5–54.6 Ma indicates the current range of differing usages of the Paleocene–Eocene boundary (after Berggren et al., 1995, p. 139). (Continued on next two pages.)

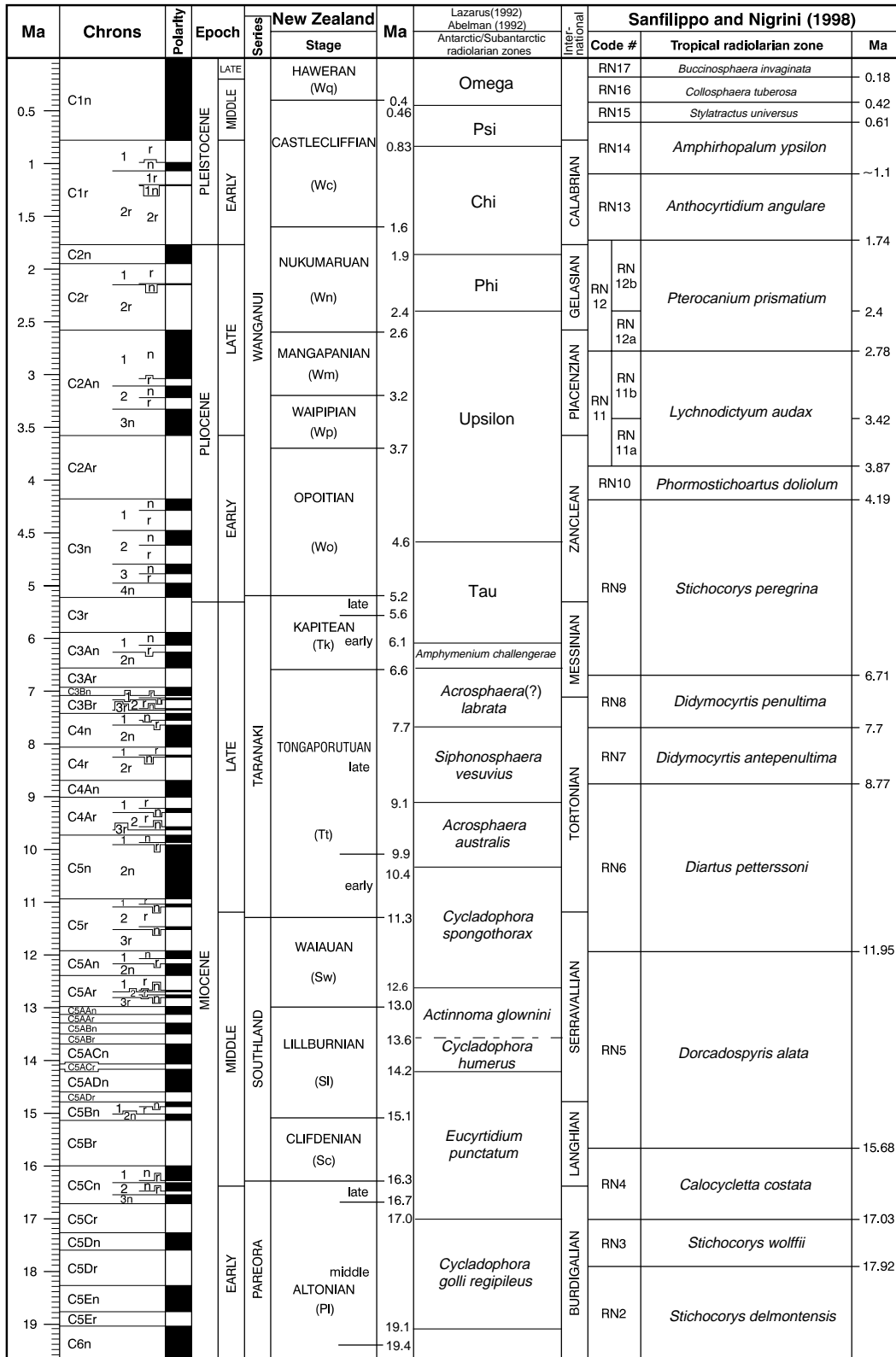


Figure F10 (continued).

Ma	Chron	Polarity	Epoch	New Zealand		Ma	Takemura (1992) Abelman (1992), Hollis(1977) South Pacific radiolarian zone	Inter- national	Sanfilippo and Nigrini (1998)										
				Series	Stage				Code #	Tropical radiolarian zone	Ma								
19	C5Dr		MIOCENE	PAREORA	middle	19.4	<i>Cycladophora golli regipileus</i>	BURDIGALIAN	RN2	<i>Stichocorys delmontensis</i>									
	C5En				ALTONIAN (Pl)														
	C5Er				early														
20	C6N				EARLY	PAREORA		20.2	<i>Cyrtocapsella longithorax</i>	BURDIGALIAN	RN2	<i>Stichocorys delmontensis</i>	20.53						
	C6r																		
21	C6An	1 n 2n					MIOCENE	PAREORA		22.4	<i>Cycladophora antiqua</i>	AQUITANIAN	RN1	<i>Cyrtocapsella tetrapera</i>	23.62				
	C6Ar								OTAIAN (Po)										
22	C6AAr	1 r 2n							EARLY	PAREORA		22.5	<i>Cycladophora antiqua</i>	AQUITANIAN	RN1	<i>Cyrtocapsella tetrapera</i>	23.62		
	C6Bn																		
23	C6Br										MIOCENE	PAREORA		25.0	<i>Lychnocanoma conica</i>	AQUITANIAN	RN1	<i>Cyrtocapsella tetrapera</i>	23.62
	C6Cn		WAITAKIAN (Lw)																
24	C6Cr		EARLY	PAREORA										25.0	<i>Lychnocanoma conica</i>	AQUITANIAN	RN1	<i>Cyrtocapsella tetrapera</i>	23.62
	C7n																		
25	C7r				MIOCENE	PAREORA								27.1	<i>Lychnocanoma conica</i>	AQUITANIAN	RN1	<i>Cyrtocapsella tetrapera</i>	23.62
	C7An																		
26	C7Ar						EARLY	PAREORA						27.5	<i>Lychnocanoma conica</i>	AQUITANIAN	RN1	<i>Cyrtocapsella tetrapera</i>	23.62
	C8n												DUNTRONIAN (Ld)						
27	C8r								MIOCENE	PAREORA				27.5	<i>Lychnocanoma conica</i>	AQUITANIAN	RN1	<i>Cyrtocapsella tetrapera</i>	23.62
	C9n																		
28	C9r										LATE	LANDON		30.0	<i>Axoprunum(?) irregularis</i>	RUPELIAN	RP20	<i>Theocyrtis tuberosa</i>	~28.8
	C10n												late						
29	C10r		EARLY	LANDON										30.0	<i>Axoprunum(?) irregularis</i>	RUPELIAN	RP20	<i>Theocyrtis tuberosa</i>	~28.8
	C11n												WHAINGAROAN						
30	C11r				MIOCENE	LANDON								33.0	<i>Eucyrtidium spinosum</i>	PRIABONIAN	RP18	<i>Calocyclus bandyca</i>	~36.4
	C12n																		
31	C12r						EARLY	LANDON						33.0	<i>Eucyrtidium spinosum</i>	PRIABONIAN	RP18	<i>Calocyclus bandyca</i>	~36.4
	C13n												(Lwh) early						
32	C13r								MIOCENE	LANDON				34.3	<i>Eucyrtidium spinosum</i>	PRIABONIAN	RP19	<i>Cryptocarpium ornatum</i>	~32.8
	C15n																		
33	C15r										LATE	ARNOLD		35.5	<i>Eucyrtidium spinosum</i>	PRIABONIAN	RP18	<i>Calocyclus bandyca</i>	~36.4
	C16n												RUNANGAN (Ar)						
34	C16r		EARLY	ARNOLD										37.0	<i>Lithapium mitra</i>	BARTONIAN	RP17	<i>Cryptocarpium azyx</i>	~37.7
	C17n												KAIATAN (Ak)						
35	C17r				MIOCENE	ARNOLD								39.0	<i>Eusyringium fistuligerum</i>	BARTONIAN	RP16	<i>Podocyrtis goetheana</i>	~38.8
	C18n												BORTONIAN						
36	C18r						MIDDLE	DANNEVIKRE						39.0	<i>Eusyringium fistuligerum</i>	BARTONIAN	RP15	<i>Podocyrtis chalara</i>	~39.5
	C19n																		
37	C19r								EARLY	DANNEVIKRE				42.0	<i>Eusyringium lagena</i>	LUTETIAN	RP14	<i>Podocyrtis mitra</i>	
	C20n												PORANGAN (Dp)						



Figure F11. A. A 32-m interval of magnetic susceptibility records from three holes at Site 1123 on the meters below seafloor (mbsf) scale. Records from different holes are offset for convenience. Matching features in adjacent holes are not aligned. B. Example of the composite section for this interval. The same records as in (A) on the meters composite depth (mcd) scale with magnetic susceptibility features aligned.

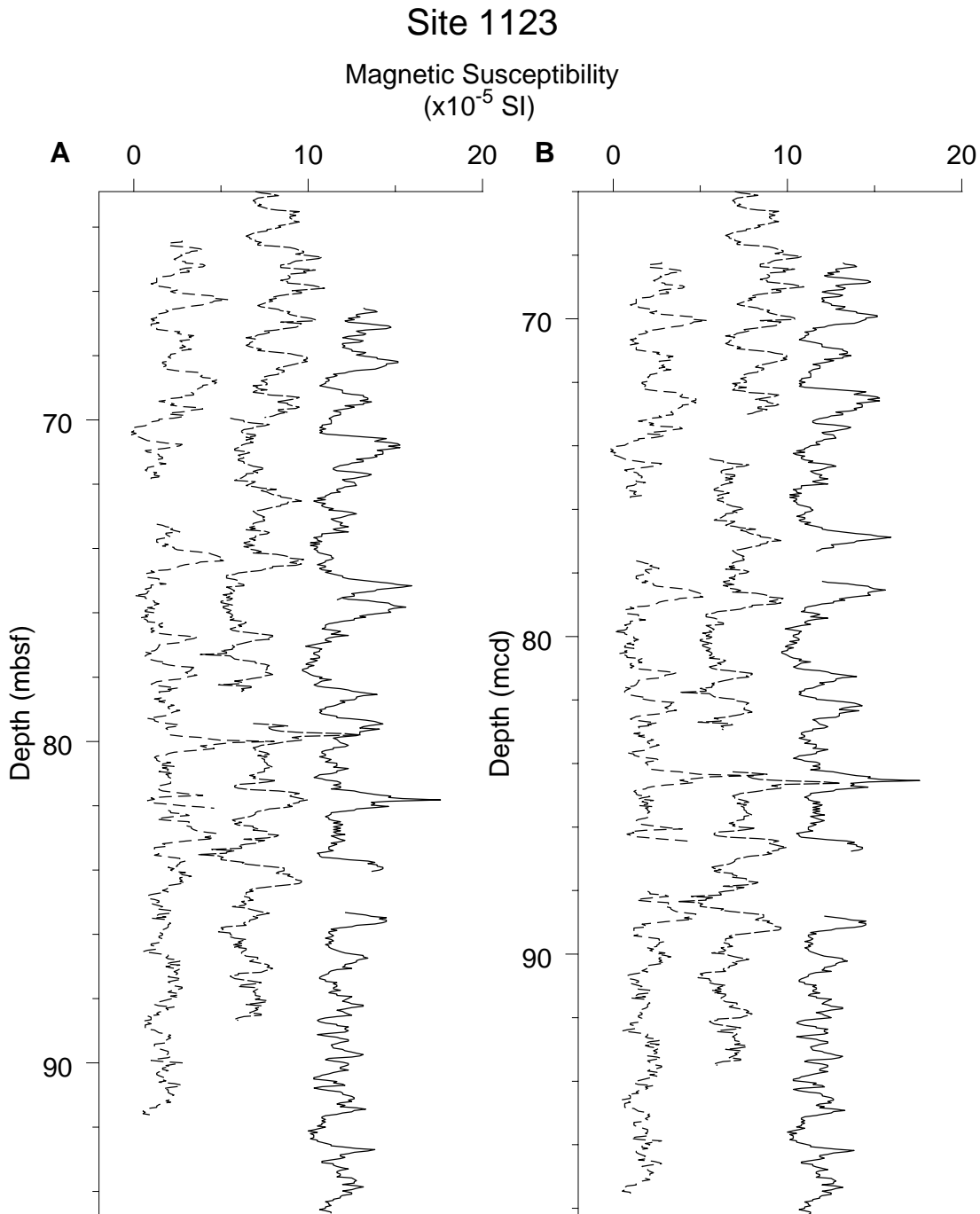


Figure F12. A. Magnetic susceptibility records from Holes 1123B and 1123C on the meters composite depth scale with splice tie points (horizontal lines) between holes. Solid curves indicate the portion of each core used in the splice. B8 indicates Core 181-1123B-8H. B. The resulting spliced magnetic susceptibility record.

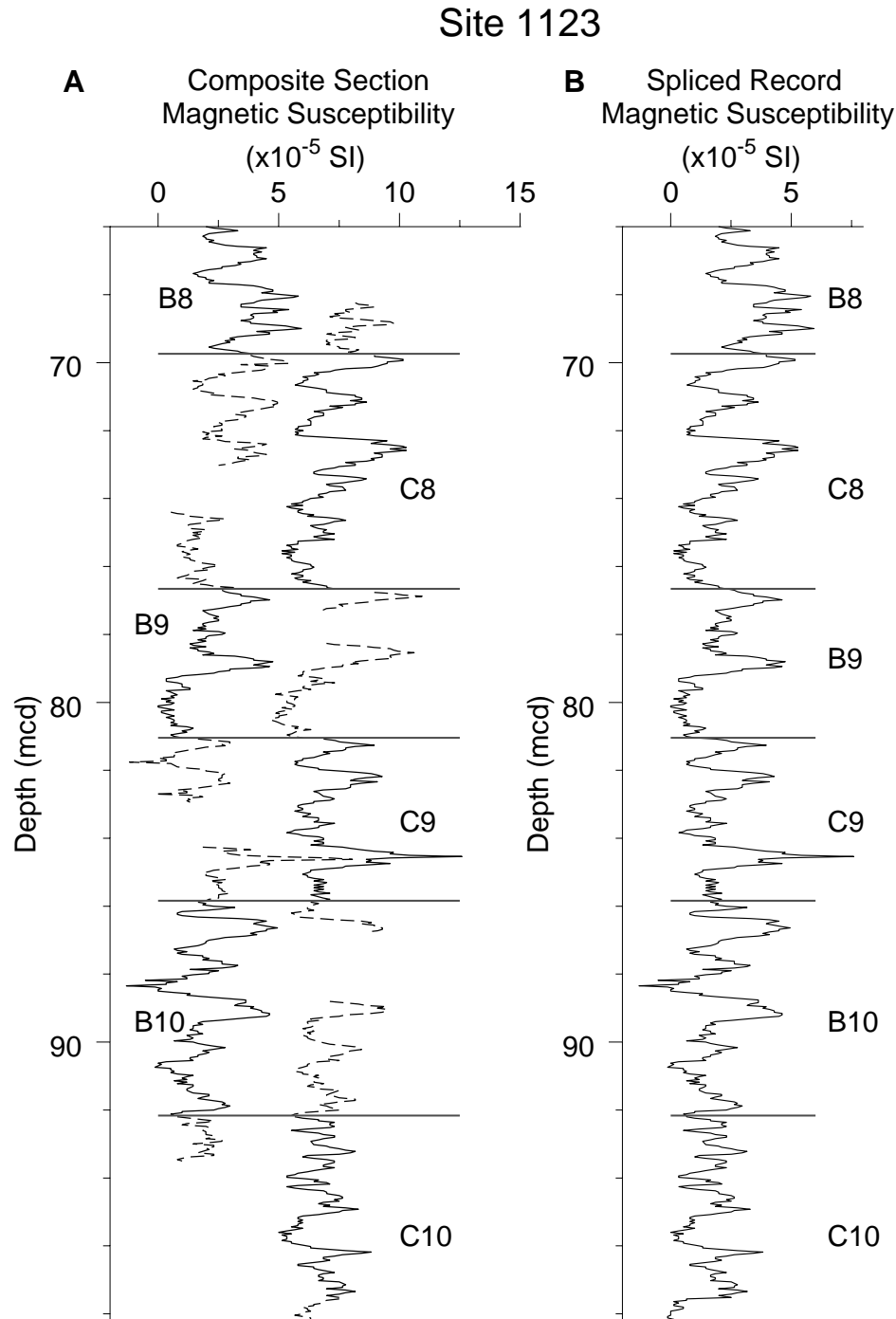


Figure F13. ODP tool strings used during Leg 181.

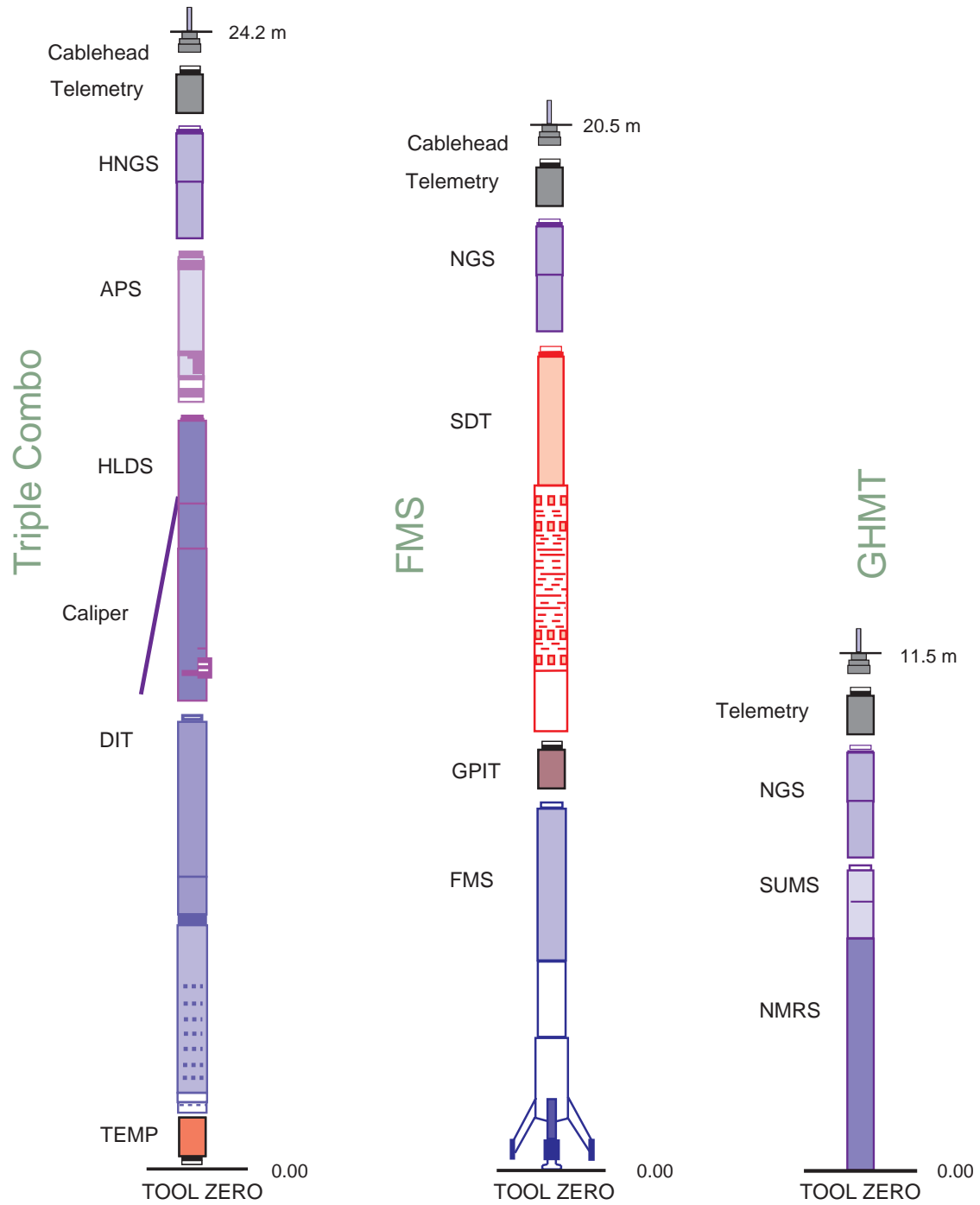
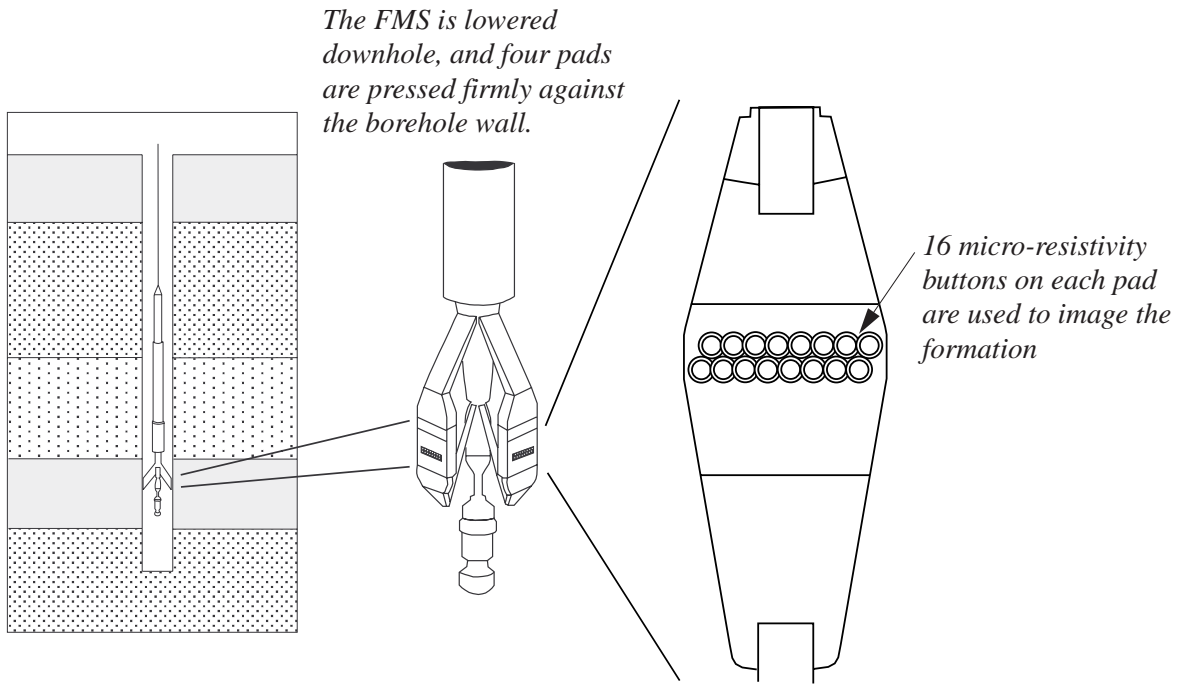


Figure F14. Schematic diagram showing the basic principles of the Formation MicroScanner (FMS).





**Table T1.** Outline of granular sediment classification scheme.

Sediment class	Major modifier	Principal name	Minor modifier
Pelagic sediment	1. Composition of pelagic grains present in major amounts.	1. Ooze 2. Chalk 3. Limestone 4. Radiolarite	1. Composition of pelagic grains present in minor amounts.
	2. Size and shape of clastic grains present in major amounts.	5. Diatomite 6. Spiculite 7. Chert	2. Size and shape of clastic grains present in minor amounts.
Siliciclastic sediment	1. Composition of all grains present in major amounts.	1. Gravel 2. Sand	1. Composition of all grains present in minor amounts.
	2. Grain shape (optional).	3. Silt	2. Size and shape and composition of siliciclastic grains present as matrix (coarse-grained clastic sediments only).
	3. Sediment color (optional).	4. Clay	
Volcaniclastic sediment	1. Composition of volcaniclasts present in major amounts.	1. Breccia	1. Composition of all volcaniclasts present in minor amounts.
	2. Composition of all pelagic grains present in major amounts.	2. Lapilli	2. Composition of all pelagic grains present in minor amounts.
	3. Size and shape of siliciclastic grains present in major amounts.	3. Tephra	3. Size and shape of siliciclastic grains present in minor amounts.

Note: This table is also available in [ASCII format](#).

Table T2. Calcareous nannofossil datums used during Leg 181.

Age (Ma)	Nannofossil events	References
0.085	Bottom acme <i>Emiliana huxleyi</i>	Berggren et al. (1995a)
0.16	LO <i>Helicosphaera inversa</i>	Sato and Kameo (1996)
0.24	FO <i>Emiliana huxleyi</i>	Naish et al. (1998)
0.42	LO <i>Pseudoemiliana lacunosa</i>	Sato and Kameo (1996)
0.78	Top acme <i>Gephyrocapsa parallela</i>	Matsuoka and Okada (1989)
0.85	LO <i>Reticulofenestra asanoi</i>	Sato and Kameo (1996)
0.90	Top dominance <i>Gephyrocapsa</i> (small)	Young et al. (1994)
0.95	FO <i>Gephyrocapsa parallela</i>	Sato and Kameo (1996)
1.14	Bottom dominance <i>Gephyrocapsa</i> (small)	Young et al. (1994)
1.16	FO <i>Reticulofenestra asanoi</i>	Sato and Kameo (1996)
1.20	LO <i>Gephyrocapsa</i> (large)	Sato and Kameo (1996)
1.26	LO <i>Helicosphaera sellii</i>	Sato and Kameo (1996)
1.44	FO <i>Gephyrocapsa</i> (large)	Sato and Kameo (1996)
1.60	LO <i>Calcidiscus macintyreii</i>	Raffi et al. (1993)
1.67	FO <i>Gephyrocapsa</i> (medium)	Raffi and Flores (1995)
1.96	LO <i>Discoaster brouweri</i>	Raffi and Flores (1995)
2.30	LO <i>Discoaster pentaradiatus</i>	Wei (1993)
2.61	LO <i>Discoaster surculus</i>	Raffi and Flores (1995)
2.76	LO <i>Discoaster tamalis</i>	Raffi and Flores (1995)
3.54	LO <i>Sphenolithus neoabies</i>	Spencer-Cervato et al. (1994)
3.82	LO <i>Reticulofenestra pseudoumbilicus</i>	Raffi and Flores (1995)
~3.88	Acme <i>Gephyrocapsa</i> (small)	Rio (1992)
4.0	FO <i>Pseudoemiliana lacunosa</i>	Gartner (1990)
4.13	FO <i>Discoaster asymmetricus</i>	Shackleton et al. (1995)
5.56	LO <i>Discoaster quinqueramus</i>	Raffi and Flores (1995)
7.39	FO <i>Amaurolithus primus</i>	Backman and Raffi (1997)
7.73	LO <i>Minylitha convallis</i>	Shackleton et al. (1995)
9.34	FO <i>Minylitha convallis</i>	Raffi and Flores (1995)
9.64	LO <i>Cantinaster calyculus</i>	Backman and Raffi (1997)
10.5	FO <i>Discoaster bellus</i>	Gartner (1992)
10.79	FO <i>Cantinaster coalitus</i>	Backman and Raffi (1997)
10.94	LO <i>Coccolithus miopelagicus</i>	Backman and Raffi (1997)
12.34	FO <i>Calcidiscus macintyreii</i>	Raffi and Flores (1995)
12.65	LO <i>Calcidiscus premacintyreii</i>	Raffi and Flores (1995)
13.19	LO <i>Cyclicargolithus floridanus</i>	Raffi and Flores (1995)
13.52	LO <i>Sphenolithus heteromorphus</i>	Backman and Raffi (1997)
16.21	LO acme <i>Discoaster deflandrei</i>	Raffi and Flores (1995)
17.40	FO <i>Calcidiscus premacintyreii</i>	Backman and Raffi (1997)
17.80	LO <i>Sphenolithus dissimilis</i>	Gartner (1992)
18.20	FO <i>Calcidiscus leptoporus</i>	Gartner (1992)
18.30	LO <i>Sphenolithus belemnus</i>	Berggren et al. (1995b)
18.60	FO <i>Sphenolithus heteromorphus</i>	Backman et al. (1990)
19.20	FO <i>Sphenolithus belemnus</i>	Berggren et al. (1995b)
19.80	FO <i>Geminolithella rotula</i>	Young et al. (1994)
22.30	LO <i>Ilseolithina fusa</i>	Gartner (1992)
23.20	FO <i>Discoaster druggii</i>	Berggren et al. (1995b)
23.6	LO <i>Sphenolithus umbrellus</i>	Berggren et al. (1995b)
23.9	LO <i>Dictyococcites bisectus</i>	Berggren et al. (1995b)
24.3	LO <i>Sphenolithus delphix</i>	Berggren et al. (1995b)
26.1	LO <i>Chiasmolithus altus</i>	Berggren et al. (1995b)
27.5	FO <i>Sphenolithus distentus</i>	Berggren et al. (1995b)
31.3	LO <i>Reticulofenestra umbilicus</i>	Morgans et al. (1996)
32.8	LO <i>Ericsonia formosa</i>	Berggren et al. (1995b)
33.30	Acme <i>Clausicoccus subdistichus</i>	Berggren et al. (1995b)
~34.6	LO <i>Discoaster saipanensis</i>	Berggren et al. (1995b)
35.5	FO <i>Isthmolithus recurvus</i>	Morgans et al. (1996)
38.0	FO <i>Dictyococcites bisectus</i>	Berggren et al. (1995b)
58.3	LO <i>Hornibrookina teuriensis</i>	Berggren et al. (1995b)
59.7	FO <i>Fasciculites tympaniformis</i>	Morgans et al. (1996)
60.6	FO <i>Sphenolithus primus</i>	Berggren et al. (1995b)
60.7	FO <i>Chiasmolithus bidens</i>	Berggren et al. (1995b)
64.5	FO <i>Cruciplacolithus tenuis</i>	Berggren et al. (1995b)
64.9	FO <i>Hornibrookina teuriensis</i>	Berggren et al. (1995b)
65.0	LO <i>Micula</i> spp.	Berggren et al. (1995b)

Note: This table is also available in [ASCII format](#).

Table T3. Foraminiferal and bolboformid datums used during Leg 181. (See table note. Continued on next two pages.)

Age (Ma)	NZ stage	Foraminiferal event	References
~0.2	Wq	FO <i>Globorotalia cavemula</i>	Hornibrook (1982)
0.34	Wc/Wq	Boundary	Naish et al. (1998)
0.45	Wc	FO <i>Globorotalia hirsuta</i>	Pujol & Duprat (1983)
0.62	Wc	LO <i>Plectofrondicularia advena</i> , <i>P. pellucida</i>	Weinholz & Lutze (1989)
~0.6	Wc	LO <i>Globorotalia puncticuloides</i>	Hornibrook (1982); Hornibrook & Jenkins (1994), modified this leg
~0.7	Wc	FCO <i>Globorotalia inflata</i> in subantarctic	Hornibrook & Jenkins (1994), modified this leg
~0.7	Wc	LCO <i>Globorotalia puncticuloides</i>	Hornibrook & Jenkins (1994), modified this leg
~0.8	Wc	FO <i>Globorotalia truncatulinoidea</i> in subantarctic	Scott et al. (1990); Hornibrook & Jenkins (1994), modified this leg
~1	Wc	LO <i>Globorotalia tosaensis</i> s.s. morphotypes	Scott et al. (1990)
1.07	Wn/Wc	Boundary	Naish et al. (1998)
~1.1	Wn/Wc	LO <i>Haeslerella pliocenica</i>	Hornibrook et al. (1990)
1.81		Pliocene/Pleistocene boundary	Ogg et al. (1998)
2.1	Wn	LO <i>Globorotalia crassaformis</i> (dextral)	Morgans et al. (1996)
~2.5	Wn	FO <i>Globorotalia crassaformis</i>	Scott et al. (1990)
2.58	Wm/Wn	Boundary	Morgans et al. (1996); Naish et al. (1998)
2.6	Wm/Wn	FO <i>Globorotalia crassula</i>	Scott et al. (1990); Hornibrook et al. (1989)
3.0	Wp/Wm	Boundary	Morgans et al. (1996)
3.0	Wp/Wm	FO <i>Globorotalia crassaformis</i> (dextral)	Morgans et al. (1996)
3.0	Wp/Wm	FO <i>Globorotalia tosaensis</i>	Scott et al. (1990)
3.0	Wp/Wm	LO <i>Globorotalia crassaconica</i>	Scott et al. (1990)
3.2	Wp	LO <i>Globorotalia praehirsuta</i>	Scott et al. (1990)
3.4	Wp	LO <i>Globorotalia subconomiozea</i>	Scott et al. (1990); Hornibrook (1982)
3.4	Wp	LO <i>Globorotalia pliozea</i>	Hornibrook (1982)
3.6	u Wp	FO <i>Globorotalia puncticuloides</i>	Scott et al. (1990)
3.6	Wp	FO <i>Globorotalia praehirsuta</i>	Scott et al. (1990)
3.6	Wo/Wp	Boundary	Morgans et al. (1996)
3.6	Wo/Wp	LO <i>Hopkinsina mioindex</i>	Hornibrook et al. (1989); Boersma (1986)
3.6	Wo/Wp	LO <i>Uvigerina hispida</i>	Hornibrook et al. (1989); Boersma (1986)
3.6	Wo/Wp	FO <i>Globorotalia inflata triangula</i>	Scott et al. (1990)
3.6	Wo/Wp	LCO <i>Globorotalia pliozea</i>	Scott et al. (1990)
3.7	Wo	FO <i>Globorotalia inflata</i>	Morgans et al. (1996)
3.7	Wo	LO <i>Globorotalia puncticulata</i> s.s.	Scott et al. (1990)
4.2	Wo	LO <i>Zeaglobigerina nepenthes</i>	Berggren et al. (1996)
4.3	Wo	LO <i>Globorotalia margaritae</i>	Ogg et al. (1998)
~4.7	Wo	FO <i>Globorotalia crassaconica</i>	Scott et al. (1990)
~4.8	Wo	LO <i>Globorotalia mons</i>	Scott et al. (1990)
5.2		Miocene/Pliocene boundary	
5.2	Tk/Wo	Boundary	Morgans et al. (1996)
5.2	Tk/Wo	FO <i>Globorotalia puncticulata</i> s.s.	Morgans et al. (1996)
5.2	Tk/Wo	LO <i>Globorotalia sphericomiozea</i>	Scott et al. (1990); Hornibrook and Jenkins (1994)
5.2	Tk/Wo	LO <i>Globorotalia juanai</i>	Scott et al. (1990)
5.2	Tk/Wo	FO <i>Globorotalia crassaformis</i>	Scott et al. (1990)
5.4	Tk/Wo	FO <i>Globorotalia margaritae</i>	Scott et al. (1990); Srinivasan and Sinha (1992)
5.4	Tk	FO <i>Globorotalia pliozea</i>	Scott et al. (1990)
5.5	Tk	FO <i>Globorotalia mons</i>	Scott et al. (1990)
5.6	l/u Tk	FO <i>Globorotalia sphericomiozea</i>	Morgans et al. (1996); Roberts et al. (1994)
5.6	l/u Tk	LO <i>Globorotalia miotumida</i>	Morgans et al. (1996)
~6.6	Tt/Tk	Boundary	Morgans et al. (1996)
~6.6	Tt/Tk	FO <i>Bolivinita pliozea</i>	Morgans et al. (1996)
~6.6	u Tk	FO <i>Globorotalia juanai</i>	Scott et al. (1990)
~7	u Tk	LO <i>Bolboforma pentaspinoso</i>	Grützmacher (1993)
~8	u Tt	LO <i>Rectuvigerina ongleyi</i>	Boersma (1986); Hornibrook et al. (1989)
9.2	Tt	FCO <i>Neogloboquadrina pachyderma</i>	Berggren (1992)
9.9	u/l Tt	LO <i>Globoquadrina dehiscens</i>	Morgans et al. (1996); Wright and Vella (1988); M. Crundwell, p.c. (1999)
10.0	l Tt	LO <i>Globorotalia miotumida</i> (dextral)	M. Crundwell, p.c. (1999)
10.1	l Tt	FO <i>Globorotalia miotumida</i> (dextral) (Tukemokihī coiling event)	M. Crundwell, p.c. (1999)
~10.3	l Tt	LO <i>Globorotalia panda</i>	Scott et al. (1990); Scott (1995)
~10.5	l Tt	LO <i>Orbulina suturalis</i>	Jenkins (1967)
~10.7	l Tt	LO <i>Globorotalia miotumida</i> (dextral)	Scott (1995); M. Crundwell, p.c. (1999)
~10.5	l Tt	LO <i>Bolboforma subfragoris</i>	Grützmacher (1993)
~11	lTt	LO <i>Neogloboquadrina continua</i>	Kennett & Srinivasan (1983)
10.9	l Tt	FO <i>Globorotalia miotumida</i> (dextral) (Kaiti event)	Scott (1995); M. Crundwell, p.c. (1999)
10.9	l Tt	LO <i>Paragloborotalia mayeri</i>	Scott (1995); M. Crundwell, p.c. (1999)
11.3	Sw/Tt	FO <i>Neogloboquadrina pachyderma</i>	Hornibrook et al. (1989); Scott, p.c. (1999)
11.3	Sw/Tt	Boundary	Morgans et al. (1996)
11.3	Sw/Tt	FO <i>Bolivinita pohana</i>	Morgans et al. (1996)
11.5	u Sw	FO <i>Bolboforma pentaspinoso</i>	Grützmacher (1993)

Table T3 (continued).

Age (Ma)	NZ stage	Foraminiferal event	References
11.5	u Sw	FO <i>Bolboforma subfragoris</i>	Grützmacher (1993)
11.5	u Sw	FO <i>Globorotalia scitula</i>	Scott et al. (1990)
11.8	u Sw	FO <i>Globigerina nepenthes</i>	Ogg et al. (1998)
13	SI/Sw	Boundary	Morgans et al. (1996)
13	SI/Sw	LO <i>Globorotalia conica</i>	Morgans et al. (1996); Scott (1991)
13	SI/Sw	LO <i>Globorotalia amuria</i>	Morgans et al. (1996); Scott (1991)
13	SI/Sw	LO <i>Fohsella peripheroronda</i>	Morgans et al. (1996); Scott (1991)
13.2	SI	FCO <i>Paragloborotalia mayeri</i> s.s.	Scott (1991); Scott et al. (1990)
~13.2	SI	FO <i>Globorotalia miotumida</i>	Scott et al. (1990)
~13.2	SI	LO <i>Globorotalia praemenardii</i>	Scott et al. (1990)
~13.2	SI	LO <i>Globigerinoides bisphericus</i>	Hornibrook et al. (1989)
~14.5	I SI	FO <i>Orbulina universa</i>	Scott, p.c. (1999)
14.8	I SI	LO <i>Praeorbulina glomerosa</i>	Berggren et al. (1995)
14.8	I SI	LO <i>Praeorbulina circularis</i>	Kennett and Srinivasan (1983)
15	SI	FO <i>Globorotalia panda</i>	Scott et al. (1990)
15.1	Sc/SI	Boundary	Morgans et al. (1996)
15.1	Sc/SI	FO <i>Orbulina suturalis</i>	Berggren et al. (1995); Morgans et al. (1996)
~15.1	Sc	LO <i>Rectuvigerina rerensis</i>	Hornibrook et al. (1989); Boersma (1986)
15.6	mSc	FO <i>Praeorbulina circularis</i>	Jenkins (1967); Kennett and Srinivasan (1983)
15.8	Sc	FO <i>Globorotalia praemenardii</i>	Scott et al. (1990)
15.9	Sc	LO <i>Globorotalia miozea</i> s.s.	Scott et al. (1990); Berggren (1992)
~16	Sc	FO <i>Globorotalia conica</i>	Scott et al. (1990)
16	Sc	FO <i>Paragloborotalia mayeri</i>	Scott et al. (1991)
16.3	PI/Sc	Boundary	Morgans et al. (1996)
16.3	PI/Sc	FO <i>Praeorbulina curva</i>	Berggren et al. (1985); Morgans et al. (1996)
16.3	PI/Sc	LO <i>Globorotalia zealandica</i>	Scott et al. (1990)
16.3	PI/Sc	LO <i>Paragloborotalia bella</i>	Scott et al. (1990)
16.4	u PI	FO <i>Planulina wuellerstorfi</i>	Boersma (1986)
16.4	u PI	LO <i>Catapsydrax stainforthi</i>	Kennett and Srinivasan (1983)
16.7	m/u PI	FO <i>Globorotalia miozea</i>	Morgans et al. (1996)
16.7	m/u PI	LO <i>Globorotalia praescitula</i>	Scott et al. (1990)
16.7	m/u PI	LCO <i>Globorotalia zealandica</i>	Scott et al. (1990)
~17	u PI	FO <i>Globigerinoides bisphericus</i>	Hornibrook et al. (1989)
~17	u PI	FO <i>Fohsella peripheroronda</i>	Scott et al. (1990)
~17	m PI	Reappearance <i>Globoquadrina dehiscens</i>	Scott et al. (1995)
~17.8	m PI	LO <i>Catapsydrax dissimilis</i>	Morgans et al., unpubl. data
~18.5	m PI	FO <i>Sphaeroidinellopsis disjuncta</i>	Hornibrook et al. (1989)
~18.6	l/m PI	Local disappearance <i>Globoquadrina dehiscens</i>	Scott et al. (1995)
18.6	l/m PI	FO <i>Globorotalia zealandica</i>	Morgans et al., unpubl. data
18.5	l/m PI	LO <i>Globorotalia incognita</i>	Morgans et al., unpubl. data
~19	I PI	FO <i>Globigerinoides trilobus</i>	Hornibrook et al. (1989)
~19	I PI	FO <i>Globorotalia bella</i>	Morgans et al., unpubl. data
19	Po/PI	Boundary	Morgans et al., unpubl. data
19	Po/PI	FO <i>Globorotalia praescitula</i>	Morgans et al., unpubl. data
21.6	Po	FO <i>Globorotalia incognita</i>	Scott et al. (1990); Berggren (1992)
22	I Po	FO <i>Spiroloculina novozealandica</i>	Morgans et al., in press
22.1	Lw/Po	Boundary	Morgans et al., in press
22.1	Lw/Po	FO <i>Ehrenbergina marwicki</i>	Morgans et al., in press
~22.2	I Lw	FO <i>Zeaglobigerina connecta</i>	Hornibrook et al. (1989)
22.5	I Lw	LO <i>Globigerina brazieri</i>	Morgans et al., in press
22.5	l/u Lw	LO <i>Globigerina euapertura</i>	Morgans et al., in press
~23	Lw	FO <i>Zeaglobigerina woodi</i>	Hornibrook et al. (1989)
23.8		Oligocene/Miocene Boundary	
24	I Lw	FO <i>Globigerina brazieri</i>	Hornibrook et al. (1989)
~25	I Lw	FO <i>Rectuvigerina rerensis</i>	Hornibrook et al. (1989); Boersma (1986)
25	Ld/Lw	Boundary	Morgans et al. (1996)
25	Ld/Lw	FO <i>Globoquadrina dehiscens</i>	Morgans et al. (1996)
27.1	Lwh/Ld	Boundary	Morgans et al. (1996)
27.1	Lwh/Ld	LO <i>Paragloborotalia opima opima</i>	Berggren et al. (1995)
27.1	Lwh/Ld	FO <i>Notorotalia spinosa</i>	Hornibrook et al. (1989); Morgans et al. (1996)
27	Lwh/Ld	LO <i>Rotaliatina sulcigera</i>	Hornibrook et al. (1989)
28.5	u Lwh	LO <i>Jenkinsina samwelli</i>	Jenkins & Srinivasan (1986)
28.5	u Lwh	LCO <i>Chiloguembelina cubensis</i>	Li et al. (1992)
29.7	u Lwh	FO <i>Tenuitellinata juvenilis</i>	Li et al. (1992)
30	l/u Lwh	LO <i>Subbotina angiporoides</i>	Berggren (1992); Morgans et al. (1996)
30.3	I Lwh	LO <i>Turborotalia ampliapertura</i>	Ogg et al. (1998)
30.6	I Lwh	FO <i>Paragloborotalia opima opima</i>	Berggren et al. (1995)
~32	I Lwh	FO <i>Tenuitella munda</i>	Jenkins & Srinivasan (1986); Hornibrook et al. (1989)
~32	I Lwh	LCO <i>Paragloborotalia gemma</i>	Jenkins & Srinivasan (1986); Hornibrook et al. (1989)
~32	I Lwh	LO <i>Globigerina brevis</i>	Jenkins & Srinivasan (1986); Hornibrook et al. (1989)
~33	I Lwh	LO <i>Uvigerina bortotara</i>	Hornibrook et al. (1989); Boersma (1986)

Table T3 (continued).

Age (Ma)	NZ stage	Foraminiferal event	References
~33.5	I Lwh	LO <i>Pseudohastigerina micra</i>	Jenkins & Srinivasan (1986); Hornibrook et al. (1989)
~33.5	I Lwh	LO <i>Globorotalia insolita</i>	Jenkins & Srinivasan (1986); Hornibrook et al. (1989)
33.7		Eocene/Oligocene Boundary	
~34	I Lwh	LO <i>Cibicidoides parki</i>	Hornibrook et al. (1989)
34.3	Ar/Lwh	Boundary	Morgans et al. (1996)
34.3	Ar/Lwh	LO <i>Nuttallides truempyi</i>	van Morkhoven et al. (1986)
34.3	Ar/Lwh	LO <i>Globigerinatheka index</i>	Morgans et al. (1996)
~34.8	Ar	LO <i>Ponticulasphaera semiinvoluta</i>	Jenkins (1967)
~35	Ar	FO <i>Paragloborotalia gemma</i>	Jenkins & Srinivasan (1986); Hornibrook et al. (1989)
~35	Ar	FO <i>Globigerina brevis</i>	Jenkins & Srinivasan (1986); Hornibrook et al. (1989)
35.5	Ar	FO <i>Turborotalia ampliapertura</i>	Jenkins & Srinivasan (1986); Hornibrook et al. (1989)
35.5	Ak/Ar	Boundary	Morgans et al. (1996)
35.5	Ak/Ar	FO <i>Sphaeroidina bulloides</i>	Hornibrook et al. (1989)
35.5	Ak/Ar	FO <i>Bolivina pontis</i>	Morgans et al. (1996)
37	Ab/Ak	Boundary	Morgans et al. (1996)
42	Dp/Ab	Boundary	Morgans et al. (1996)
42	Dp/Ab	FO <i>Globigerinatheka index</i> s.s.	Morgans et al. (1996)
55.5		Paleocene/Eocene Boundary	
55.5	Dt/Dw	Boundary	Morgans et al. (1996)
~55.5	Dt/Dw	LO <i>Rzehakina epigona</i>	Hornibrook et al. (1989)
~55.5	Dt/Dw	LO <i>Spiroplectammina spectabilis</i>	Hornibrook et al. (1989)
~55.5	Dt/Dw	LO <i>Conotrochammina whangaia</i>	Hornibrook et al. (1989)
~55.5	Dt/Dw	LO <i>Alabamina creta</i>	Hornibrook et al. (1989)
~55.5	Dt/Dw	LO <i>Nuttallides florealis</i>	Hornibrook et al. (1989)
~55.5	Dt/Dw	LO <i>Valvulineria teuriensis</i>	Hornibrook et al. (1989)
~63	Dt	FO <i>Allomorphina conica</i>	Hornibrook et al. (1989)
~63	Dt	FO <i>Nuttallides carinotruempyi</i>	Hornibrook et al. (1989)
~63	Dt	FO <i>Nuttallides florealis</i>	Hornibrook et al. (1989)

Note: FO = first occurrence, LO = last occurrence, FCO = first common occurrence, p.c. = personal communication. For other abbreviations, see Figure F7, p. 46. This table is also available in [ASCII format](#).

Table T4. Age assignments of biostratigraphic diatom zones used during Leg 181.

Zone	Reference	Top (Ma)	Base (Ma)	Datum used to define base
Neogene				
<i>Thalassiosira lentiginosa</i> Subzone c	1	0	0.18	
<i>Thalassiosira lentiginosa</i> Subzone b	1	0.18	0.42	
<i>Thalassiosira lentiginosa</i> Subzone a	1	0.42	0.65	<i>F. reinholdii</i> LO
<i>Actinocyclus ingens</i> Subzone c	1	0.65	1.07	
<i>Actinocyclus ingens</i> Subzone b	1	1.07	1.30	
<i>Actinocyclus ingens</i> Subzone a	1	1.30	1.80	<i>P. barboi</i> LO, ? <i>T. elliptipora</i>
<i>Proboscia barboi</i>	1	1.77	2.00	<i>T. kolbei</i> LO
<i>Thalassiosira kolbei</i> / <i>Fragilariopsis matuyamae</i>	1	2.00	2.50	<i>T. vulnifica</i> LO, ? <i>F. matuyamae</i>
<i>Thalassiosira vulnifica</i>	1	2.50	2.63	<i>F. interfrigidaria</i> LO, <i>T. insigna</i> LO
<i>Thalassiosira insigna</i>	2	2.63	3.26	<i>T. vulnifica</i> FO
<i>Fragilariopsis interfrigidaria</i>	2	3.26	3.80	<i>F. interfrigidaria</i> FO
<i>Fragilariopsis barronii</i>	2	3.80	4.44	<i>F. barronii</i> FO, <i>T. complicata</i> FO
<i>Thalassiosira inura</i>	2	4.44	4.92	<i>T. inura</i> FO
<i>Thalassiosira oestrupii</i>	2	4.92	5.56	<i>T. oestrupii</i> FO
<i>Fragilariopsis reinholdii</i>	2	5.56	8.10	<i>F. reinholdii</i> FO
<i>Actinocyclus ingens</i> var. <i>ovalis</i>	2	8.10	8.68	<i>C. intersectus</i> FO, <i>A. ingens</i> var. <i>ovalis</i> FO
<i>Thalassiosira torokina</i>	2	8.68	9.01	<i>T. torokina</i> FO
<i>Asteromphalus kennettii</i>	2	9.01	10.23	<i>T. kennettii</i> FO
<i>Denticulopsis hustedtii</i>	2	10.23	10.63	<i>D. dimorpha</i> LO
<i>Denticulopsis dimorpha</i>	2	10.63	11.67	<i>N. denticuloides</i> LO
<i>Denticulopsis dimorpha</i> / <i>Nitzschia denticuloides</i>	2	11.67	12.20	<i>D. dimorpha</i> FO
<i>Denticulopsis praedimorpha</i>	2	12.20	12.84	<i>D. praedimorpha</i> FO
<i>Nitzschia denticuloides</i>	2	12.84	13.51	<i>N. grossepunctata</i> LO, <i>N. denticuloides</i> FO
<i>Denticulopsis hustedtii</i> / <i>Nitzschia grossepunctata</i>	2	13.51	14.17	<i>D. hustedtii</i> FO
<i>Actinocyclus ingens</i> var. <i>nodus</i>	2	14.17	14.38	<i>A. ingens</i> var. <i>nodus</i> FO
<i>Nitzschia grossepunctata</i>	2	14.38	15.38	<i>N. grossepunctata</i> FO
<i>A. ingens</i> / <i>D. maccollumii</i>	2	15.38	16.20	<i>A. ingens</i> FO
<i>Denticulopsis maccollumii</i>	2	16.20	16.75	<i>D. maccollumii</i> FO
<i>Crucidentacula kanayae</i>	2	16.75	17.72	<i>C. kanayae</i> FO
<i>Thalassiosira fraga</i>	2	17.72	20.79	<i>T. fraga</i> FO
<i>Thalassiosira spumellaroides</i>	2	20.79	22.58	<i>T. spumellaroides</i> FO
Oligocene				
<i>Rocella gelida</i>	2	22.58	26.50	<i>R. gelida</i> FO
<i>Lisitzinia ornata</i>	2	26.50	27.95	<i>L. ornata</i> FO
<i>Azpeitia gombosii</i>	2	27.95	28.35	<i>A. gombosii</i> FO
<i>Rocella vigilans</i>	2	28.35	30.24	<i>R. vigilans</i> (small) FO
<i>Cavitatus jouseanus</i>	2	30.24	30.62	<i>C. jouseanus</i> FO
<i>Rhizosolenia gravida</i> / <i>oligocaenica</i>	2	30.62	33.22	<i>R. oligocaenica</i> FO

Note: References: 1 = Gersonde and Barcena (in press), 2 = Gersonde et al. (1999). This table is also available in [ASCII format](#).

Table T5. Ages of biostratigraphically useful radiolarian datums in the New Zealand region.

Age (Ma)	Radiolarian event	Source
0.18	FO <i>Buccinosphaera invaginata</i>	Johnson et al. (1989)
0.46	LO <i>Stylatractus univertus</i>	Caulet (1991)
0.83	LO <i>Pterocanium trilobum</i>	Lazarus (1992)
1.81	Pliocene/Pleistocene boundary	
1.92	LO <i>Eucyrtidium calvertense</i>	Lazarus (1992)
1.93	FO <i>Lithelius nautiloides</i>	Caulet (1991)
1.93	FO <i>Triceraspyris antarctica</i>	Caulet (1991)
2.42	LO <i>Helotholus vema</i>	Lazarus (1992)
2.44	LO <i>Desmospyris spongiosa</i>	Lazarus (1992)
2.61	FO <i>Cycladophora davisiana</i>	Lazarus (1992)
3.5	LO <i>Prunopyle titan</i>	Lazarus (1992)
4.57	FO <i>Helotholus vema</i>	Lazarus (1992)
4.6-4.62	LO <i>Helotholus praeveva</i>	Caulet (1991)
4.98-5.01	FO <i>Desmospyris spongiosa</i>	Caulet (1991)
5.01-5.11	FO <i>Prunopyle titan</i>	Caulet (1991)
5.03	LCO <i>Lychnocanoma grande</i>	Lazarus (1992)
5.2	Miocene/Pliocene boundary	
6.1	LO <i>Amphymenium challengerae</i>	Lazarus (1992)
6.58	FO <i>Amphymenium challengerae</i>	Lazarus (1992)
6.79	FO <i>Lamprocyrtis heteroporos</i>	Morely and Nigrini (1995)
7.71	FO <i>Acrosphaera? labrata</i>	Lazarus (1992)
9.12	LO <i>Cycladophora spongothorax</i>	Lazarus (1992)
9.22	LO <i>Stichocorys peregrina</i>	Lazarus (1992)
9.32	LCO <i>Ceratocyrtis stigi</i>	Lazarus (1992)
9.83	FCO <i>Ceratocyrtis stigi</i>	Lazarus (1992)
10.36	FO <i>Acrosphaera australis</i>	Lazarus (1992)
10.53	LO <i>Cycladophora humerus</i>	Lazarus (1992)
10.61	FO <i>Eucyrtidium pseudoinflatum</i>	Lazarus (1992)
10.77	LO <i>Actinomma glownini</i>	Lazarus (1992)
12.55	FO <i>Cycladophora spongothorax</i>	Lazarus (1992)
12.68	FO <i>Dendrospyris megalcephalis</i>	Lazarus (1992)
13.61	FO <i>Actinomma glownini</i>	Lazarus (1992)
14.18	FO <i>Cycladophora humerus</i>	Lazarus (1992)
17.02	FO <i>Eucyrtidium punctatum</i>	Lazarus (1992)
(19.11	FO <i>Cycladophora golli regipileus</i>	Lazarus (1992)
20.72	FO <i>Cyrtocapsella longithorx</i>	Lazarus (1992)
22.48	FO <i>Cyrtocapsella tetrapera</i>	Harwood et al. (1992)
23.35-24.73	LO <i>Lithomelissa sphaerocephalis</i>	Takemura and Ling (1997)
23.8	Oligocene/Miocene boundary	
23.94-25.26	FO <i>Cycladophora campanula</i>	Caulet (1991)
23.94-25.26	FO <i>Gondwanaria hister</i>	Caulet (1991)
24.12-28.75	LO <i>Axoprunum irregularis</i>	Takemura and Ling (1997)
26.77-30.05	LO <i>Eucyrtidium antiquum</i>	Caulet (1991)
26.77-30.05	LO <i>Lophocyrtis longiventer</i>	Caulet (1991)
?28.28-29.40	FO <i>Calocyclus</i> sp. A	Takemura and Ling (1997)
?28.28-29.40	LO <i>Lithomelissa challengerae</i>	Takemura and Ling (1997)
28.75-30.10	LO <i>Lychnocanoma conica</i>	Takemura and Ling (1997)
30.48-733.06	LO <i>Calocyclus</i> cf. <i>semipolita</i>	Takemura and Ling (1997)
30.94-34.66	FO <i>Axoprunum irregularis</i>	Takemura and Ling (1997)
30.94-34.66	FO <i>Eucyrtidium antiquum</i>	Takemura and Ling (1997)
30.94-34.66	LO <i>Eucyrtidium spinosum</i>	Takemura and Ling (1997)

Note: FO = first occurrence, LO = last occurrence, FCO = first common occurrence, LCO = last common occurrence. This table is also available in [ASCII format](#).

**Table T6.** Tool strings used and properties measured.

Tool string	Tool	Measurement	Measurement interval (cm)	Approximate vertical resolution (cm)
Triple combination	HNGS	Natural gamma	15	45
	APS	Porosity	5 and 15	30
	HLDS	Bulk density, PEF	2.5 and 15	15/45
	DIT	Resistivity	2.5 and 15	200/150/75
	TEMP	Temperature	1 per s	—
FMS-sonic	NGS	Natural gamma	15	45
	SDT	Orientation	15	—
	GPIT	Sonic velocity	15	120
	FMS	Microresistivity	0.25	0.5
GHMT	NGS	Natural gamma	15	45
	SUMS	Susceptibility	5 and 15	35
	NMRS	Total field	5 and 15	45

Note: PEF = photoelectric factor; see [“Downhole Measurements,”](#) p. 29, for other abbreviations. This table is also available in [ASCII format](#).